Analyses of Fibroblast Growth Factor Signaling in Lung Fibrosis

Inaugural Dissertation
submitted to the
Faculty of Medicine
in partial fulfillment of the requirements
for the PhD-Degree
in the Faculties of Veterinary Medicine and Medicine
of the Justus Liebig University Giessen

by
(BreAnne MacKenzie)

of
(Waterbury, Connecticut USA)
Giessen (2013)

From the Department of Internal Medicine

Director / Chairman: Prof. Dr. Werner Seeger

Faculty of Medicine of the Justus Liebig University Giessen

First Supervisor and Committee Member: Prof. Dr. Saverio Bellusci

Second Supervisor and Committee Member: Dr. Mohammad Hajihosseini

Committee Members (Chair):

Committee Member:

Date of Doctoral Defense:

Declaration

“I declare that I have completed this dissertation single-handedly without the unauthorized help of a second party and only with the assistance acknowledged therein. I have appropriately acknowledged and referenced all text passages that are derived literally from or are based on the content of published or unpublished work of others, and all information that relates to verbal communications. I have abided by the principles of good scientific conduct laid down in the charter of the Justus Liebig University of Giessen in carrying out the investigations described in the dissertation.”

Giessen October 2013

Summary (English)

Increased *fibroblast growth factor 10* (*Fgf10*) expression in vivo and administration of exogenous FGF7 recombinant protein enhance lung repair due to bleomycin injury by sending survival signals to lung epithelial cells via tyrosine kinase fibroblast growth factor receptor 2b (Fgfr2b). Given the prophylactic effects of FGF7 and therapeutic effects of FGF10 during bleomycin injury in mice, it was hypothesized that activation of the Fgfr2b endogenous pathway is critical for lung repair after bleomycin injury in mice. Furthermore, as new studies for the treatment of Idiopathic Pulmonary Fibrosis (IPF) have begun to target tyrosine kinases, the aim was to 1) assess the levels of FGF10 and FGF7 signaling in end-stage IPF lungs, 2) assess the level of recruitment of the endogenous Fgfr2b pathway after bleomycin lung injury in mice, and 3) assess the effect of FGF10 treatment on IPF fibroblasts in vitro.

Compared to donor, non-IPF controls, *FGF7* and *FGF10* transcripts were increased in end-stage IPF patient lung homogenates. However, receptors as well as downstream targets of FGF7 and 10 were significantly decreased. In contrast, wild type mice undergoing spontaneous repair after bleomycin injury, expressed *Fgf10* and downstream targets from 14 days post injury, indicating potential recruitment of this pathway during repair. Using three different genetic mouse lines congenitally deficient in endogenous Fgfr2b signaling, we found that *Fgf10* deficient animals incurred the highest trend towards increased fibrosis. Surprisingly, in a fourth mouse line allowing for induction of a soluble, dominant negative Fgfr2b receptor, induced mice did not show increased bleomycin-induced fibrosis compared to non-induced controls. Thus FGFR2b ligands signaling seemed to be recruited in a model of spontaneous repair, and dysregulated in non-repairing IPF patients. Thus the endogenous FGFR2b pathway may be redundant with other repair pathways in mice, as attenuating it did not result in a significant increase in bleomycin-induced fibrosis.

IPF fibroblasts responded to FGF10 treatment by decreasing their size, increasing proliferation and increasing expression of lipofibroblast markers. In addition, FGF10 inhibited transforming growth factor beta (TGF-β) stimulated induction of TGF-β signaling downstream target, pSMAD3. Likewise the ability of FGF10 to reduce cell size and inhibit TGF-β signaling in IPF fibroblasts, suggests that it could effectively mediate a contractile to synthetic-like phenotype, which may be an important step towards UIP lesion repair.

Taken together, this work highlights and discusses 1) the attenuation of FGFR2b ligand signaling in end-stage IPF, 2) FGFR2b signaling recruitment in wild type mice during bleomycin injury, yet redundant role in injury, and 3) the potential therapeutic effect of FGF10 given the effects of treatment on IPF fibroblasts.

Zusammenfassung (Deutsch)

Eine in-vivo erhöhte Expression von Fibroblasten-Wachstumsfaktor 10 (FGF10) und exogene Verabreichung von rekombinanten FGF7 Protein fördert über Signalwege des Tyrosinkinase-abhängigen Fibroblastenwachstumsfaktor-Rezeptors r2b (Fgfr2b) an das Lungenepithel die Lungenregeneration nach Bleomycin-induzierter Lungenfibrose. Angesichts der prophylaktischen Wirkungen von FGF7 und therapeutischen Wirkungen von FGF10 für die Bleomycin-induzierte Lungenschädigung im Mausmodell, lautet unsere Hypothese, dass die Aktivierung des endogenen FGFR2b Signalweges in diesem Zusammenhang eine kritische Rolle spielt. Darüber hinaus, wird in neuen klinischen Studien zur Behandlung von idiopathischer pulmonaler Fibrose (IPF) die Blockade von Tyrosin-Kinasen untersucht. Die vorliegende Arbeit hat folgendes zum Ziel: 1) Das Ausmaß der pulmonalen FGF10 und FGF7 Signalwege im Endstadium von IPF zu beurteilen, 2) Das Ausmaß der Aktivierung des endogenem FGFR2b Signalweges nach Bleomycin-induzierte Lungenschädigung bei Mäusen zu evaluieren und 3) Den Effekt der Behandlung von IPF Fibroblasten mit FGF10 in-vitro zu untersuchen.

Im Vergleich zum Spender (Kontrollgruppe ohne IPF), waren FGF7 und FGF10 Transkripte in Lungenhomogenaten von IPF Patienten im Endstadium erhöht. Allerdings waren die Expression der Rezeptoren sowie nachgeschaltete Signalwege von FGF7 und 10 signifikant erniedrigt. Im Gegensatz dazu wiesen Wildtyp-Mäuse, die ab Tag 14 nach Bleomycin-induzierte Lungenschädigung eine spontane Lungenregeneration zeigten, eine Aktivierung des FGF10 Signalweges auf. Dies weist darauf hin, dass der FGF 10 Signalweg eine potentielle Rolle während der Lungenregeneration spielen könnte. Unter den drei verwendeten verschiedenen genetischen Mauslinien mit kongenital reduziertem endogenem FGFR2b Signalweg, stellten wir fest, dass die konstitutiv FGF10 defizienten Mäuse den höchsten Trend zur vermehrten Fibrosebildung zeigten. Überraschenderweise, zeigte sich in einer vierten transgenen Mauslinie, in der die Expression eines dominant negativen FGFR2b Rezeptor induziert werden kann, in der Gruppe mit induzierte Blockade des FGFR2B Signalweges im Vergleich zur Kontrollgruppe keine vermehrte Fibrosebildung. Schlußfolgern einerseits wird, dass der FGFR2b Signalweg bei der spontanen Regeneration rekrutiert wird und in nicht-regenerierenden IPF-Patienten im Endstadium fehlreguliert ist. Andererseits, scheint neben dem endogenen FGFR2b Signalweg andere regenerative Signalwege zu existieren, da eine Blockade dieser nicht zur vermehrten Fibrosebildung führte. Obwohl es kann mit anderen Reparaturwege bei Mäusen redundant sein, als mildernde es nicht in einem deutlichen Anstieg der Bleomycin-induzierten Fibrose führen. IPF Fibroblasten reagierten auf die in-vitro FGF10 Behandlung mit eine Reduktion der Zellgröße sowei eine Erhöhung der Proliferation und der Expression von Marker für Lipofibroblasten. Darüber hinaus führte die in-vitro Behandlung mit FGF10 zur Hemmung des TGF-ß (transformierenden Wachstumsfaktor beta) Signalweges, was an der Reduktion des nachgeschalteten Signalproteins pSMAD3 gezeigt werden konnte.

Die Fähigkeit von FGF10, die Zellgröße der IPF Fibroblasten zu reduzieren und den TGF-β Signalweg zu hemmen, deutet darauf hin, dass FGF10 womöglich in der Lage sein könnte, die Veränderungen der Fibroblasten vom kontraktilen zum synthetischen Phänotyp zu fördern. Dies stellt ein wichtiger Schritt in der Regeneration der UIP (Usual Interstitial Pneumonia) Läsionen dar. Zusammenfassend handelt die vorliegende Arbeit von 1) der Abschächung des endogenen FGFR2b Signalweges im Endstadium von IPF Patienten, 2) der Rekrutierung des FGFR2b Signalweges im Rahmen der spontanen Regeneration nach Bleomycin-induzierter Lungenschädigung bei Wildtyp-Mäusen und 3) der potentiellen therapeutisch Wirkung von FGF10 auf der Grundlage der in-vitro Daten an IPF Fibroblasten.

Table of Contents

I. List of figures……..xi

II. List of tables…….xv

III. Abbreviations……..xvii

Part 1. Introduction……..……1

1.1 FGF signaling in the context of the lung……...1

1.1.1 Discovery and categorization of FGF ligands ……..1

1.1.2 General characteristics of FGF/FGFR structure and signaling…….....4

1.1.3 FGF7 signaling and regulation……6

1.1.4 FGF10 signaling and regulation……..7

1.1.5 FGFR2-IIIb signaling and regulation……..9

1.1.6 FGFR1-IIIb signaling and regulation……10

1.2 The Human Adult Lung……..……..12

1.2.1 Airway anatomy and cell types of the adult human lung……..12

1.3 Intersection of the lung and fibroblast growth factors……15

1.3.1 *FGF* mutations resulting in abnormal lung phenotypes……15

1.4 Interstitial lung diseases……19

1.4.1 ILD Overview……19

1.4.2 Idiopathic pulmonary fibrosis (IPF) ……..19

1.4.2.1 Familial IPF – Molecular links to the pathogenesis of IPF…...21

1.4.2.2 Putative mechanisms of sporadic IPF ……...22

1.4.2.3 Current treatments for IPF patients…….23

1.5 Introduction to mouse models of ILDs……25

1.5.1 Discovery and clinical use of bleomycin……..25

1.5.2 Bleomycin-induced pulmonary disease (humans)…….26

1.5.3 Bleomycin-induced pulmonary disease (mice)……...28

1.5.4 Effect of FGFs on bleomycin-induced pulmonary disease in mice….30

Part 2. Aims of this Study……..32

Part 3. Materials and Methods……..33

3.1 Procurement of human lung tissue specimens……33

3.2 Laser-assisted micro-dissection of human lung tissue……..33

3.2.1 RNA extraction for microarray……...33

3.2.2 Microarray hybridization and scanning……34

3.2.3 Microarray data analysis……34

3.3 Bleomycin injury……35

3.3.1 Generation of mice…….35

3.3.2 Establishing the dosage of bleomycin…….36

3.3.3 Delivery of bleomycin.……36

3.3.4 Monitoring physiological response post-injury……36

3.3.5 Mouse experiment protocols……..…37

3.4 Acquisition of lung function measurements……..37

3.4.1 Statistical analyses of SCIREQ data……38

3.5 Histological preparation and analyses of the left lung……...39

3.5.1 Masson's trichrome stain……39

3.5.2 Hematoxylin and eosin stain……..40

3.5.2.1 Ashcroft Score (% confluent fibrosis) ……40

3.5.2.1.1 Statistical analyses of Ashcroft Score……41

3.5.3 TUNEL assay for apoptosis……41

3.5.4 Immunofluroescence……..…41

3.5.4.1 Quantification of immunostaining……..…42

3.5.4.1.1 Statistical analyses of immunostaining……42

3.6 Collection of RNA for qPCR……42

3.6.1 cDNA synthesis and quantitative PCR……43

3.6.2 Mouse primers……43

3.7 Hydroxyproline content assay……..…..46

3.7.1 Hydroxyproline content analysis……..…..46

3.8 Primary culture of human lung fibroblasts……..…47

3.8.1 Culturing and passaging ……...47

3.8.2 Treatment with rhFGF1, rhFGF10 and TGF-β……48

3.8.3 Treatment with Rosiglitazone……48

3.8.4 Harvesting cells for RNA……48

3.8.4.1 Making cDNA……49

3.8.4.2 Human primers……45

3.8.5 Immunohistochemistry of cells……..49

3.8.6 Oil Red O staining……...50

3.8.7 Protein isolation and quantification……..50

3.8.8 Statistical Analyses……51

3.8.9 Quantification of immunofluorescent microscopy……..51

3.9 Primary culture of MLE-12 cells……51

3.9.1 Culturing and passaging……51

3.9.2 RNA isolation……...51

3.9.3 Protein isolation and quantification……..51

3.9.4 Western blot……51

3.10 Delegation of work done on animal experiments……..……51

Part 4. Results……..……..……..……..……..……53

4.1 FGF signaling is dysregulated in IPF lungs……...53

4.1.2 Epithelial FGF signaling is blunted in IPF lungs (microarray)……..53

4.1.3 qPCR transcriptome analysis of IPF vs. Donor lungs (qPCR)…….55

4.2 Bleomycin-injury mouse model does not recapitulate end-stage IPF phenotype……...57

4.3 FGF10/FGF7 signaling is blunted in end-stage IPF patients and activated in mice recovering from bleomycin-induced lung injury by 14 dpi……60

4.3.1 p-Akt and p-ERK are activated and total FGFR2 and FRS are increased in patients with IPF……60

4.4 Summary: FGF signaling is necessary to repair the lung after injury…65

4.5 Attenuating FGF ligands signaling in mice……68

4.5.1 Validation of the construct……69

4.5.2 Doxycycline from 7 dpi had no effect on survival……71

4.6 Ubiquitous attenuation of FGFR2b ligands activity during bleomycin injury led to moderately increased fibrosis……72

4.7 *Fgfr2b*$^{+/-}$ mice incurred more bleomycin-induced fibrosis than *WT*……76

4.8 *Fgf7* knockout mice showed no hindrance in repair at 28……..78

4.9 *Fgf7* knockout mice were more vulnerable to acute lung injury…..…...80

4.10 Spontaneous resolution was significantly hindered in *Fgf10*$^{+/-}$ mice....82

4.11 Fibrotic foci of bleomycin-injured *Fgf10*$^{+/-}$ mice are more active than *WT* mice…….84

4.12 Primary culture of human lung fibroblasts express FGF ligands and receptors…….……..……86

4.13 Impact of rhFGF10 treatment on Donor and IPF fibroblasts……...……88

4.13.1 IPF fibroblasts exhibit robust proliferation response……..88

4.13.1.1 MLE-12 cells respond to FGF1 and FGF10…….....90

4.13.2 Increase in FGF7 and FGFR1b/FGFR2b in IPF cells…..……..91

4.13.3 Impact of FGF10 treatment on *FGFR2b* expression…….……92

4.13.4 Increase in lipid droplets ..……93

4.14 FGF10 and rosiglitazone treatment of IPF fibroblasts led to a more lipofibroblast-like phenotype ..……94

4.14.1 Decreased size of SMA+ cells……...94

4.14.2 Increased expression of C/EBPα……..…96

4.14.3 Impact on *FGFR1b* expression……..…97

4.15 pre-treatment of IPF fibroblasts with FGF10 hindered TGF-β signaling……99

4.15.1 Decreased TGF-β signaling……..…99

4.15.2 Decreased number of SMA+ cells……..101

Part 5. Discussion……..……..……..……..……..……..…102

5.1 Analyzing the resolution of bleomycin-induced fibrosis in mice may be more relevant to IPF than analyses at earlier stages……..…..102

5.2 FGF signaling is activated in bleomycin-treated mice and attenuated in end-stage IPF patients…….……....103

5.3 Exogenous FGF7 may protect the epithelium from acute lung injury but is unlikely to promote fibrotic lesion resolution……..…....104

5.4 FGFR2b-independent FGF10 signaling may promote fibrosis resolution in mice……..105

5.5 FGF10 pushes IPF fibroblasts towards a lipofibroblast-like phenotype….107

5.6 FGF10 tempers TGFß1 signaling in IPF fibroblasts……..108

5.7 Model of the therapeutic use of FGF10 for end-stage IPF……...109

5.8 Future analyses of the role of FGF10 in lung progenitor cells are critical..112

Part 6.Conclusion……..……..……..……..……..……..……..114

Part 7.Summary/Zusammenfassung.....iv

Part 8.References.....116

Part 9. Acknowledgments.....131

Part 10. Curriculum vitae.....136

List of Figures

Fig1. Evolutionary relationships within the mouse *Fgf* gen e family and C. intestinalis *Fgf11/12/13/14*……3

Fig2. FGFR splicing isoforms confer FGF ligand and therefore temporal and tissue specificity for the activation of PI3K, PLC and Ras/MAPK signaling pathways……...5

Fig3. Major cell types of the human lung……...14

Fig4. Microarray profile indicating decreased FGF signaling in IPF lungs……..…….54

Fig5. Transcriptome analyses of IPF patients vs. donor by qPCR…….……..…57

Fig6. Heterogeneity in response of bleomycin to wild type injured animals and limited collagen deposition compared to end-stage IPF……...59

Fig7a. Transcriptome analysis of members of the FGF7 and 10 signaling pathway in human IPF and bleomycin-treated mice…….……63

Fig7b. Proteome analysis of members of FGF downstream targets in IPF vs. donor lung homogenates…….…….……..……65

Fig8. Bleomycin mouse model experiment schematic……..……67

Fig9. Validation of *Rosa26*$^{rtTA/+}$*;tet(O)solFgfr2b*/+ mice……..…69

Fig10. Survival curve for bleomycin-injured wild type mice fed doxycycline chow from 7 dpi……..……...……71

List of Figures

Fig11a. Impact of FGFR2b signaling attenuation from 6 dpi on fibrosis formation in mice……..73

Fig11b. Impact of FGFR2b signaling attenuation from 14 dpi on fibrosis formation in mice……75

Fig12. Decrease in endogenous *Fgfr2b* expression leads to increased fibrosis following bleomycin injury……...77

Fig13. Absence of endogenous *Fgf7* had no significant impact on fibrotic repair….79

Fig14. Absence of endogenous *Fgf7* led to increased acute lung injury following bleomycin administration…….81

Fig15. Decrease in endogenous *Fgf10* expression led to increased fibrosis following bleomycin injury…….83

Fig16. Decreased *Fgf10* expression leads to persistence of fibrotic lesions with increased proliferation, decreased epithelial markers, and increased smooth muscle actin after bleomycin injury……..……85

Fig17. Primary culture of human lung fibroblasts express *FGF* ligands and receptors……..…….87

Fig18a. IPF fibroblasts exhibit robust proliferation response to FGF10 compared to non-treated and donor cells…….89

Fig18b. MLE-12 cells respond to FGF1 and FGF10 treatment……..90

List of Figures

Fig19. FGF10 treatment results in a trend towards an increase in FGF7 expression by IPF fibroblasts……91

Fig20. FGF10 treatment results in a trend towards an increase in FGFR1b and FGFR2b expression in IPF fibroblasts……..92

Fig21. FGF10 treatment of lung fibroblasts increase in lipid droplets……..…….93

Fig22. Rosiglitazone and FGF10 decreased the size of SMA+ IPF fibroblast…...……95

Fig23. FGF10 and Rosiglitazone resulted in an increase in CEBP/α+ cells…..……96

Fig24. Rosiglitazone treatment increased *FGFR1* expression…….……98

Fig25. FGF10 hinders TGF-β signaling in IPF fibroblasts……..99

Fig26. FGF10 reduces the number of SMA+ IPF fibroblasts……...……101

Fig27. Model of the inhibition of TGF-β signaling by FGF10 in IPF……..111

Fig28. Model for therapeutic effects of FGF10 on end-stage IPF lungs……..113

Fig29. Lung progenitor cells are recruited during injury/repair……...…….115

List of Tables

Tab1. Summary of *FGF10, FGF7, FGFR1-IIIb, FGFR2-IIIb* expression in the lung...11

Tab2. *FGFR1/2* and *FGF7/10* mutations resulting in syndromes with respiratory phenotype or implicated in lung cancer……..…….……..…18

Tab3. Delivery methods of bleomycin…….…….……30

Tab4. Anesthesia dosages……..……...…….36

Tab5. Daily physiological response chart.…….…….……37

Tab6. Protocols for mouse experiments...…….…….……37

Tab7. Lung function read-out summary……..……38

Tab8. Mouse primers……..…..…..……44

List of Tables

Tab9. Human primers……..……..….45

Tab10. Delegation of animal work……..…….….51

Acta2/α-SMA	smooth muscle actin
AECI	alveolar epithelial cell type I
AECII	alveolar epithelial cell type II
ALI	acute lung injury
ARDS	acute respiratory distress syndrome
BADJ	broncho-alveolar duct junction
BAL	broncho-alveolar lavage
BALF	broncho alveolar lavage fluid
Bek	Fibroblast growth factor 2; isoforms b,c
Blmpf1	bleomycin-induced pulmonary fibrosis 1
BOOP	bronchiolitis obliterans organizing pneumonia
BSA	bovine serum albumin
CC10	Clara cell-specific 10 kDA protein
CCSP	Clara cell secretory protein 16 kDA
CEBP/α	CCAAT/enhancer binding protein alpha
CFA	cryptogenic fibrosing alveolitis
cmH20	centimeters of water
cmH20/s	centimeters of water/second
Col1a1	Collagen type 1 alpha 1
COP	cryptogenic organizing pneumonia
COPD	chronic obstructive pulmonary disorder
DAD	diffuse alveolar damage
DIP	desquamative interstitial pneumonia
DL (CO)	diffusion capacity for carbon monoxide
DMEM	Dulbecco's Modified Eagle Medium
DNA	deoxyribonucleic acid
Don	Donor
DOX	doxycycline
dpi	days post injury
E	embryonic stage
ECM	extra cellular matrix
ER	endoplasmic reticulum
Etv4/5	ETS translocation variant 4 or 5
F-IIP	familial - idiopathic interstitial pneumonitis
FEV1	forced expiratory volume
FGF	Fibroblast growth factor
FGFR	fibroblast growth factor receptor
Flg	Fibroblast growth factor receptor; 1 isoforms b,c
FVC	forced vital capacity
g.o.f.	gain of function
^{3}H	tritium (hydrogen-3)

H&E	Hematoxylin and eosin stain
HRCT	high-resolution computed tomography
i.t.	intra-tracheal
i.v.	intra-venous
IIP	idiopathic interstitial pneumonia
IL1-β	interleukin 1 beta
ILD	Interstitial lung disease
IP	interstitial pneumonia
IPF	idiopathic pulmonary fibrosis
IVC	inspiratory vital capacity
KGF/FGF7	Keratinocyte growth factor / Fibroblast growth factor 7
FGF10	Fibroblast growth factor 10
FGFR1-IIIb	Fibroblast growth factor receptor 1 isoform 3b
FGFR1-IIIc	Fibroblast growth factor receptor 1 isoform 3c
FGFR2-IIIb	Fibroblast growth factor receptor 2 isoform 3b
FGFR2-IIIc	Fibroblast growth factor receptor 2 isoform 3c
FRS2α	Fibroblast growth factor receptor substrate 2 alpha
l.o.f.	loss of function
LADD	lacrimal-auricular dental digital syndrome
LIP	lymphoid interstitial pneumonia
LOD	logarithm of odds
MAPK	mitogen-activated protein kinase
MHC	major histocompatibility complex
NSIP	nonspecific interstitial pneumonia
pAKT	phosphorylated Akt
PBS	phospho-buffered saline
PCR	polymerase chain reaction
PEEP	positive end expiratory pressure
pERK	phosphorylated Erk1/Erk2
PFA	paraformaldehyde
PI3K	phosphoinositide 3-kinase
PN	post natal day
PPARγ	peroxisome proliferation activator receptor gamma
qPCR	quantitative polymerase chain reaction
RB-ILD	respiratory bronchiololitis-associated interstitial lung disease
rhFGF10	recombinant human FGF10
RNA	ribonucleic acid
Rosi	rosiglitazone
rtTA	reverse tetracycline transactivator
SFTPC/SpC	surfactant protein C
Spry2	sprouty 2
Spry4	sprouty 4

tet(O)	tetracycline binding site
TGF-β	transforming growth factor beta
TKD	tyrosine kinase domaine
TLC	total lung capacity
TUNEL	Terminal deoxynucleotidyl transferase dUTP nick-end labeling
UIP	usual interstitial pneumonia
UPR	unfolded protein response
ΔP	change in pressure
ΔV	change in volume
µg	microgram
µl	microliter
µm	micrometer

Part 1. Introduction

1.1 FGF signaling in the context of the lung

1.1.1 Discovery and categorization of FGF ligands

The mitogenic activity of “growth” factors was first observed by treating connective tissue with “tissue juices” extracted from various animals and organs in the early 1900’s. The aim of these studies was to improve suture healing after surgeries. “If the factors that bring about the multiplication of cells and the growth of tissues were discovered, it would perhaps become possible to activate artificially the processes of repair,” wrote surgeon and Nobel prize winner for physiology, Alexis Carrel in 1912 in the Journal of Experimental Medicine (Carrel, 1913). He observed that while “embryo juice” had the most “activating power” on the density and outgrowth of chicken embryo heart explants, “tissue juice” extracts from different organs also improved cultures with variable efficiencies. Later, in the 1930s, experiments were performed in order to identify an organ in adult fowl whose “tissue juice” had the most potent effect on periosteal fibroblasts (Trowell and Willmer, 1938). Brain extracts contained the most potent growth promoting properties, followed by thyroid, testis, ovaries, bone marrow, liver, kidney, and muscle extracts. Following this seminal observation, scientists worked to identify and isolate these potent factors. Finally, in the 1970’s and 80’s, the first two fibroblast growth factor (FGF) ligands were isolated from bovine brain and pituitary gland respectively: “acidic” FGF (FGF1) and “basic” FGF (FGF2) (Böhlen et al., 1985; Gospodarowicz, 1975). Thus the name “fibroblast growth factor” came from the observation that *in vitro*, FGF1 and 2 could induce the proliferation of fibroblasts. Since then, FGFs have been identified not only in vertebrates and invertebrates (Burdine et al., 1998) but even in the genome of viruses (Popovici et al., 2005). *Fgf*-like sequences have not however been found in unicellular organisms such as *Escherichia coli* or *Saccharomyces cerevisiae*.

In mammals, *Fgfs* 1-10 and 16-23, have been studied and characterized. According to phylogeny and sequence homology, they have been clustered into seven subfamilies (Fig 1A): *Fgf-1/2, Fgf-3/7/10/22, Fgf-4/5/6, Fgf-8/17/18, Fgf-11/12/13/14, Fgf-9/16/20, and Fgf-15/21/23* (Itoh and Ornitz, 2008). The

hormone-like (*hFgf*s); *Fgf15* in mouse and its ortholog *FGF21* in human, as well as *Fgf23* (mouse and human), require cofactors (Klothos) to bind and activate FGF receptors and control important metabolic functions (Adams et al., 2012; Kuro-o, 2008). The intracrine FGFs, or (*iFgf*s) (*Fgf-11/12/13/14*), are not secreted and do not require interaction with receptors for signaling, but rather signal via voltage gated sodium channels (Wang et al., 2011). Lastly, FGFs belonging to the following subfamilies: *Fgf-1/2/5*, *Fgf-3/4/6*, *Fgf-7/10/22*, *Fgf-8/17/18* and *Fgf-9/16/20*, are between 20 – 30 kDA in size, glycosylated, secreted, form dimers, and signal in a paracrine manner via FGF receptors (FGFRs) in the presence of heparan sulfate proteoglycans (HSPGs). Interestingly, the coding regions of *iFgfs* are divided by four introns, while the coding regions of canonical *Fgfs* and *hFgfs* are divided by two introns; all of whose core locations are highly conserved. Many studies suggest that introns are relics of primordial genes (de Roos, 2007; Rogozin et al., 2005) thus indicating that the *iFgf* subfamily is the likely ancestor of canonical *Fgf* ligand families (Fig 1B).

This project is focused on the *Fgf7* canonical subfamily, whose ligands signal in a paracrine fashion via receptors FGFR1 and FGFR2 (Itoh and Ornitz, 2011). The gene predecessors of the canonical *Fgf* subfamilies and *hFgfs* were derived from an *Fgf13-like* ancestral gene via gene duplication followed by translocation and accompanied by the loss of two introns. In addition, canonical *Fgf4* ligand acquired a cleavable amino terminal signal sequence in the first exon. Given that *Fgf4* is required at the earliest stages of development, an *Fgf4-like* gene may be the ancestor for all *Fgf* ligands in the canonical subfamilies. Taken together, a model for the evolution of the *Fgf7* subfamily was created (Fig 1B): First, an *Fgf13-like* gene gave rise to *Fgf4*. Later, *Fgf5, Fgf8, Fgf9*, and *Fgf10* were generated from an *Fgf4-like* gene via gene duplications and translocations with conserved secreted signal sequences and intron positions (Itoh and Ornitz, 2008). An *Fgf10-like* gene is thus thought to be the ancestor of other members of the *Fgf-7* family (*Fgf-7/10/22*). Notably, although *Fgf3* is a member of the *Fgf7* subfamily according to phylogenetic and functional analysis, gene location analysis indicates that *Fgf3* is linked rather to *Fgf4* and *Fgf6*.

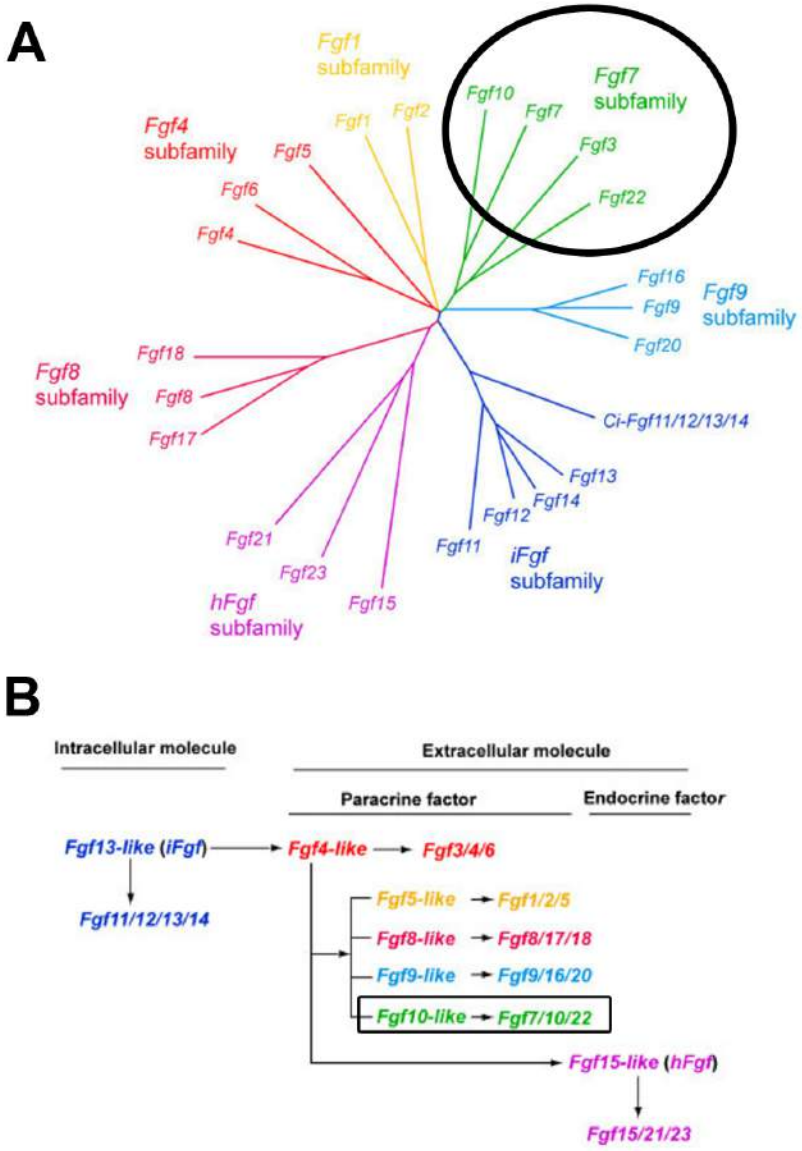

Figure 1. Evolutionary relationships within the mouse *Fgf* gene family and C. intestinalis *Fgf11/12/13/14*.

(A) Ancestral relationships and subfamilies of FGF genes. Black circle indicates family of interest. (B) Functional evolutionary history of ancestors of the mouse *Fgf* gene family. Black rectangle indicates family of interest.

Figure adapted from (Itoh and Ornitz, 2008).

1.1.2 General characteristics of FGF/FGFR structure and signaling

Each of the four *FGFR*s encode up to 20 exons and is comprised of an extracellular region composed of two to three immunoglobulin-like (Ig) domains, a single pass transmembrane segment, and an intracellular tyrosine kinase domain (Johnson and Williams, 1993). Tissue specific and ligand specific signaling is achieved by alternative splicing of exons 7 – 9 in the C-terminal end which encode the third Ig extracellular domain of FGFRs-1, -2, and -3. These receptors are spliced into isoforms “IIIb” and “IIIc”; “III” referring to the third IgG domain (Fig 2 A,B). These isoforms allow for both ligand and tissue expression specificity (Zhang et al., 2006).

FGF ligands bind two at a time leading to receptor dimerization in the presence of heparan sulfate proteoglycans (HSPG). This results in the transphosphorylation of the dimerized receptors and activation of the intracellular tyrosine kinase domain of the receptor. FGFR signaling is largely mediated through a single membrane-bound tyrosine phosphorylated docking protein, FGF receptor substrate 2 alpha (FRS2α). When FRS2α tyrosite sites are phosphorylated (pTyr), it recruits four molecules of the adaptor protein Grb2 and two molecules of the protein tyrosine phosphatase Shp2 (Gotoh, 2008; Hadari et al., 2001; Zhang et al., 2008). Activated cytoplasmic intracellular signaling cascades include: Ras/MAPK, PI3K/Akt, and PLC*γ*/PKC. These pathways regulate the transcription of a variety of target genes that control functions such as cell proliferation, migration, differentiation, or survival (Fig 2B).

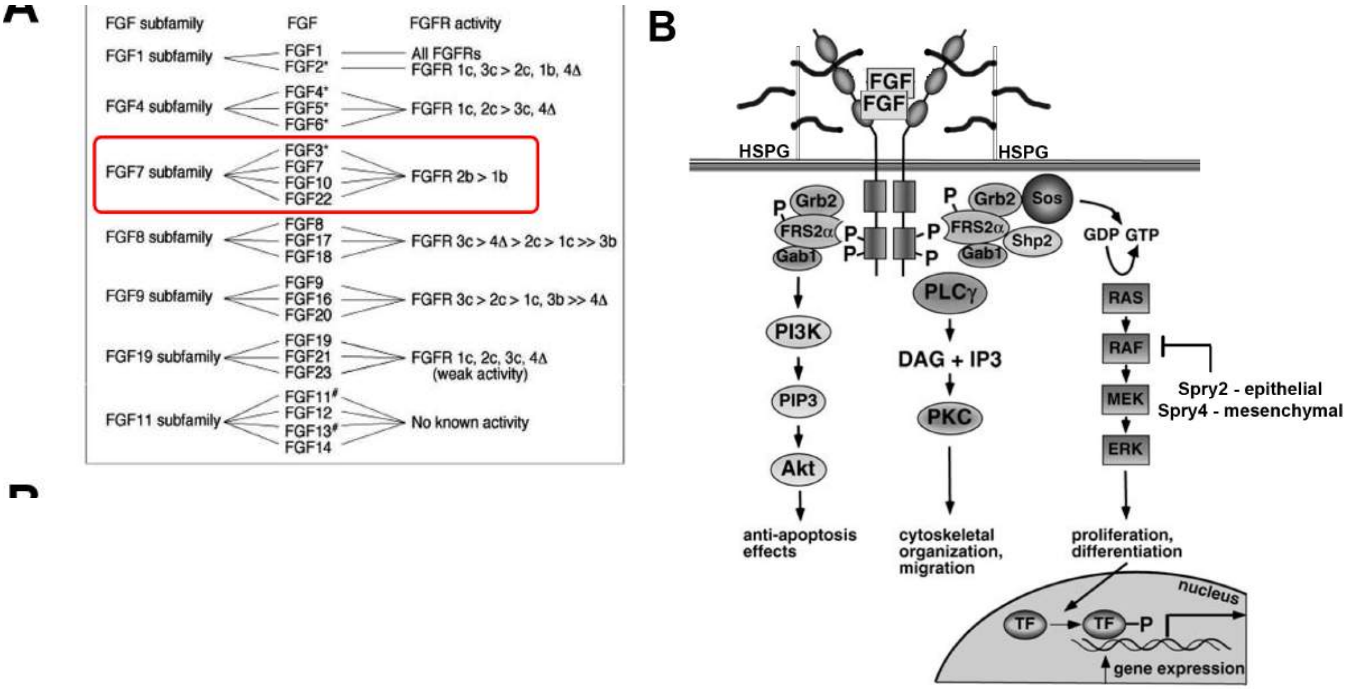

Figure 2. FGFR splicing isoforms confer FGF ligand and therefore temporal and tissue specificity for the activation of PI3K, PLC*γ* and Ras/MAPK signaling pathways.

(A) Based on *in vitro* studies using BaF3 cells, FGF7 and FGF10 signal mainly via FGFR2b, but also have some affinity to FGFR1b. (B) FGFs bind to FGFRs in the presence of HSPGs stimulating receptor phosphorylation and the binding of the FGF receptor docking protein FRS2α. FRS2α phosphorylation recruits Grb2 and Gab1 adaptor proteins, as well as the protein tyrosine phosphatase Shp2, and directs signaling to either PI3K or Ras-MAPK pathways. Activation of the PLCγ pathway stimulates PKC. These pathways control a variety of cellular behaviors involved in development and repair.

Figure adapted from (Wagner and Siddiqui, 2007; Zhang et al., 2006).

1.1.3 FGF7 signaling and regulation

FGF7, otherwise known as keratinocyte growth factor (KGF), binds with high affinity and exclusively to FGFR2-IIIb (Cheon et al., 1994; Mason et al., 1994). While FGF7 shows potent mitogenic activity on epithelial cells, as FGFR2-IIIb is expressed exclusively on epithelial cells, no corresponding activity on fibroblasts, endothelial cells, melanocytes, or other non-epithelial targets of FGF action have been observed (Aaronson et al., 1991). In addition to high receptor specificity, a precise conformation of HSPGs with specific charge densities between stromal and epithelial cells in the ECM, are also necessary in order for FGFR2-IIIb to access stromal-derived FGF7 (Luo et al., 2006a; Luo et al., 2006b). *In vitro* studies showed that FGF7 induced activation of FGFR2-IIIb, elicited tyrosine phosphorylation not only of FRS2α, but also of the insulin receptor substrate 4 (IRS4), the canonical extracellular signal regulated kinase 2 (ERK2, MAPK2), and cyclin-dependent protein kinase (CDK2) (Luo et al., 2009).

In the lung, FGF7 plays an important role in mediating the proliferation, migration and differentiation of AEC2 cells (Deterding et al., 1996). Treatment of isolated adult lung type II cells (AEC2) with FGF7 increases expression of the surfactant-associated proteins *SP-A* and *SP-B*, with no effect on *SP-C* mRNA expression (Sugahara et al., 1995). In addition it has been shown to regulate fluid balance in the fetal lung (Zhou et al., 1996) possibly via up-regulation of aquaporin-5 (*AQP5*) expression, an epithelial water channel (Tichelaar, 2000). Interestingly, FGF7 also stimulates lipogenesis in rat AEC2 cells by inducing expression of lipogenic enzymes and transport proteins regulated by transcription factors CCAAT/enhancer-binding protein (C/EBP) isoforms and sterol regulatory element-binding proteins (SREBP), but not peroxisome proliferation activator receptor gamma (PPARγ). Notably, FGF7 induces fatty acid synthase, stearoyl-CoA desaturase-1 (SCD-1), which activates fatty acid synthesis in AEC2 cells (Mason et al., 2003).

Regulation of FGF7 by lung fibroblasts is poorly characterized. However, inflammatory mediators are known activators, including interleukin 1 beta (IL-1β) which appears to be the most potent cytokine inducer of FGF7 expression in

fibroblasts (Chedid et al., 1994; Li and Tseng, 1997; Marchand-Adam et al., 2005). The stimulation of FGF7 expression by IL-1β and to a lesser extent by other cytokines such as IL-6, transforming growth factor alpha (TGFα), and platelet-derived growth factor (PDGF) may be the mechanism by which FGF7 is induced during inflammation, where it has been shown to promote re-epithelialization and wound healing.

1.1.4 FGF10 signaling and regulation

While both FGF7 and FGF10 bind with high affinity to FGFR2-IIIb (Igarashi, 1998), they may induce different target genes in the lung and thereby play different functional roles during development and homeostasis. Regulation of *Fgf10* however, is only partly understood during lung development and still less characterized in the adult lung.

During development, *Fgf10* is expressed in the distal mesenchyme where it induces budding and outgrowth of early lung endoderm (Bellusci et al., 1997) and induces chemotaxis in distal lung epithelium (Weaver et al., 2000). While *Fgf7* knockouts are viable (De Moerlooze et al., 2000; Guo et al., 1996; Sekine et al., 1999), absence of *Fgf10* or *Fgfr2b* results in complete lung agenesis. *Fgf10* expression peaks at E18.5 (Bellusci et al., 1997), and blocking FGF10 with a soluble dominant negative receptor from E14.5, results in decreased lung morphogenesis and emphysema (Hokuto et al., 2003). In addition, *Fgf10* hypomorphs display vascular defects associated with decreased expression of vascular markers *Pecam* and *Laminin*, a reduction of WNT signaling, as well as significant lung hypoplasia (Ramasamy et al., 2007). These results demonstrate that a threshold of *Fgf10* is required for the formation and maintenance of multiple mesenchymal and epithelial cell progenitor populations in the lung. Also, like FGF7, O-sulfated groups in heparin sulfates were found to be critical for FGF10 signaling activation in the epithelium during lung bud formation (Izvolsky et al., 2003).

Known negative regulators of FGF10 during lung development include TGFβ (Lebeche et al., 1999), SHH (Bellusci et al., 1997) and BMP4 (Weaver et

al., 2000). Positive regulators include FGF9 (De Langhe et al., 2006; del Moral et al., 2006) which has been shown to upregulate *Fgf10* expression likely via *Tbx4/5* as well as WNT2 (Goss et al., 2011). In order to identify early lung specific, epithelial targets of FGF10 signaling, mesenchyme free E11.5 primary epithelial lung cultures were treated with FGF10 and a DNA microarray followed by in situ hybridization was performed (Lü et al., 2005). This analyses revealed upregulation of genes associated with cell rearrangement and migration, inflammatory processes, lipid metabolism as well as BMP and WNT receptors (Lü et al., 2005).

In addition to FGFR2-IIIb, FGF10 also binds to FGFR1-IIIb (Luo et al., 1998). This may be the mechanism by which FGF10 maintains lipofibroblast progenitors in the lung, as the FGFR1-IIIb isoform is expressed on cells of both epithelial and mesenchymal cell lineages (Beer, 2000). Interestingly, FGF10 also partly contributes to the expression of *C/ebpβ* through an autocrine (possibly via FGFR1-IIIb) or paracrine (FGFR2-IIIb) mechanism (Sakaue et al., 2002). *In vivo* data supports this finding, as *Fgf10*$^{-/-}$ mouse embryos lack white adipose tissue (Asaki et al., 2004b).

While FGFR2b ligands have been shown to be critical for the maintenance of ameloblast progenitors which are required for the regeneration of adult mouse incisors (Parsa et al., 2010), whether FGF10 signaling is required for the preservation or maintenance of lung epithelium or mesenchymal progenitors during adult lung homeostasis is unknown. However, FGF10 has been shown to be an important mediator of lung repair after injury. In mice injured with naphthalene, WNT7b was shown to activate *Fgf10* after injury (Volckaert et al., 2011). In this case, in order to stimulate re-epithelialization, FGF10 coming from smooth muscle actin positive (SMA+) cells signaled to variant Clara cells; a putative epithelial progenitor cell that is SPC+; CC10+; cytochrome p450 negative, and therefore immune to naphthalene. Moreover, epithelial specific over-expression of *Fgf10* was found to be protective against bleomycin induced fibrosis partly by inhibiting TGFβ and by triggering an increase in CD41+CD25+Foxp31+ T-regulatory cells (Gupte et al., 2009).

Recently, more insight into the difference between FGF7/FGFR2b and FGF10/FGFR2b downstream targets and signaling events have been discovered (Francavilla et. al. *in press* Molecular Cell 2013). This study showed that FGF10 specifically induces Y734 phosphorylation of FGFR2-IIIb which recruits p85; a regulatory subunit of PI3K. p85 functions as a scaffold protein for the adaptor protein: SH3 domain binding protein 4 (SH3BP4). This complex functions as a molecular switch for receptor recycling. Thus, the FGF10/FGFR2b signal stimulates receptor recycling and prolonged signaling resulting in cell migration, while FGF7/FGFR2b signaling results in transient signaling, receptor degradation and proliferation.

1.1.5 FGFR2-IIIb signaling and regulation

FGFR2-IIIb is expressed by differentiated epithelial cells in a variety of tissues where it functions to maintain epithelial cell homeostasis. It is also under stringent co-factor control (HSPGs) (Finch et al., 1989). While FGFR2-IIIb signaling supports epithelial cell proliferation, it is self-limited and often occurs in parallel with differentiation (Belleudi et al., 2011; Matsubara et al., 1998; Yan et al., 1993). Moreover, loss of stromal-epithelial compartmental homeostasis concurrent with loss of *FGFR2-IIIb* has been associated with malignancy (Wang et al., 2004). Furthermore, exon switching from the *IIIb* variant of *FGFR2* to the *IIIc* variant was accompanied with malignant progression in prostate cancer (Jin et al., 2003). Interestingly, down-regulation of *FGFR2-IIIb* was associated with malignant transformation in keratinocytes (Finch and Rubin, 2006) while re-expression of *FGFR2-IIIb* resulted in growth inhibition and induction of differentiation in prostate (Matsubara et al., 1998), bladder (Bernard-Pierrot et al., 2004; Ricol et al., 1999), and human salivary gland carcinoma cells (Drugan et al., 1998). While normal FGFR2-IIIb signaling may act as a “tumor suppressor”, mutations associated with increases, or aberrant signaling (for example *FGFR2-IIIb* expression in the mesenchyme) have been implicated in the pathogenesis of gastric, lung, breast, ovarian cancer and endometrial cancer (Katoh, 2008).

Sprouty 2 (SPRY2) is an epithelial specific, negative regulator of FGFRs. *SPRY2* promoter contains *ETS-1* and *CREB* binding elements (Ding et al., 2003) indicating it is an ERK1/2 cascade target. Growth factor stimulation of FGFR2-IIIb results in SRC kinases binding to FRS2 (Li et al., 2004) which in turn results in the phosphorylation of several tyrosines on SPRY2 (Mason et al., 2004; Rubin et al., 2005), thus SRC kinases also play a key role in controlling FGFR signaling dynamics (Sandilands et al., 2007). Furthermore, *Etv4* is also an epithelial transcriptional target of FGFR2-IIIb signaling (Firnberg and Neubüser, 2002; Liu et al., 2003).

1.1.6 FGFR1-IIIb signaling and regulation

The highest levels of *FGFR1-IIIb* expression are found in sebaceous glands and in the neurons of the hippocampus and the cerebellum. However, it is also expressed in the kidney, lung, skeletal muscle, heart, testis, and intestine (Beer, 2000). Furthermore, *FGFR1-IIIb* is expressed in the pancreas where it can modulate functions that regulate cell proliferation, adhesion, and movement (Liu et al., 2007b). FGFR1-IIIb binds FGF1 with highest affinity, and has a lower relative affinity to FGF10 (Beer et al., 2000; Zhang et al., 2006). Mice carrying an in-frame stop codon in the *IIIb* exon of *Fgfr1*, were viable and fertile (Partanen et al., 1998). Like the FGFR2-IIIb isoform, FGFR1-IIIb also showed tumor-suppressor qualities; for example re-expression of this isoform in pancreatic cancer cells inhibited their malignant phenotype (Liu et al., 2007a).

In the lung, *FGFR1-IIIb* expression has been detected in whole lung homogenates and rat lung fibroblasts cell lines (*Rehan* and *Bellusci* unpublished data). Thus FGF10 may signal in an autocrine fashion to mesenchymal derived cells such as lipofibroblasts in the lung in order to promote surfactant homeostasis or repair after injury. *Spry4* is also a mesenchymal target and negative regulator of FGF signaling in the mesenchyme (de Maximy et al., 1999). Like SPRY2, it blocks FGF signaling by inhibiting the MAPK pathway.

	FGF10	*FGF7*	*FGFR1-IIIb*	*FGFR2-IIIb*
Embryonic Development	distal tips of mesenchyme from E9.5[1] , PBSMCs[5] lipofibroblast progenitors[8]	through-out mesenchyme from E14.5[2]	unknown; mutation is not lethal[3]; putative epithelium[3]	epithelium from E9.5[4]
Alveologenesis	lipofibroblast progenitors[8]	lung fibroblasts, "stromal" cells[6]	putative lipofibroblasts progenitors[12]	epithelial progenitors[1]
Adult Lung	PBSMCs after epithelial injury[1] stromal cells[11] lipofibroblasts[12]	lung fibroblasts, "stromal" cells[6]	putative: lipofibroblasts[12] basal respiratory cells[9]	respiratory epithelium[9], variant Clara cells[10,*]

Table 1. Summary of *FGF10, FGF7, FGFR1-IIIb, FGFR2-IIIb* expression patterns in the lung

(Finch et al., 1995)[2] (Partanen et al., 1998)[3] (Peters et al., 1992)[4] (Mailleux et al., 2005)[5] (Chelly et al., 1999)[6] (El Agha et al., 2012)[7,8] (Hughes, 1997)[9] (Volckaert et al., 2011)[10] (El Agha et al., 2013 *in revision*)[11] (Bellusci Lab, Unpublished Data)[12]

*variant Clara cells: cytochrome P450 negative, CC10+;SPC+; putative stem cells of bronchio-alveolar duct junction (BADJ)

1.2 The Human Adult Lung

1.2.1 Airway anatomy and cell types of the adult human lung

As in the case of other vertebrates, the human lung is the primary organ of respiration, or the exchange of carbon dioxide for oxygen. The human lung is divided into two asymmetrical sides: the left lung is made up of two lobes, and the right lung, three. Air enters through the mouth or nose, travels through the oropharynx or nasopharynx; and continues to the larynx and trachea. After the trachea, it then enters a progressively subdividing system of bronchi and bronchioles. Finally, it reaches the alveoli where oxygen passes into the bloodstream and where carbon dioxide is released from the bloodstream into the alveolar compartments and exhaled. Lung structure can thus be divided into “conductive” airways and “respiratory” airways. The conductive airway assures that air is delivered to the “respiratory airways” where gas exchange takes place. The first main structure of the conducting airway is the trachea. The trachea, or windpipe, is a ringed-cartilaginous tube lined with smooth, pseudostratified, columnar epithelial cells and mucin secreting goblet cells, all of which are anchored to the basement membrane by basal cells. The trachea then divides into the two main bronchi, which enter either, the right or left lobe. The right main bronchus divides into three lobar bronchi, the right bronchi into two lobar bronchi. These lobular bronchae are then segmented into still narrower airways which segment further into bronchioles. Bronchioles lack both cartilage and mucin producing cells and are the last structures to comprise the conducting airway. A mixed population of ciliated and non-ciliated epithelial cells line the conducting airways of mice and humans. The non-ciliated cells are Clara cells characterized by apical protrusions that secrete Clara cell secretory protein (CCSP), which has antioxidant and surfactant-like immune-modulatory properties. In healthy humans, there are few Clara cells in the large conducting airways, but their numbers progressively increase in more distal airways (Coppens et al., 2007) .

The respiratory airway begins where the bronchioles end. The bronchioles terminate into alveolar sacs; the structure where they meet, the alveolar ducts, marks the beginning of the respiratory airway, as gas exchange takes place here.

Each alveolar sac is wrapped in a fine mesh of capillaries covering about 70% of its area and each lung contains about 300 million alveoli. Alveoli are comprised primarily of Type I pneumocytes (simple squamous alveolar cells), which are also called alveolar epithelial cells (AECI). AECIs account for 95% of alveolar cells. They are the site of gas exchange, they provide structural support for the alveoli, help manage lung fluid homeostasis, have very little mitotic activity, and are very susceptible to injury (Kathuria et al., 2007). Partial pressure differences allow oxygen (in the alveoli) and carbon dioxide (in the red blood cells) to exchange places via passive diffusion (Maina and West, 2005). Type II pneumocytes (AECII) only account for approximately 5% of alveolar cells. However, they are mitotically active, they secrete and are able to alter surfactant composition, they participate in both the immune and inflammatory responses, and they can also proliferate and transform into AECIs to repair alveolar walls (Wang, Manzer, McConville, & Mason, 2006).

While epithelial cells make up the majority of the respiratory airways, they could not maintain their shape during the cycles of alveolar expansion and collapse during respiration without support by interstitial fibroblasts or “stromal” cells. Several different fibroblasts are present in the adult lung. Alveolar myofibroblasts, sometimes called alveolar smooth muscle cells, assist in extracellular matrix (ECM) production and support alveolar structure. Lipofibroblasts are distinguished by the presence of large, cytoplasmic lipid droplets, and assist AECII cells with surfactant production particularly during alveologenesis (Vaccaro and Brody, 1978). Surfactant proteins are small, hydrophobic and hydrophilic proteins, secreted by AECIIs, which are crucial for both the establishment and maintenance of lung alveolar structure and function.

The lung parenchyma is defined as the tissues and spaces that surround the air sacs of the lung. Cells such as fibroblasts, monocytes, and macrophages fill the delicate space between the basement membranes of AECI and AECII cells; the area known as the interstitium, and contribute to the circulatory, immune and structural support system of the lung.

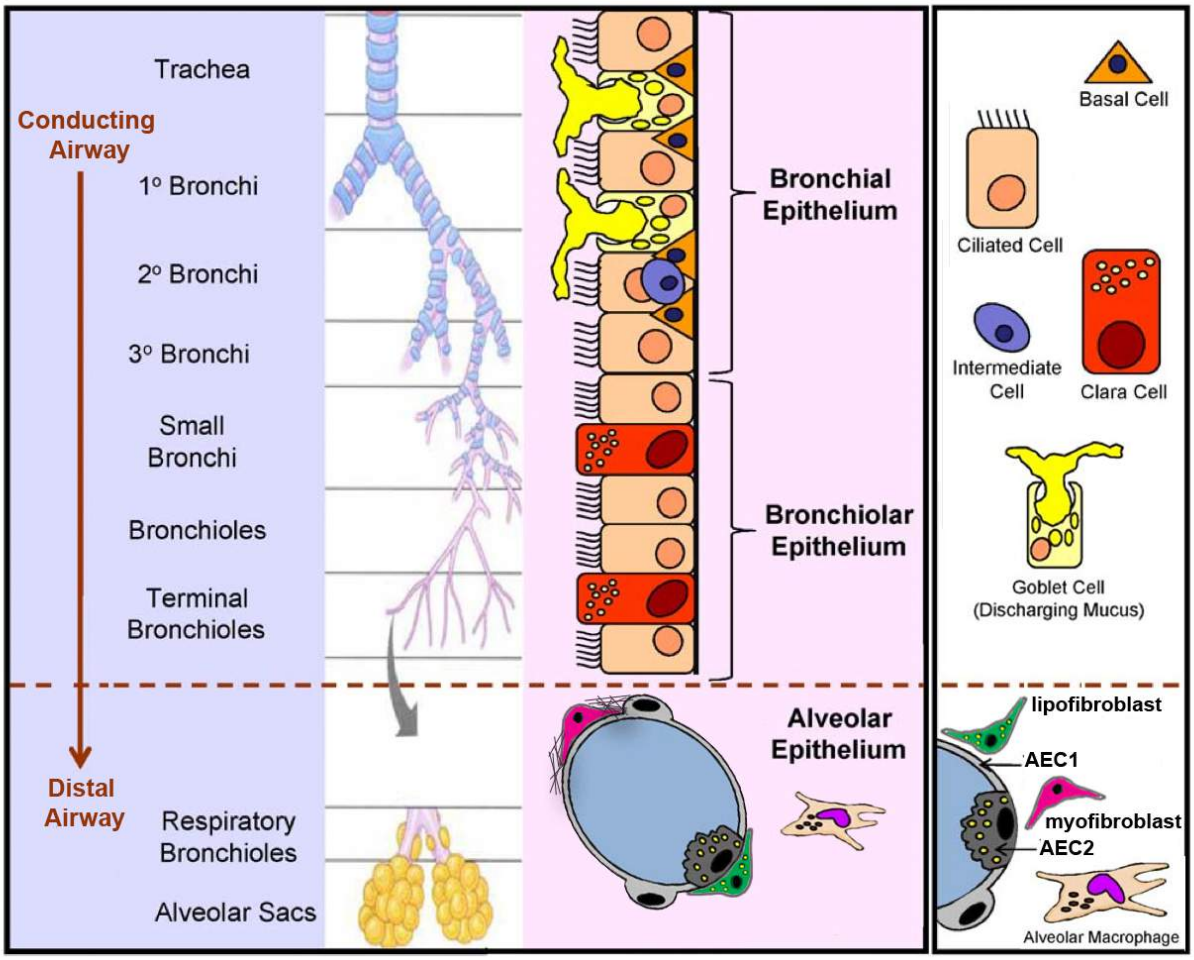

Figure 3. Major cell types of the human lung

The lung is composed of the conducting and respiratory airways each of which is composed of special cell types. The conducting airways are composed of basal, ciliated, Clara, intermediate and goblet cells, as well as differentiating or 'intermediate' cells. The respiratory airways are mainly composed of AEC1 cells, but also include AEC2, lipofibroblast, myofibroblasts, and alveolar macrophages. Not featured here: other immune cells, as well as endothelial cells composing the capillaries that line the alveolar sacs, and neuroendocrine cells.

Figure adapted from (Bérubé et al., 2010)

70 square meters of alveolar membrane space makes the lung by far the largest surface of the human body in contact with the outside world. Because the lung surface is so vulnerable to foreign agents breathed in from the environment; it has evolved a first line of defense against the detection and elimination of bacteria and viruses, otherwise called the “innate immunity”. Alveolar macrophages are part of the innate immunity as they recognize microbial or viral motifs on the organism’s surface. Intruders are opsonized or marked by macrophages and subsequently discarded by phagocytosis. Even the surfactant proteins, SP-A and SP-D, assist in the clearance of pathogens by opsonizing the target for eradication by leukocytes. In addition, humans have also evolved an “adaptive immunity”, which responds to the innate signals by mounting antigen specific antibodies against both microbes and viruses.

1.3 Intersection of the lung and fibroblast growth factors

1.3.1 *FGF* mutations can result in abnormal lung phenotypes

Given that FGFs are so important for the normal embryonic development of a wide range of tissues, it’s not surprising that a single germ line mutation in either *FGF* receptor or ligand results in the manifestation of genetic syndromes. Genetic disorders or “syndromes” refer to complex clinical pathologies that have more than one identifying feature or symptom resulting from one or more genetic defects. There are many known heritable and spontaneous genetic mutations in *FGF* genes that have adverse effects on just about every organs development. Germline loss and gain of function mutations in *FGF10, FGFR1,* and *FGFR2b* result in improper signaling during embryonic development and manifest as syndromes. In addition, SNPs in *FGF7* have been associated with COPD. These mutations and their effects on the respiratory system are summarized in Table 2.

Gain of function (g.o.f.) mutations in *FGFR1* (Pfeiffer 1, Osteo-glophonic dysplasia) and *FGFR2* (Apert, Crouzon, Pfeiffer 1,2, and 3, and Beare-Stevenson) occur more frequently than loss of function mutations and can result in the premature fusion of the skull or digits; craniosynostosis and syndactyly

respectively (Albuisson et al., 2005; Dutt et al., 2011; Ibrahimi et al., 2004; Katoh, 2008; Meyers et al., 1996; Seo et al., 2012; Snyder-Warwick et al., 2010; Vargas et al., 2003; Wilkie et al., 1995). This affects the individual's ability to see, hear, use their hands and feet, and occasionally has a detrimental effect on intelligence. Mice that carry a typical Apert point mutation *Fgfr2c*$^{+/S252W}$ (Wilkie et al., 1995), or a splicing mutation that causes *Fgfr2c* g.o.f (Hajihosseini et al., 2001), in addition to mice hemizygous for *Fgfr2c* (*Fgfr2c*$^{+/\Delta}$) (Hajihosseini et al., 2009) exhibit an Apert syndrome-like phenotype including cranial synostosis, digit syndactyly and a tracheal sleeve. Moreover, while humans with Apert Syndrome may exhibit absence of interlobular fissures, mice lack the entire medial and accessory lobes of the lung due to developmental patterning defects. In the Apert's mouse, it was found that the b isoform of *FGFR2*, which is normally expressed strictly in the epithelium, was ectopically expressed in the mesenchyme. During development, ectopic expression of *FGFR2b* in the mesenchyme, led to mesenchymal autocrine FGF10 signaling; including in the trachea progenitor cells, which resulted in a tracheal sleeve phenotype. Interestingly, the Apert's syndrome-like phenotype of the *Fgfr2c*$^{+/\Delta}$ mice was rescued when these mice were crossed with *Fgf10*$^{+/-}$ mice (De Langhe et al., 2006; Hajihosseini et al., 2009; Tiozzo et al., 2009).

In terms of airway abnormalities, g.o.f. mutations in both *FGFR1* and *FGFR2* can cause the premature fusion of the palatal shelves during development resulting in smaller naso-pharyngeal cavities or a deviated nasal septum. In addition, both tracheal and bronchial development is affected. Instead of cartilaginous rings, the trachea is sometimes incased in a continuous cartilaginous sleeve, and the bronchial tree is hypoplastic or angulated. A small or malformed, upper airway architecture can cause chronic upper airway obstruction; especially during sleep which causes apnea, cyanosis, right ventricular hypertrophy and a predisposition to pneumonia. In addition, a l.o.f. mutation in *FGFR1* can result in Kallmann syndrome, two of the manifestations of which are cleft palate and the inability to smell (anosmia) (Albuisson et al., 2005).

To date, only l.o.f. mutations for *FGF10* have been reported. These

mutations can result in non-syndromic cleft lip or palate, which can usually be fixed with surgery (Riley et al., 2007). Depending on the severity of the mutation, aplasia of lacrimal and salivary glands (ALSG), or the more severe form, lacrimal-auricular-dental-digital, (LADD) can also occur (Entesarian et al., 2007; Francannet et al., 1994). Some patients with LADD develop hypoplasia of the left lung vasculature and mild hypoplasia of the left pulmonary artery. Interestingly, *FGF10* haplo-insufficient patients showed a non-reversible airway obstruction when compared with both predicted reference values and siblings with normal *FGF10* alleles. Significantly reduced forced expiratory volume (FEV_1) (68% of predicted) and FEV_1/IVC (0.6; normally above 0.70–0.75) were consistent with obstructive lung disease. Although individuals had a normal total lung capacity (TLC), they had slightly reduced inspiratory vital capacity (IVC) (83% of predicted). The degree of chronic obstructive pulmonary disease (COPD) was classified as moderate or stage II COPD (FEV_1/IVC < lower limit of normal (LLN) and 60% ≤FEV_1 <69% of predicted). Thus far, these findings provide the most direct connection between FGF10 and human lung function (Klar et al., 2011). Interestingly, a recent study showed that SNPs correlating with both increased or decreased expression of *FGF7* was also associated with the development of COPD (Brehm et al., 2011; Xu et al., 2012).

In summary, loss of function mutations in *FGF10* and gain of function in *FGFR2b*, the quintessential ligand/receptor pair for lung development, leads to respiratory organ dysfunction and susceptibility to respiratory disease. In addition, an isoform switch from *FGFR2-IIIb* expression to *FGFR2-IIIc* in epithelial cells has been implicated in lung cancers (Dutt et al., 2011).

Table 2. *FGFR1/2* and *FGF7/10* mutations resulting in syndromes with respiratory phenotype or lung cancer

Gene/ location	Syndrome	Type of mutation	amino acids/genetic phenotype	Airway Phenotype	Citation
***FGFR1*/ 8p12**	Pfeiffer type 1	g.o.f.	P252R	upper airway obstruction ,tracheal sleeve, hypoplastic bronchial tree, deviated nasal septum	Moore 1995, Imbrami 2004, Hockstein 2004, Gupta 2011
	Kallmann	l.o.f.; autosomal dominant	C277Y, V607M, R622X, W666R >40	anosmia, cleft palate	Dodé 2003
	Osteo-glophonic dysplasia	g.o.f autosomal dominant	Y372C	hypophosphatemia, reduction in [calcitriol]-> poor inspiratory effort with atelectasis-> predisposed to pneumonia.	White 2005, Shankar 2010
	x	increased copy number in tumors	approx. 20% increase by FISH	non-squamous cell lung cancer	Dutt A 2011
***FGFR2*/ 10q26**	Apert	g.o.f.	P253R, C255G, S252W	tracheal sleeve; also angulated, short, stenotic trachea, obstructive sleep apnea, cyanosis, right ventricular hypertrophy	Cohen 1992, Imbrami 2004
	Crouzon	g.o.f autosomal dominant	Y105C, S252L, S267P, Y281C, Q289P,W290G, W290R, L292E, W301C…	upper airway obstruction, tracheal sleeve	1996 Meyers, 2011 Robin
	Pfeiffer types 1,2 and 3	g.o.f autosomal dominant for 1, de novo for 2, 3	S351C, W290C, C342R	upper airway obstruction, tracheal sleeve, hypoplastic bronchial tree, deviated nasal septum	Moore 1995, 2011 Robin
	Beare-Stevenson	g.o.f., de novo	S372C, Y375C	respiratory distress due to upper airway obstruction	Vargas 2003 Fonesca 2008
	x	FGFR2b to FGFR2c, gene amp. or missense	K660E,D283N, I380V, R612T	non-squamous cell lung cancer, lung squamous cell carcinoma, adenocarcinoma	Seo 2012, Katoh 2008
***FGF10* 5p13-p12**	Aplasia of lacrimal and salivary glands	l.o.f autosomal dominant	G138E, R80S	None	2007 Entesarian
	Lacrimal-auricular-dental-digital	l.o.f autosomal dominant	H207R, C106F	hypoplasia of the left lung vasculature, mild hypoplasia of the left pulmonary artery	1994 Franncannet, 2007 Entesarian
	non-syndromic cleft lip and palate	l.o.f autosomal dominant	S59F	none	2007 Riley
	x	haplo-insufficiency	loss of one *FGF10* allele from birth	chronic obstructive pulmonary disease like phenotype	Klar 2011
***FGF7* 15q15-q21.1**	x	increase/ decrease expression	SNPs	COPD	Brehm 2011; Xu 2012

1.4 Introduction to interstitial lung diseases

1.4.1 ILD Overview

Interstitial lung diseases (ILDs), or diffuse parenchymal lung diseases (DPLDs) are a heterogeneous group of non-neoplastic disorders that result in damage to the lung parenchyma (alveolar tissue including respiratory bronchioles), due to either fibrosis (scarring) or inflammation. ILDs can have both distinct and unknown causes, albeit with overlapping clinical pathologies and diverse histopathological signatures, leading to much confusion over the histological and clinical terminology. Prognoses for ILD patients range from excellent to fatal. ILDs with known etiologies are often treatable, while ILDs with unknown causes are not. Therefore it is critical to achieve the utmost diagnostic accuracy via a thorough, multi-step differential diagnosis process that spans multiple medical disciplines. Thankfully for ILD patients, the combined efforts of pulmonologists, radiologists, and pathologists of the American Thoracic Society (ATS) and the European Respiratory Society (ERS), have led to an international consensus for the accurate categorization of hundreds of ILDs (American Thoracic and European Respiratory Society, 2002)

Patients suffering from ILDs usually cough and exhibit dyspnea (shortness of breath) on exertion. While onset and progression are variable, tachypnea, reduced chest expansion, bibasilar end-inspiratory dry crackles, and finger clubbing (25 – 50%) are also common. ILD patients exhibiting these clinical symptoms will also exhibit a typical histopathological signature in the lung called an “interstitial pneumonia” (IP); “interstitial” refers to the “stromal cells” or fibroblasts supporting the alveolus, “pneumonia”, is the general term describing abnormalities caused either by fibrosis, inflammation or both. While clinical and histopathological signs of ILDs are very similar, prognoses vary from treatable to palliative.

1.4.2 Idiopathic pulmonary fibrosis (IPF)

The most important distinction among IPs is between idiopathic pulmonary fibrosis (IPF) (non-treatable) and the other IPs, which include nonspecific

interstitial pneumonia (NSIP), cryptogenic organizing pneumonia (COP), acute interstitial pneumonia (AIP), respiratory bronchiololitis-associated interstitial lung disease (RB-ILD), desquamative interstitial pneumonia (DIP), and lymphoid interstitial pneumonia (LIP) (American Thoracic and European Respiratory Society, 2002). IPF, sometimes called cryptogenic fibrosing alveolitis (CFA), is an ILD for which there is no known cause and no known treatment. The prevalence of IPF is estimated to be between 14 and 42.7 per 100,000; usually presents itself during or after the 5th decade of life and is more common in males (Gribbin et al., 2006; Olson et al., 2007). The incidence of IPF is 6.8 to 16.3 per 100,000, and this figure has been rising for the last 30 years. Diagnosis of IPF is a death sentence, with a median survival of 3-5 years after diagnosis and a 5-year survival rate of 10-15% (Lewis and Scullion, 2012). Many patients suffer a gradual decline in lung function until death. However, unpredictable, acute episodes of respiratory failure may also result in death. IPF is the most common and most lethal type of idiopathic interstitial pneumonia (IIP); accounting for approximately 55% of lung diseases classified as IIPs; thus its histologic pattern was named “UIP” or usual interstitial pneumonia.

Pulmonologists begin the differential diagnostic for IPF by taking a detailed patient history, physical examination, chest x-ray, and finally a spirometry test to FEV_1 and TLC. With this first batch of tests, it can be determined whether the patient has 1) a history of exposure to environmental toxins, drugs, chemicals, or tobacco use, family history of lung disease and symptom duration 2) whether the radiographs show one of the characteristics of IPs including both typical peripheral reticular opacity in peripheral, subpleural and basal areas, as well as ‘honeycombing’ which is defined by visualization of multiple lucent shadows from 2 to 10 mm in size on the radiograph, often indicating end-stage IPF, and finally 3) the lung function test; which can also help to determine the stage of disease progression. A pulse oximetry test to check blood oxygen levels, and a six-minute walk test to assess exercise capacity may also be performed if lung function is poor. Patients with unclear radiograph results then undergo a high-resolution computed tomography (HRCT) scan to see whether patchy, subpleural

UIP or honeycombing, together with traction bronchiectasis (irreversible dilation of the bronchial tree) are present. If the diagnosis is still unclear, and UIP cannot be detected, a bronchoscopy may be needed to visually assess the bronchioles, in addition to a bronchoalveolar lavage to examine the cells in the airway. The last resort is a surgical lung biopsy in which a surgeon goes through the ribs and collects a piece of lung for histological analyses. This so-called "transbronchial" biopsy is in fact usually necessary *unless* the patient presents with a clear clinical/radiological picture of IPF. Histologically, UIP presents with dense, patchy, collagenous scars that are often surrounded by fibroblastic foci of loose organizing connective tissue and cystic changes, often bordering intact lung tissue. Importantly, IPF patients should lack active sarcoidosis or Langerhans lesions, inflammation, granulomas, inorganic dust deposits, and eosinophilia.

1.4.2.1 Familial IPF – Molecular links to the pathogenesis of IPF

Between 1-5% of IPF patients have a first degree relative with IPF. However, the histopathology of the familial (F-IIP) and the non-familial forms of IPF (sporadic IPF) are characterized by 'usual interstitial pneumonia' (UIP) and are to date pathologically indistinguishable. One molecular link to the familial form of IPF has been found to be related to surfactant protein folding defects caused by a mutation in the gene *SFTPC*. Protein folding defects cause stress in the endoplasmic reticulum (ER) and result in an "unfolded protein response" (UPR) by AECII cells that may result in the inability of AECII cells to re-epithelialize a damaged area of the lung in both F-IIP and sporadic IPF patients (Korfei et al., 2008; Kropski et al., 2013).

Hermansky-Pudlak, is a rare, autosomal recessive syndrome characterized by skin and hair hypopigmentation, photophobia, platelet dysfunction and cellular storage disorders resulting in ceroid accumulation in the lung and kidneys. Mutations in *HPS* genes located on chromosome 10q2; which is interestingly, near *FGFR2*, results in lethal pulmonary fibrosis in Hermansky-Pudlak syndrome (HPS) type 1 in the fourth and fifth decades of life (Gahl et al., 2002).

1.4.2.2 Putative mechanisms of sporadic IPF

While it is clear that our delicate air filtration system protects us from the daily onslaught of foreign pathogens via innate and adaptive immune responses, what happens when the alveolar membrane itself is destroyed or damaged by cellular toxins or blunt injury? How does an alveolus repair itself after it is damaged? What causes the formation of a UIP lesion, and how long does it take for it to form? Does a defective repair mechanism; i.e., the formation and persistence of a fibrotic mass in response to foreign assaults, rather than the replenishing of AECI cells, spur the beginning of IPF? Is an IPF patient's "epithelial repair on-switch" or "scar resolution off-switch" simply defective? Is epithelial cell injury absolutely necessary for the formation of a UIP lesion? Do some individuals have more efficient epithelial repair mechanisms than others? Do all IPF patients have defective AEC2 cells? The questions of how and why IPF disease begins and how it progresses are still unanswered; hence it is still referred to as "idiopathic" pulmonary fibrosis. It is hypothesized, however, that IPF progresses slowly over many years, but that an IPF patient will not be referred to a pulmonologist until it is already "too late". Although no one knows for certain how IPF begins, the dominant paradigm asserts that the on-set of IPF begins when AECII cells turn defective.

In 1973, the first evidence for the clonal expansion and differentiation of AECII into AECI cells was observed in rats treated with nitric oxide (NO) indicating the importance of type two cells in lung homeostasis and barrier maintenance (Evans et al., 1973). Normally, the lung maintains the alveolar epithelial barrier by replacing damaged AECI cells that derive from AECIIs. AECII cell injury can occur as a result of both external and internal injury. For example, repeated environmental toxin exposure combined with an internal protein-folding defect and shorter than average telomeres all contribute to the incapability of the AECII cells to replenish the damaged area by "re-epithelializing" it with AECI cells. The lung, programmed to protect the gas exchange barrier at all costs, thus in theory responds to a defective epithelial barrier by sending a barrage of fibroblasts to clog the leak, thus marking the onset of UIP lesion.

Recently, it was shown that lineage-labeled AEC2s in 3-D culture gave rise to self-renewing “alveolospheres,” which contained both AEC2s and cells expressing multiple AEC1 markers. Interestingly, growth and differentiation of the so-called alveolospheres occurred most readily when co-cultured with primary PDGFRα+ lung stromal cells and lipofibroblasts (Barkauskas et al., 2013a); thus suggesting that mesenchymal-epithelial cross-talk is essential for repair. However the signals required for clonal expansion, and differentiation of AEC2s are yet to be defined.

The second part of the UIP paradigm focuses on the hyperfibrotic response of the lung to epithelial injury. It is currently hypothesized that in order to fix a leaky epithelial barrier, interstitial fibroblasts, which usually help to maintain the structure of the alveolus and traffic lipids for surfactant production, become “activated”. These “activated myofibroblasts” turn “bad”, and begin to secrete too much collagen and ECM. While the resulting UIP lesion is often described as “scar-like” the lesion is in fact anything but a scar. In normal wound healing processes, scars contain fibroblasts that secrete an *organized* collagen scaffold that allows for tissue repair. UIP lesions are rather disorganized clusters of chaotic fibroblasts secreting excessive amounts of collagen and matrix. Unlike scars, these collagenous foci are not re-absorbed but rather propagate and expand sporadically throughout the lung impeding lung function and rapidly deteriorating the patient’s quality of life. While some investigators hypothesize that the lesions appear wherever the barrier is broken; i.e., wherever AECII cells are dysfunctional, others suggest an intrinsic fibroblast disorder. In any case, it is still unknown why and how these lesions appear; thus our inability to re-capitulate IPF accurately in animal models is one of the reasons for the plethora of studies reporting “successful” animal studies amidst the failure of clinical trials.

1.4.2.3 Current treatments for IPF patients

The fact that IPF seems to appear out of nowhere, and is un-responsive to typical anti-fibrotics, anti-inflammatories, or anti-receptor tyrosine kinase antibodies, is frustrating not only for patients, but also for clinicians and scientists

alike (Loomis-King et al., 2013). It has been suggested that IPF patients undergo a long progressive pre-symptomatic phase characterized by chronic inflammation, which would be one explanation for the weakening and eventual irreversible damage of the epithelial barrier. However, given that the proposed chronic inflammation period is “asymptomatic” it is impossible to characterize the histopathologic phenotype of IPF during the early stages. What clinicians and scientists are presented with is rather a snapshot of an end-stage, lethal lung disease. The unresponsiveness of IPF patients to typical treatments may lie in the fact that the pathogenesis of IPF is, to date, under characterized. Therefore, it may be critical to first identify the cell types that are responsible for UIP formation. Next, once a common molecule or marker for the pathogenic cells is found, a strategy to reverse or stagnate IPFs progression by targeting these cells for apoptosis, could theoretically halt the disease. However, too much apoptosis may also result in collapse of the alveolus, which is also counter-productive when the goal is to try to improve or at least maintain lung function. Alternatively, targeting activated myofibroblasts for trans-differentiation, while protecting surviving epithelium may also spur *de novo* alveolar structure formation, as long the existing epithelial cells are not responsible for pathogenic progression (Marmai et al., 2011).

Pirfenidone initially appeared to slow the progression of pulmonary fibrosis in HPS patients with significant residual lung function. While a random coefficients model showed no significant difference, using data restricted to patients with an initial forced vital capacity (FVC) >50% of predicted, both statistical models showed the pirfenidone group losing FVC ($p<0.022$), FEV_1 ($p<0.0007$), TLC ($p<0.001$), and diffusion capacity for lung carbon dioxide, DL(CO) ($p<0.122$) at a rate that was approximately 8%/year slower than the placebo group (Gahl et al., 2002). However, a double blind study repeated in 2011 showed no significant difference between the groups (Gahl et al., 2002; O’Brien et al., 2011). The use of Pirfenidone continues to be debated since for the majority of individuals treated, the drug side-affects not only further reduced their quality of life but also had a very limited effect on the rate of disease

progression. The small percentage of patients that the drug claims to 'help' experience at the most, a 9% decrease in the rate of progression as measured by FVC, at the cost of many side effects (Jenkins, 2013; Raghu and Thickett, 2013).

1.5 Introduction to mouse models of ILDs

1.5.1 Discovery and clinical use of bleomycin

The bleomycin mouse model, the most commonly used and described mouse model of IPF, cannot be introduced without first describing the history of the discovery, and the subsequent use of bleomycin in the clinic. Bleomycin is a chelating molecule of high molecular weight; 1415 kDa, that causes DNA scission, and was first isolated from Streptomyces verticillus, (*S. verticillus*) by a Japanese researcher, Hamao Umezawa in 1963. After observing its deadly effect on squamous carcinoma cells, Dr. Umezawa published his discovery in 1966 (Umezawa et al., 1972). Based on these results and following toxicology studies reporting the ability of bleomycin to cleave DNA site-specifically (D'Andrea and Haseltine, 1978), researchers quickly developed clinical protocols for the treatment of squamous cell cancers. However, by 1970, it became clear that despite the absence of hematopoietic toxicity or immunosuppression, bleomycin had toxic effects on the skin, muscosa and lungs. Moreover, while some lesions were successfully annihilated, prognosis after treatment was unpredictable as response to treatment was heterogeneous (Mathé, 1970). Despite the unpredictability of the patient's response, the drug continues to be used today for the treatment of testicular cancer, lymphoma, and squamous cell cancers of the head, neck, cervix, penis and other sites. It is also used to treat cancer that has spread to the lungs, in order to prevent fluid from building up between the lungs and chest wall (American Cancer Society, 2010) and most recently off-label use has been reported for the removal of plantar warts by intralesional injection (McLaughlin and Shafritz, 2011) .

The heterogeneity in cancer treatment response to bleomycin treatment, both in terms of tumor regression and side effects, prompted mechanistic studies

of how bleomycin is metabolized by both tumors and the body. In one of the first studies published in 1968, mice were subcutaneously injected with ^{3}H-bleomycin and harvested one hour later. Interestingly, the lung and the skin contained the highest concentration of un-metabolized drug, while the liver, kidney, peritoneum other organs metabolized it more efficiently (Umezawa et al., 1968). The ability to metabolize bleomycin was also found to be weaker in older mice (28 weeks) compared to younger mice (3 or 5 weeks) with almost double the radioactivity in the lungs of older mice; a result which was in accordance with clinical observations (Ohkoshi and Oka, 1984).

The differential response by *organs* to bleomycin is related to the level of a bleomycin-inactivating enzyme; a hexameric ring barrel structure, called bleomycin hydrolase. The bleomycin hydrolase gene (*BLMH*) is conserved in bacteria, yeast, birds, reptiles, and mammals. In yeast, it is in fact the well-known '*Gal6*', a key regulator of galactose inducible genes. Umezawa was the first to discover and describe its action in mice and human tissues, and the first to isolate it from the liver; the organ with the highest concentration. He found that the enzyme inactivated bleomycin by hydrolyzing the carboxamide group of the β-amino-alanine moiety of bleomycin molecule (Umezawa et al., 1974). In the case of tumors, all those that were studied were reported to be able to metabolize bleomycin; although, bleomycin hydrolase activity did not always reflect the level of inactivation of bleomycin (Lazo et al., 1982). Later, genetic variations in the gene were discovered to play a role in the prognosis of cancer treatment with bleomycin and are described in the next section.

1.5.2 Bleomycin-induced pulmonary disease (humans)

Humans, rather than rodents, with bleomycin induced pulmonary disease, were perhaps the first inadvertent experimental models of IPF. The lung, the organ with the least amount of *BLMH* expression in both humans and mice (Lazo and Humphreys, 1983) is the most susceptible organ to the negative side effects of bleomycin cancer treatment; particularly, the development of lethal pulmonary fibrosis after protracted intravenous treatment. Overall, approximately 20% of

patients treated with bleomycin will develop clinical pulmonary disease and as many as 1% will die from pulmonary consequences of bleomycin therapy (Limper, 2004). Pre-existing renal disease is the best predictor for bleomycin lung toxicity. The half-life of the drug, which is normally metabolized within 2-5 hours can increase up to 30 hours in patients with renal disease (Alberts et al., 1978). Normally, between 50 to 70% of a dose of bleomycin is excreted by the kidneys, in its original form, within the first 24 h (McLeod et al., 1987). In patients with reduced glomerular filtration rate (creatinine clearance <35 mL/min), the drug half-life is increased leading to longer exposure in the lung and higher incidence of bleomycin induced lung disease. In addition to kidney disease, age, cumulative exposure to bleomycin, and pre-existing lung disease also significantly contributes to bleomycin induced lung disease.

Lethality of bleomycin pulmonary toxicity seems to depend on whether the patient survives an acute event, in which case they may improve substantially (Froudarakis et al., 2013). However, once significant fibrosis is present, it can progress insidiously, despite corticosteroid administration, and may be difficult to distinguish from IPF/UIP. More frequently, an acute onset of bleomycin hypersensitivity is described where the patient presents with fever, and peripheral blood or BAL eosinophilia. Discontinuation of bleomycin corticosteroid regimen usually reverses this hypersensitivity variant of bleomycin pneumonitis. Lastly, a rare, but clinically important, presentation of bleomycin pneumonitis can occur, the clinical presentation of nodular pulmonary lesions that mimic tumor metastasis. The nodular lesions of bleomycin pneumonitis often display the histologic pattern of bronchiolitis obliterans with organizing pneumonitis (BOOP). BOOP-like histologic patters have also been described in association with other chemotherapeutic agents, including cyclophosphamide, methotrexate, mitomycin, chlorambucil, and interferon, as well as nonchemotherapeutic agents, including amiodarone, gold, and nitrofurantoin (Cohen et al., 1989; Santrach et al., 1989).

1.5.3 Bleomycin-induced pulmonary disease in mice

Despite the fact that IPF remains an idiopathic disease; a disease without a known cause, researchers have searched for ways to recapitulate the histopathological phenotype of IPF (UIP lesions). While almost any substance that causes non-lethal DNA damage or cellular toxicity can be sprayed into the lung and result in fibrotic response, bleomycin remains the best characterized agent partly due to its translational potential; as it is frequently used as a chemotherapeutic agent in humans, and partly because of its relatively low cost. Rats and mice are the most frequently used subjects due to their amenability to laboratory experiments; though rat lung architecture is more similar to humans than that of the mouse. Although bleomycin treated rodents, incur fibrotic lesions, decreased lung function, and increased collagen deposition, the lesions themselves are nevertheless distinct from UIP lesions and may explain why drugs found to attenuate bleomycin-induced lung fibrosis have no effect on UIP. Interestingly, bleomycin lesions in rodent lungs do not resemble lesions incurred by humans receiving bleomycin as chemotherapy treatment (Borzone et al., 2001). Notably, they lack fibroblastic foci, hyperplastic epithelium, and temporal heterogeneity. Moreover, rodents are able to spontaneous recover if they do not die of acute lung injury (ALI), which is characterized by an influx of neutrophils during the first week. The lesions that Borzone et al. described at 21 – 28 days post injury (dpi) that resulted from intra-tracheal installation of bleomycin in rats: mural inflammation, fibrosis at the level of the bronchioles and emphysematous changes, resemble COPD much more than IPF. Recently, a study showed that bleomycin administration induces molecular changes in the lung that are directly relevant to “active” stages of IPF rather than a the end-stage of a slowly progressing disease. Using gene set enrichment analysis the authors showed that genes differentially expressed during the fibrotic phase of the single challenge bleomycin model were significantly enriched in the expression profiles of IPF patients (Peng et al., 2013). Moreover, genes involved in mitotic processes were expressed at higher levels in lung tissues from bleomycin-treated mice and IPF patients as well as fibroblasts isolated from IPF patients

with rapidly progressing disease. Thus, while bleomycin injury in rodents may not be progressive, it may be a decent model for patients with rapidly progressing IPF.

In a further attempt to recapitulate the IPF phenotype in mice, the transient expression of IL-1β or TGF-β was induced after bleomycin exposure in order to achieve the formation of fibroblastic foci and honeycombing features, (Kolb et al., 2001; Liu et al., 2001); however while inflammatory cell infiltrates are sometimes found in IPF lungs, whether inflammation plays an important role in IPF pathogenesis, especially at the end stage of the disease, is debated, especially given the resistance to corticosteroid and immunosuppressant therapies (Collard et al., 2004).

Additionally confounding for investigators is the fact that mice, like humans, show a differential response to bleomycin metabolism. Some strains are particularly sensitive, while others are resistant, thus indicating a genetic component. A genetic study comparing C3Hf/Kam (bleomycin immune) and C57BL/6J (bleomycin sensitive) mouse strains showed highly significant linkage to two loci: 1) a locus on chromosome 17 in the major histocompatibility complex (MHC), locus of determination, (LOD) = 17.4, named *Blmpf1*, which was found to be highly significant in both males and females, and accounts for approximately 20% of the phenotypic variance and 2) a locus on chromosome 11, LOD = 5.6, named *Blmpf2*, which was found to be significant in males only (Haston et al., 2002). Further complicating the model, in MHC congenic mice of different, inbred strain backgrounds and strain-specific genetic factors in addition to the MHC genotype influence susceptibility to bleomycin lung injury. Therefore, most researchers use young female mice from an inbred background strain with wild type littermate controls for their experiments.

Bleomycin lung injury phenotype and outcome is also dependent on the method of administration. It can be administered via single or multiple intra-tracheal installations with a micro-sprayer, sub-cutaneous implantation of a mini-pump, which uses osmotic diffusion of the product for up to 10 days, intravenously, or trans-tracheally. Direct tracheal installation results in the acute

destruction of the respiratory airway epithelium and often results in ALI, which is characterized by an influx of neutrophils. The time frame for the end of ALI; characterized by a reduction of neutrophils, and the beginning of scar formation, is dependent not only on the delivery method, but also the dosage, age, sex and genetic background of the mouse. In general, inflammation peaks between 1 and 10 dpi and begins to wane between 10 and 21 dpi. A larger dose is needed when delivering bleomycin systemically via either intra-venous or osmotic mini-pump in order to achieve a fibrotic reaction in the lung.

Table 3. Delivery methods of bleomycin

Method	Dose	Cost	Main disadvantages
intra-tracheal (i.t.)	0.8 – 5.0U/kg	low	death due to ALI with high dose, insufficient injury if too low
multiple i.t.	0.2 – 1.0U/kg per dose	medium	labor intensive, risk of ALI death, surgical stress
trans-tracheal	0.2 – 1.0U/kg	low	surgery, death due to ALI
intra-venous	50-300U/mouse	low	model for chemotherapy induced lung fibrosis but less relevant for IPF
osmotic mini pump	50-300U/mouse	high	labor intensive, diffuse lesions, expensive pumps

After bleomycin administration, the next step is to worsen, reduce, or eradicate either the inflammatory or fibrotic response by administering a treatment to the experimental group. Thus studies that aim to find a difference between groups intrinsically require a homogenous response by the animals to the injury. Therefore littermate, age, and sex-matched controls are absolutely crucial, as is using the same batch of bleomycin since drug activity can vary. Outcome of the experimental group is measured not only by survival and overall health condition, but also by lung function as well as assessment of collagen deposition, quantification of the extent of fibrosis (Ashcroft score), and gene expression profiling.

1.5.4 Effects of FGFs on bleomycin-induced pulmonary disease in mice

Although the pathomechanism of IPF is not yet fully understood, chronic injury, especially injury leading to chronic endoplasmic reticulum (ER) stress in AECII cells, followed by extensive apoptosis, is generally accepted as a key

pathological event (Korfei et al., 2008). Hence protecting AECIIs against apoptosis, is considered to be a potential therapeutic approach. FGF7 (Deterding et al., 1997; Li et al., 2010; Sakamoto et al., 2011; Yi et al., 1996) and FGF10 (Gupte et al., 2009), as well as hepatocyte growth factor (HGF) (Gazdhar et al., 2013) were all found to diminish the extent of epithelial injury and apoptosis and to attenuate lung fibrosis in the bleomycin model of lung fibrosis. Moreover, *Fgf10* overexpression (Gupte et al., 2009), unlike recombinant FGF7 treatment (Sugahara et al., 1998) was found to result in an accelerated resolution of lung fibrosis in the bleomycin model. The mechanism by which FGF10 accelerated recovery may have been due to inhibition of TGFβ and the recruitment of T-regulatory cells. Furthermore endogenous *Fgf10* produced by the peribronchial smooth muscle cells appeared to be critical for amplification of bronchial epithelial progenitors in response to naphthalene injury in mice (Volckaert et al., 2011) suggesting that FGF10 acts to preserve or amplify lung progenitor cells. In addition to mouse models, few experiments have been performed with IPF cells and FGFs. However, in an experiment performed with IPF fibroblasts, FGF7 expression upon IL-1β stimulation was found to be decreased in donor vs. IPF fibroblasts (Marchand-Adam et al., 2005). Finally, one study showed that humans genetically deficient in *Fgf10* exhibited decreased lung function (Klar et al., 2011). Thus while clear links have been demonstrated between FGFs and lung repair, the exact mechanism of action must be elucidated.

Part 2. Aims of this Study

Previous studies in mouse injury models have clearly shown that exogenous FGF7 can protect the lung from injury and that FGF10 can trigger a repair response by acting directly on lung progenitor cells. Given these results and the importance of FGF signaling in lung development, this study aimed to find out whether expression of *FGF10, FGF7, FGFR1b* and *FGFR2b* in the lungs of humans with end-stage IPF was dysregulated. In addition, this project aimed to demonstrate whether endogenous FGF7 and 10 signaling in mice plays a role in the repair process of bleomycin-induced fibrotic lesions.

In summary, the aims were as followed:

1) **To identify whether FGF signaling was dysregulated in IPF patients using RNA and protein isolated from donor and IPF lung homogenates.**

2) **To test whether repair after bleomycin-induced lung fibrosis was defective in mice genetically deficient in *Fgf7, Fgfr2b, Fgf10,* and/or all FGFR2b ligand signaling.**

3) **Identify the mechanism of action of FGF10 on primary cultures of IPF and donor lung fibroblasts.**

Part 3 Materials and Methods

3.1 Procurement of human lung tissue specimens used for microarray or primary culture of human lung fibroblasts

Lung tissues were collected from patients undergoing lung transplants for interstitial lung disease at the Universities of Giessen, Germany or Vienna, Austria. Non-transplanted donor lung tissue showing no evidence of interstitial lung disease served as healthy controls. The institutional ethics committee approved the protocol and tissue usage, and informed consent was obtained before lung transplantation. Explanted lungs were directly rinsed until free from blood and preserved in ice-cold preservation buffer. Next, tissue samples were immediately frozen for later mRNA extraction.

3.2 Laser-assisted microdissection of human lung tissue

Laser assisted microdissection of donor and IPF lung tissue was performed as described previously (Kwapiszewska et al., 2005). Cryosections from lung tissue were mounted on glass slides; to limit storage time, only 10 slides were performed at time. After short hematoxylin staining, septa were micro-dissected under optical control using the Laser Microbeam System (P.A.L.M., Bernried, Germany). Next, cells were isolated using a sterile, 30-gauge needle. Needles and adherent cells were transferred into a reaction tube containing 200ul of RNA lysis buffer. Total cellular RNA was isolated with the RNeasy kit (Qiagen, Valencia, CA) and purified according to the kit's protocol.

3.2.1 RNA extraction for microarray

RNA was isolated using the RNeasy kit (QIAgen, Hilden, Germany) following the kit instructions. Reverse Transcription, pre-amplification, and fluorescent labeling. Total RNA was reverse-transcribed, pre-amplified, and labeled using the BD Atlas SMART Fluorescent Probe Amplification Kit (Clontech Laboratories, Heidelberg, Germany). RNA from laser-microdissected material was used quantitatively. According to pilot experiments and based on quantitative real-time PCR measurements of reference genes, the estimated

amount was 5-50 ng total RNA. From homogenates, aliquots containing 50 ng total RNA were reverse transcribed. cDNA was amplified with 22 SMART PCR cycles. The dsDNA products were labeled by four additional PCR cycles in the presence of aminoallylated UTP, then coupled with mono-functional reactive Cy3- and Cy5-dyes (Amersham, Freiburg, Germany). The labeled dsDNA was purified with the QIAquick PCR Purification Kit (Qiagen). Absorbance spectra were measured with the ND-1000 (Nanodrop, Montchanin, DE). The concentrations of the nucleic acids (RNA, dsDNA) were estimated from the absorbance at 260 nm; absorbance values at 550 nm and 650 nm were used to calculate the amount of incorporated Cy3 and Cy5, respectively.

3.2.2 Microarray hybridization and scanning

Labeled dsDNA containing 40 pmol incorporated Cy-dyes of each sample were subjected to hybridization. IPF and donor samples were competitively hybridized on Agilent whole human genome arrays (Gene Expression Omnibus: G4112A) spotted with 44k 60-mer oligonucleotides according to Agilent's protocol (Version 4.1; Agilent, Santa Clara, CA). The hybridization was performed for 18 hrs at 60°C while continuously rotating the Agilent hybridization chambers in a standard *in situ* hybridization oven. After hybridization, slides were washed according to the Agilent protocol.

3.2.3 Microarray data analysis

Slides were scanned with the Axon 4100A (Molecular Devices, Munich, Germany). Photomultiplier tube (PMT) gains were adjusted to use the entire dynamic range of the scanner, yielding similar intensity histograms for both channels (Cy3 and Cy5). Image analysis was done with GenePix 5.0 (Molecular Devices), further data processing was performed using R (R Development Core Team, 2009) and the limma package (Smyth, 2004). Spots were weighted with factors between 0 (worst) and 1 (best) according to percentage of pixels with an intensity higher than the mean local background + 2 SD, homogeneity (coefficient of variation of the pixel intensities), and saturation (% pixels in saturation) for both

channels. M and A values were calculated using the mean intensities. The M-versus-A values were normalized by a weighted LOESS correction.

Candidate selection was based on a moderated t-statistic controlling the false discovery rate (Hochberg and Benjamini, 1990). Genes were ranked for differential expression by a moderated Welsh-t-statistic. The selected 773 candidates were subjected to a pathway analysis using PathwayExpress (Khatri et al., 2007). Pathways were ranked by the PathwayExpress impact factor. Pathways with impact factors greater than 1 and with more than three regulated genes were considered relevant.

3.3 Bleomycin-induced lung injury on mice

3.3.1 Generation of mice

CMV-Cre mice (Sauer, 1998) were crossed with *rtTA*^{flox} mice (Gossen and Bujard, 1992) to generate mice expressing *rtTA* under the ubiquitous *Rosa26* promoter. This constitutive *Rosa26*$^{rtTA/+}$ mouse line was then crossed with the *tet(O)solFgfr2b* responder line to generate *Rosa26*$^{rtTA/+}$*;tet(O)sFgfr2b/+* heterozygous animals, allowing ubiquitous expression of soluble decoy FGFR2b receptor (Parsa et al., 2010). All mice were generated on a CD1 mixed background. Attenuation of FGFR2b ligands activity was achieved by administration of doxycycline-containing food; normal rodent diet with 0.0625% doxycycline (Harlan Teklad). Mice were genotyped as described previously (Belteki et al., 2005; Hokuto et al., 2003; Schwenk et al., 1995). To generate *Fgfr2b*$^{+/-}$ or *Fgf10*$^{+/-}$ mice*, CMV-Cre* mice (Schwenk et al., 1995) on a C57BL/6J background were crossed with either *Fgfr2b*$^{flox/flox}$ (De Moerlooze et al., 2000) or *Fgf10*$^{flox/flox}$ (Abler et al., 2009; Urness et al., 2010) mice (also C57BL/6). *Fgfr2b*$^{+/-}$ and *Fgf10*$^{+/-}$ mice were crossed with C57BL/6 wild type mice to generate *Fgfr2b*$^{+/-}$ (or *Fgf10*$^{+/-}$) experimental and corresponding *Fgfr2b*$^{+/+}$ (or *Fgf10*$^{+/+}$) littermate controls. *Fgf7*$^{-/-}$ animals were obtained from Jackson Laboratory (Stock number: 004161), and backcrossed for several generations on a C57BL6 background. Corresponding genetically matched C57BL/6 mice were used as controls.

3.3.2 Establishing the dosage of bleomycin

Each genetic background of mouse used required a dosage finding experiment in order to determine the dose of bleomycin needed to cause robust fibrosis with minimal death (<10-30%) due to acute lung injury.

3.3.3 Delivery of bleomycin

Mice were anesthetized with a non-lethal dosage (i.p.) of a ketamine/dormitor solution (Table 4). When they no longer responded to a light forceps pinch between the toes, Bepanthene was placed over the eyes to prevent dryness, and they were gently placed on a stand at a 45° angle, to hang from their incisors on a rubber band. A light was positioned over the mouth and trans-tracheally for visualization of the larynx. A blunt forceps was used to pull the tongue gently to one side and open the mouth. Once the larynx was located, the trachea was intubated with a 20 G plastic catheter. Next the microsprayer (PennCentury) was filled with 200 ul bleomycin or saline solution, positioned inside the catheter, and sprayed. Mice resumed spontaneous breathing shortly after being sprayed and were placed in a cage positioned partially over a 37°C heating pad. Mice were kept under observation until consciousness and stable physical condition were regained. Mice who did not recover due to mechanical injury were euthanized with an overdose of ketamine/dormitor (see Table 4).

Table 4. Anesthesia dosages for bleomycin treatment and end point lung function measurement

anesthesia dose (i.p.) for bleomycin treatment (i.t.)	0.6ul/g Ketamine 10% (100mg/mL)	0.3ul/g Dormitor 10% (0.5mg/mL)
lethal anesthesia dose (i.p.) for end point lung function test	1.2ul/g Ketamine 10% (100mg/mL)	0.6ul/g Dormitor 10% (0.5mg/mL)

3.3.4 Monitoring of the physiological response post-injury

After injury, mice were monitored daily for physiological signs of suffering (Table 5). Reduced activity, grooming, and weight, as well as briefly abnormal respiration were common between 1 and 4 dpi followed by a steady recovery.

Mice suffering from acute lung injury, marked by prolonged periods of abnormal respiration and weight reduction were euthanized between 5 and 10 dpi. However, mice that recovered to 10 dpi, usually survived until 28 dpi. Occasionally some mice with normal breathing would be removed from the study before 14 dpi due to a reduction of more than 20% of the initial weight. All mice were anaesthetized (i.p.) with a ketamine/dormitor solution appropriate for either deep sleep or death as needed (Table 4).

Table 5. Daily physiological response chart

Daily physiological response chart total score < (6) or weight loss <20%; animal euthanized				
Spontaneous Activity	**Grooming**	**Weight Reduction**	**Physiological Temperature**	**Respiration**
normal (0)	normal (0)	<5% (0)	0.5 ºC (0)	normal (0)
reduced (1)	reduced grooming (1)	5-10%(1)	<1 ºC (2)	briefly abnormal (1)
isolates (2)	very reduced grooming (2)	10-20%(2)	1-2 ºC (2)	extended abnormal (2)
apathetic (3)	matted fur (3)	>20%(3)	>2 ºC (3)	permanently abnormal (3)

3.3.5 Mouse experiments were performed according to approved protocols

Table 6. Mouse experiment protocols

Fig.	Experiment	Site	Protocol
Fig 6	5U/kg bleo i.t. wild type	CHLA*	193-12
Fig 9	DOX admin. (validation *Rosa26$^{rtTA+/}$;tet(O)solFgfr2b/+*)	CHLA	193-12
Fig 10	3.5U/kg bleo i.t. and DOX from 7 dpi	CHLA	193-12
Fig 11a	1.0U/kg bleo i.t. and d7 – 28 DOX *Rosa26$^{rtTA+/}$;tet(O)solFgfr2b/+*	CHLA/JLU**	73/2012
Fig 11b	2.0U/kg bleo i.t. and d14 – 28 DOX *Rosa26$^{rtTA+/}$;tet(O)solFgfr2b/+*	CHLA	193-12
Fig 12	3.5U/kg bleo i.t. *Fgfr2b$^{+/-}$*	CHLA	193-12
Fig 13	3.5U/kg bleo i.t. *Fgf7$^{-/-}$*	JLU	72/2012
Fig 14	3.5U/kg bleo i.t. *Fgf7$^{-/-}$*	JLU	72/2012
Fig 15	3.5U/kg bleo i.t. *Fgf10$^{+/-}$*	CHLA	193-12

*CHLA; Children's Hospital Los Angeles; **JLU; Justus Liebig Universität, Giessen

3.4 Acquisition of lung function measurements (forced oscillation plethysmography)

Post bleomycin injury analyses were begun with end point lung function measurements after the mice were appropriately anaesthetized (Table 7). Lung function was analyzed using the SCIREQ flexiVent forced oscillation

plethysmograph (emka technologies) to give an overall readout of lung function. The SCIREQ flexiVent used a computer-controlled ventilator combined with data acquisition and analysis software for the measurement of respiratory mechanics of animals. Deeply anaesthetized mice were intubated transtracheally and ventilated at a rate of 150 breaths per minute with a positive end-expiratory pressure (PEEP) between 1 and 3 cm H_2O. PEEP was calculated automatically by the software and dependent on the weight of the animal. After stable ventilation was achieved; the mouse was no longer spontaneously breathing, but the heart continued to beat, a 3 second, weight dependent, fixed volume wave form was initiated every 15 – 20 seconds 8 times. During this perturbation, "Snapshopts" of the following respiratory function parameters were taken: total respiratory compliance, or change in volume over change in pressure (ΔV mL /ΔP cmH_2O); elastance, the reciprocal of compliance which measures the lungs ability to recoil to it's original shape (ΔV mL / - ΔP cmH_2O), and resistance, or the impedance to ventilation (ΔP cmH_2O/s/ΔV mL). Sufficiently damaged bleomycin treated lungs showed a decrease in compliance along with an increase in both elastance and resistance. In the case of acute lung injury, as often was the case for measurements performed 7 or 14 dpi, airway resistance was positively increased as compared to airway compliance due to the presence of inflammatory cells in the airspaces.

Table 7. Lung function read-out Summary

Lung Function Read-Out Summary			
Injury Level	**Compliance**	**Elastance**	**Resistance**
Normal	.035 - .009	30 - 70	0.3 – 1.2
Mild	.008 - .005	80 - 150	1.3 - 2.5
Moderate	.005 - .002	160 - 300	2.6 - 4.0
Severe	< .002	< 300	< 4.0

3.4.1 Statistical analyses of SCIREQ data

Lung function measurements were taken every 15 – 20 seconds, a total of 8 times for each mouse. The average of these measurements were taken, and used as one value to represent one biological sample. To compare groups, at

least 3 mice were taken from each experimental group and an unpaired, two-tailed Student's T-test was performed in order to test whether the group means were significantly different.

3.5 Histological preparation and analyses of the left lung

The bleomycin model of IPF can vary in terms of the extent of fibrosis incurred by each of the five lobes. Therefore it is necessary to take many approaches; both physiological and molecularly, in order to obtain a comprehensive read-out of the extent of injury and to accurately and thoroughly compare experimental groups (Thannickal et al., 2004). Immediately after lung function measurements were taken, the thorax was opened, and the right bronchus was clamped to avoid contamination with paraformaldehyde (PFA). Next, transcardiac perfusion of the left lobe was performed with 15 mL phosho-buffered saline (PBS) in order to wash away the blood and prepare the left lobe for histological analysis. The left lobe was then perfused from 22 cm – 24 cm above the mouse for 1-2 min with PBS followed by 2 min with 4% PFA. The trachea was tied off with a string, and the lung was removed and placed in 4% PFA for at least 24 hrs at RT or up to one week at 4°C. Immediately afterwards, the cranial and accessory lobes were removed and placed in TRIZOL for RNA extraction. The medial and caudal lobes were washed with PBS and processed for the collagen deposition assay. These preparatory methods along with further experiments are described in detail in the sections below. Left lobes were then embedded with a Leica embedding machine and paraffin blocks were kept cold until 3 – 5 um sections were cut. These sections were used for Masson's trichrome stain, Hematoxylin and Eosin (H/E), immunofluorescence, or TUNEL stainings.

3.5.1 Masson's trichrome stain

In order to stain for collagen fibers, sections from the left lobe were deparaffinized in xylene (3 x 10 min) followed by decreasing concentrations of ethanol gradients (1 x 5 min) and re-fixed in Bouin's solution for 1 hr at 56°C. Tap

water was run for 10 min, followed by staining in Weigert's iron hematoxylin working solution for 10 min. Weigert's Hematoxylin Solution was made fresh by adding equal volumes of Solution A (1% Hematoxylin in 95% EtOH) and Solution B (1.2% Ferric Chloride Sigma F7134 and 1% Acetic Acid in distilled water) and stained the nuclei blue-black. Next, slides were run under running tap water for 5 min and rinsed in ddH_2O. Slides were then incubated for 10-20 min in Biebrich Scarlet-Acid Fuchsin Solution, which stains the cytoplasm and keratin red, and washed twice in ddH_2O. Next, the stain was differentiated in phosphomolybdic-phosphotungstic acid solution for 10-15 min or until collagen was not red. Then, sections were transferred directly to aniline blue solution, which stains the collagen fibers green-blue, and stained for 5-10 min. Afterwards, they were rinsed briefly in distilled water and differentiated in 1% acetic acid solution for 2-5 mins. Lastly, slides were rinsed briefly in distilled water and dehydrated very quickly through 95% EtOH, 100% EtOH, cleared in xylene, and mounted with clear Permamount mounting media.

3.5.2 Hematoxylin and eosin stain

3 – 5 um sections of the left lobe were deparaffinized, dipped in water and stained for Mayer's Hematoxylin solution for 1 – 3 min and washed under running tap water for up to 10min. Slides were monitored under the microscope for over and under staining. Slides were then incubated for 2 min in Eosin dye and brought back through increasing gradients of EtOH, xylene and cover slipped with Pertex mounting media.

3.5.2.1 Ashcroft score and % confluent fibrosis

Ashcroft scoring was performed blinded using a modified Ashcroft scoring protocol as described by (Hübner et al., 2008) on H and E stained sections of the left lobe. While Hübner et. al., scored multiple 20X images, we imaged with light-microscopy at the furthest objective (1.25X), which allowed for visualization of one entire section of the left lung. ImageJ was used to measure the area of the lung that was covered in confluent fibrosis; percent confluent fibrotic area per

total section area was calculated. When no confluent fibrotic areas were detected, Ashcroft score was used to assess extent of alveolar wall thickening.

3.5.2.1.1 Statistical analyses of % confluent fibrosis

Sections were measured a total of 3 times, blindly and scores were averaged. Normally the measurement system was robust such that the sample always received the same score; with the exception of lower scores, where a higher magnification was used to identify the extent of alveolar wall thickening. A Student's T-Test was used with a Mann-Whitney correction to assess whether there was a difference between two experimental groups.

3.5.3 TUNEL assay for apoptosis

The DeadEnd™ Fluorometric TUNEL System (Promega G3250) measures the fragmented DNA of apoptotic (or necrotic) cells by catalytically incorporating fluorescein-12-dUTP at 3´-OH DNA ends using the Terminal Deoxynucleotidyl Transferase, Recombinant, enzyme (rTdT), which forms a polymeric tail using the principle of the TUNEL (TdT-mediated dUTP Nick-End Labeling) assay. Briefly, slides with 3 – 5 um sections were deparaffinized, dipped in .85% saline solution, pre-fixed with 4% PFA for 15 min, washed in PBS, then incubated for 13 min in 20 ug/mL Proteinase K for antigen retrieval. The slides were then washed in PBS, and post-fixed for 5 min in 4% PFA. Sections were equilibrated in equilibration buffer for 10 min before adding the smallest volume of reaction mixture possible, and incubating for 1 hr at 37°C. The reaction was quenched for 15 min in 2X SSC buffer and washed in the dark 3 times with PBS. Sections were then counterstained with DAPI and the fluorescein-12-dUTP-labeled DNA was then visualized directly by fluorescence microscopy.

3.5.4 Immunofluorescence

For the washing steps, if the antigen of interest was nuclear, phosho-buffered saline with 0.1% Triton-X 100 (PBX) was used, if it was located on the

cell surface, phosho-buffered saline with 0.1% Tween-20 (PBT) was used. Slides were deparaffinized, and then blocked 3% bovine serum albumin (3% BSA) in PBS for 1 hr at RT. The primary antibody was diluted 1:50 – 1:200 in incubation buffer (1% BSA in PBS) and incubated for 1 – 2 hrs at RT or overnight at 4°C. Next, slides were washed with PBT or PBX 3 x 5 min. The secondary antibody was diluted in blocking buffer (1:450 – 1:1000) and incubated for 1 – 3 hrs at RT in the dark. Slides were washed again with either PBT or PBX 3 x 5 min and cover slipped with 10 ul of mounting media mounting media (VECTASHIELD) with or without 4',6-diamidino-2-phenylindole, (DAPI).

3.5.4.1. Quantification of TUNEL and/or immunofluorescent staining

In order to quantify immunofluorescent staining from sections or cell cultures, at least 6 fields of view from each biological sample or treatment group was taken. Experiments were repeated in triplicates or at least 3 biological samples were used. Either LAS software or ImageJ was used to count the total number of cells (DAPI). The section was then divided into a grid and counted, blindly, to determine the number of stained cells. Percentage of positive cells were calculated accordingly and compared.

3.5.4.1.1 Statistical analyses of immunostaining

Unpaired, two-tailed Student's T-test was performed in order to test whether the group means were significantly different.

3.6 Collection of RNA for qPCR

After lung function was performed, and the left lobe was removed for histology, the accessory and cranial lobes were removed and placed directly in 2 mL TRIZOL in a GentleMacs (Milteny Biotec) homogenizer. Tissue was homogenized for 1 min under the "RNA" setting and tubes were spun down at RT 1200 rpm for 5 min. Supernatant was collected immediately in cryovials, frozen in liquid nitrogen and stored at -80°C until RNA extraction could be performed.

Samples were brought up from -80°C and thawed on the bench for 5 min at

RT. Heavy phase-lock gel tubes (5 PRIME 2302830) eppendorfs were centrifuged for 5 min at maximum speed. The homogenized lysate was added to the separator column and incubated at RT for 3 min. 1/10 total volume of chloroform was added. Tubes were shaken for 15 s and incubated for 3 min at RT. Next, tubes were centrifuged for 15 min at 10,000 g at 4°C. The aqueous layer was extracted and added to a new eppendorf. 1.5 volumes 100% isopropanol was added. Tubes were inverted to mix and incubated for 10 min at RT. After incubation, tubes were spun down for 15 min at 10,000 g, 4°C. After the pellet was identified, the supernatant was discarded and the pellet was washed with 75% EtOH and vortexed. Lastly, tubes were centrifuged for 5 min at 8,000 g, 4°C; supernatant was discarded, and the pellet was dried on the bench until it became transparent. 30 ul of ddH_2O was added and samples were Nanodropped for RNA concentration and purity. Samples were stored at -80°C until reverse transcription was performed.

3.6.1 cDNA synthesis and quantitative PCR

cDNA was either reverse transcribed directly after RNA isolation or RNA was brought up from -80°C and thawed on ice. 2 ug of RNA was used and reverse transcription was performed in PCR tubes using Qiagen QuantiTect Reverse Transcription Kit (205313). cDNA was nanodropped and diluted to a concentration between 40 and 100 ng/ul.

Primers were designed using Roche Applied Sciences Assay Design Process. All primers were designed to span introns and blasted for specificity. Sybr Green Master Mix was used for RT-PCR with a Roche LightCycler 480 machine.

3.6.2 Mouse primers

See table 8.

Table 8. Mouse primer table

Gene	Forward Primer	Reverse Primer
Adrp	cctcagctctcctgttaggc	cactactgctgctgccattt
Cc10	gatcgccatcacaatcactg	cagatgtccgaagaagctga
C/ebpa	aaacaacgcaacgtggaga	gcggtcattgtcactggtc
col2a	agtaccggagctcgaggag	gatcacccttggcaccag
Ecad	gttgcagaaggcgctgtt	gtgttgacgtcatcgtctgc
Etv4	cagacttcgcctacgactca	gccataacccatcactccat
Etv5	gcagtttgtcccagattttca	gcagctcccgtttgatctt
Fgf1	ccgaagggcttttatacgg	tcttggaggtgtaagtgttataatgg
Fgf10	atgactgttgacatcagactcctt	cactgttcagccttttgagga
Fgf3	gattactgcggtggaagtgg	ccgttccacaaactcacactc
Fgf7	actatctgcttataaaatggctgct	gtggggcttgatcatctgac
Fgf9	tgcaggactggatttcatttag	ccaggcccactgctatactg
Fgfr1	tctggcctctacgcttgc	aggatgggagtgcatctga
Fgfr1b	ccacaggtctggtgacagtga	cgggaagtaatagctcggatg
Fgfr1c	tctggcctctacgcttgc	cttccgaggatgggagtg
Fgfr2_3_b	ccctacctcaaggtcctgaa	catccatctccgtcacattg
Fgfr2_3_c	tgcatggttgacagttctgc	tgcaggcgattaagaagacc
Fgfr2b	cctacctcaaggtcctgaagc	catccatctccgtcacattg
Fibronectin	cctctgcagacctacccaga	taaggtggccaggaatggta
HPRT	gctgacctggattac	ttggggctgtactgctta
IL-1 beta	tgtaatgaaagacggcacacc	tcttctttgggtattgcttgg
Lipase	gcgctggaggagtgttttt	ccgctctccagttgaacc
Perillipin	ggatggagacctccctgag	ctcacaggtcccgctcac
PPAR gamma	gaaagacaacggacaaatcacc	gggggtgatatgtttgaacttg
Pten	aggcacaagaggccctagat	ctgactgggaattgtgactcc
Rac1	catcagttacacgaccaatgc	cattggcagaatagttgtcaaaga
Sma	actctcttccagccatctttca	ataggtggtttcgtggatgc
SPC	ggtcctgatggagagtccac	gatgagaaggcgtttgaggt
Spry2	gagaggggttggtgcaaag	ctccatcaggtcttggcagt
Spry4	gtggagcgatgcttgtgac	caccaagggacaggcttcta
T1-alpha	cagtgttgttctgggttttgg	tggggtcacaatatcatcttca
Tbx4	ctgcatgagaaggagctgtg	gaatccgggtggacatacag
Tbx5	cgaagtgggcacagagatg	caccttcactttgtaactagggaaaca
Tgf-ß1	tggagcaacatgtggaactc	cagcagccggttaccaag
Ttf1	catgccttcagactgcacat	tctttgcacggtagtacacga
Twist1	agctacgccttctccgtct	tccttctctggaaacaatgaca

Table 8. Primer table for human whole lung homogenates or primary cultures of human lung fibroblasts.

GENE	Forward Primer	Reverse Primer
ACTA2	CTGTTCCAGCCATCCTTCAT	TCATGATGCTGTTGTAGGTGGT
ADRP	TCAGCTCCATTCTACTGTTCA CC	CCTGAATTTTCTGATTGGCACT
CC10	CTCACCCTGGTCACACTGG	CTGAAAGCTCGGGCAGAT
CEBPA	GGAGCTGAGATCCCGACA	TTCTAAGGACAGGCGTGGAG
COL1A1	ATGTTCAGCTTTGTGGACCTC	CTGTACGCAGGTGATTGGTG
ECAD	TTG ACG CCG AGAGCTACAC	GTCGACCGGTGCAATCTT
EP2	CCACCTCATTCTCCTGGC TA	AGGTCCCATTTTTCCTTTCG
ETV4	GCAGTTTGTTCCTGATTTCCA	ACTCTGGGGCTCCTTCTTG
ETV5	CATCCTACATGAGAGGGGGTTA	AAGTATAATCGGGGATCTTTTTCA
FGF1	CAATGTTTGGGCTAAGACCTG	GGCTGTGAAGGTGGTGATTT
FGF10	GAAGGAGAACTGCCCGTACA	GGCAACAACTCCGATTTCTACT
FGF3	TGGAGAACAGCGCCTACAGT	GGAGAAGAGACCCCTGATGG
FGF7	AAGGGACCCAAGAGATGAAGA	CCTTTGATTGCCACAATTCC
FGFR1	GGAGTATCTGGCCTCCAAGA	TCACATTGTCCTCTGTCACCA
FGFR1b	GCATTCGGGGATTAATAGCTC	CCACAGGTCTGGTGACAGTG
FGFR1c	ACCACCGACAAAGAGATGGA	GCAGAGTGATGGGAGAGTCC
FGFR2b	GATAAATAGTTCCAATGCAGAAGTGCT	TGCCCTATATAATTGGAGACCTTACA
FN	GCGAGAGTGCCCCTACTACA	GTTGGTGAATCGCAGGTCA
IL1-B	TACCTGTCCTGCGTGTTGAA	TCTTTGGGTAATTTTTGGGATAA
LPN1	GATGAGAAATTCTGGGCCTTT	GATGAGAAATTCTGGGCCTTT
PDPN/(T1-a)	AAATGTCGGGAAGGTACTCG	AGGGCACAGAGTCAGAAACG
PGBD	TGTCTGGTAACGGCAATGCG	CCCACGCGAATCACTCTCAT
PLIN1	ACATTAAAGGGAAGAAGTTGAAC	TTCTCCTGCTCAGGGAGGT
PPARG	CCTAAACTTCGGATCCCTCCT	TTTGTGGTTTAGTGTTGGCTTC
PTEN	GGGGAAGTAAGGACCAGAGAC	TCCAGATGATTCTTTAACAGGTAGC
PLA2	TTTTGGGGCCAAGGAACT	GTACTGGATGCCGACCATCT
PTGS2	CTTCACGCATCAGTTTTTCAAG	TCACCGTAAATATGATTTAAGTCCAC
RAC1	CTGATCAGTTACACAACCAATGC	CATTGGCAGAATAATTGTCAAAGA
SFTPC	CATAGCACCTGCAGCAAGAT	CAGCAGGGAATGCCAAAT
SMAD3	CACCACGCAGAACGTCAA	GATGGGACACCTGCAACC
SPRY2	TTTGCACATCGCAGAAAGAA	TCAGGTCTTGGAAGTGTGGTC
SPRY4	CCCCGGCTTCAGGATTTA	CTGCAAACCGCTCAATACAG
TBX5	GGCAGGTCTTTTGCGTCA	GAAGAGGTGGGATAGTTGGAGA
TBX4	CCATCGCTACAAGTTCTGTGAC	TTGTAGCTGGGGAACATCCT
TGF-B	CACGTGGAGCTGTACCAGAA	CAGCCGGTTGCTGAGGTA
TWIST2	TTTTGGGGCCAAGGAACT	GCAGCATCATTCAGAATCTCC

3.7 Hydroxyproline content assay

After lung function was performed, the right bronchus was clamped, and the medial and caudal lobes were removed and washed briefly in PBS. The tissue was then dried overnight in the hood, and either stored at 4°C or processed using Quickzyme Hydroxyproline Assay protocol directly. Dried lobes were scraped out of a cells culture plate, weighed and transferred into acid safe tubes. 6M hydrochloric acid (HCl) was added to obtain a concentration of 50 mg of tissue/mL. At the same time, a collagen standard was prepared for incubation with the samples. Standard and sample tubes were sealed tightly and incubated for 20 hrs at 95°C in a thermoblock. After incubation, tubes were cooled to RT and spun down at 13,000 x g. The supernatant of the hydrolyzed sample was diluted 10 times in 4M HCl. In addition, a collagen standard was prepared from the hydrolyzed stock solution. 35 ul of the sample and standards were pipetted into a 96-well plate. 75 ul Assay buffer was added to the wells and the plate was covered with an adhesive seal and incubated for 20 min at RT while shaking. 75 ul of detection reagent was added to each well, and plate was incubated in the dark at 60°C in an oven. The plate was then cooled on ice until the solution reached RT and an ELISA plate reader was used to measure the absorbance at 570 nm.

3.7.1 Hydroxyproline content analysis

After the A_{570} values were obtained fort he samples, a standard curve was constructed in the range of 6 - 300 ug/mL collagen. Total collagen measured in medial and caudal lobes were fit accordingly. Samples were plated in triplicate and an unpaired, two-tailed Student's T-test was performed in order to test whether the group means were significantly different.

3.8 Primary culture of human lung fibroblasts

3.8.1 Culturing and passaging

5 cm lung cubic biopsies were washed in PBS and multi-scissored in growing culture medium (DMEM with 5 – 10% FCS, 1% glutamine, and 1% Penicillin-Streptomycin (P/S) into small pieces. The small pieces were seeded in a large 75cm^2 flask allowed to grow out at 37°C, 5% CO_2 for up to one month with weekly media changes. Chunks were eventually washed away, and adherent fibroblasts remained. After the second passage, fibroblasts were frozen in 10% DMSO, 10% FCS and DMEM. These steps were usually performed before we received them. Normally, we received previously frozen aliquots of fibroblasts between 1 and 4 million cells per cryotube.

In order to bring up frozen cells for culture, media (DMEM 90%; FCS 10%; P/S 1%) was pre-warmed to 37°C and 7 mL aliquoted into 75cm^2 flasks which were also pre-warmed in incubators at 37°C 5% CO_2 for at least 30min. 10 mL of pre-warmed media were also prepared and labeled in 15 mL tubes. Cells were then removed from liquid nitrogen and placed in a 37°C water bath until thawed for approximately 1-2 min. Next, cells were immediately pipetted into the aliquoted media and centrifuged for 5 min at 100 g. Supernatant was removed and the cell pellet was resuspended in 3 mL of media. This media was then added to the pre-warmed flasks and placed in the incubator.

Human lung fibroblasts grow extremely fast and often reached 80 – 100% confluence by the following day. Before splitting, 50 mL tubes were labeled and 1X trypsin, as well as 1X PBS with 1% P/S were pre-warmed to 37°C. Cell supernatant was then aliquoted into pre-labeled 50 mL flasks, and washed twice with 10 mL 1X PBS, followed by incubation at 37°C for 2-3 min with 6 mL 1X trypsin. Flasks were spanked and adherence was monitored under the microscope. Once most cells were detached, 4 mL 1X PBS was added to the flask, and the solution was mixed, washed and pipetted back into the original supernatant in order to stop the trypsin reaction. The solution was inverted to mix, and cells were counted using a hemocytometer. 10 ul of cells were added to one side of the hemocytometer. Cells present in an area of 4 larger squares

composed of a smaller grid of 16 squares were counted. The total number of cells in this area was divided by 4 (to get the average), then multiplied by 10 (for the volume in ul used for counting), then multiplied by the dilution of cells (normally 20 mL or 20,000 ul). For example if 80 cells total were counted; 80 divided by 4 (number of squares) multiplied by 10 (ul volume used for counting) times 20,000 (ul diluted), would equal 4 million total cells. After counting, cells were spun down at 100 g for 5 min and resuspended according to the needed concentration. In order o achieve 80 – 100% confluency by the next day, for six-well plates, cells were seeded at 150 – 250,000/well; for 4 well slides, 20 – 50,000/well, and 8-well slides, 8 – 15,000/well.

3.8.2 Treatment with rhFGF1, rhFGF10 and TGF-β

25 ug rhFGF1 (R&D Systems 232-FA) was resuspended in 0.1% BSA in PBS and diluted in PBS for a final concentration of 100 ng/mL. rhFGF10 (R&D Systems 345-FG) were resuspended in 250 ul of 0.1% BSA in PBS to make a stock concentration of 100 ug/mL. Cells were serum starved for at least 12 hrs and treated with 200 – 500 ng/mL rhFGF10. 2 ug hTGF-β (R&D Systems 240-B) was resuspended in 0.1% BSA in 4 mM HCl and diluted in PBS for treatment of cells at a final concentration of 4 ng/mL.

3.8.3 Treatment with Rosiglitazone

10 mg of Rosiglitazone (R2408 Sigma) was diluted with 280 ul DMSO for a .1M solution. A working solution of 0.033 M Rosiglitazone was then made by using 1 part Rosiglitazone and 3 parts PBS. Cells were treated at a final concentration of 20 uM or 100 uM Rosiglitazone.

3.8.4 Harvesting cells for RNA

Human fibroblasts were grown in monolayers in 6 well plates to 80 – 100% confluency. Media was aspirated, cells were washed with 1X PBS briefly, and 200 ul of TRIZOL was added per well. Cells were scraped away with a cell scraper and pipetted into a cryovial. At least 3 wells were combined into one

cryovial and vortexed for at least 30 s and placed immediately in liquid nitrogen. Homogenized cell lysates were then stored in -80°C until RNA was extracted.

Heavy phase-lock gel tubes (5 PRIME 2302830) eppendorf tubes were centrifuged for 5 min at maximum speed. The homogenized lysate was added to the separator column and incubated at RT for 3 min. 1/10 total volume of chloroform was added. Tubes were shaken for at least 15 s and incubated for 3 min at RT. Next, tubes were centrifuged for 15 min at 10,000 g at 4°C. The aqueous layer was extracted and added to a new eppendorf. 1.5 volumes 100% isopropanol was added. Tubes were inverted to mix and incubated for 10 min at RT. After incubation, tubes were spun down for 15 min at 10,000 g, 4°C. After the pellet was identified, the supernatant was discarded and the pellet was washed with 75% EtOH and vortexed. Lastly, tubes were centrifuged for 5 min at 8,000 g, 4°C; supernatant was discarded, and pellet was dried on the bench until it became transparent. 30 ul of ddH_2O was added and samples were Nanodropped for RNA concentration and purity.

3.8.4.1 Making cDNA

See section 3.6.1 for cDNA.

3.8.4.2 Human primers

See Table 9 for list of human primers.

3.8.5 Immunohistochemistry of cells

Cells were rinsed briefly in PBS and immerse for 30 min in 4% PFA solution at 37ºC. Next, for the washing steps, if the antigen of interest was nuclear, PBX was used, if it was located on the cell surface, PBS was used. Cells were washed in PBS or PBX 3 x 5 min. Next, cells were covered in blocking buffer (1% BSA in PBS) for 30 min at 37ºC or 3% BSA in PBX. Blocking buffer was removed by draining with KimWipe. The primary antibody was diluted 1:50 – 1:200 in blocking buffer and incubated for 1 – 2 hrs at RT or overnight at 4°C. Next, the primary antibody solution was blotted on away with a KimWipe and cells were washed with PBS or PBX 3 x 5 min. The secondary antibody was diluted in blocking buffer (1:450 – 1:1000) and incubated for 1 hr at RT. The solution was drained or blotted with a KimWipe and cells were washed again with either PBS

or PBX 3 x 5 min. Chambers were removed, and PBS or PBX was drained. Lastly 10 ul of mounting media (VECTASHIELD mounting media with or without DAPI (UV channel) for cell nuclei staining was added and slides were cover-slipped.

3.8.6 Oil red O stain

A stock solution of Oil Red O (Sigma O-0625) was prepared: 0.35 g Oil Red O in 100 mL of isopropanol was stirred overnight on a stir plate, filtered (0.2 uM) and stored at RT. Next, a 3:2 working solution was prepared with water and filtered again. Cells were washed twice with PBS, once with 10% formalin, and incubated for up to one day in fresh 10% formalin. Formalin was then removed with a pipette and cells were washed twice with water, then 60% isopropanol for 5 min at RT. Cells were then dried with a hair dryer and 1 mL of Oil Red O working solution was added and cells were incubated for 10 min. Solution was immediately removed and cells were washed 4 times with water. Cells were imaged with light microscopy.

3.8.7 Protein isolation and quantification

Cells were washed twice with cold PBS, and then incubated with cold RIPA buffer including protease/phosphatase Inhibitor Cocktail (Cell Signaling #5872), 1 mM phenylmethylsulfonyl fluoride (PMSF), and 1 mM Sodium Orthovanadate, on ice for 2 min. Cells were then scraped with a frozen cell scraper into an eppendorf tube and spun down at 4°C for 30 min. The supernatant was then put on ice while a Bradford Assay was performed for quantification of lysate. A 1:10 dilution of the lysate was usually used. Lysates were then diluted to 1.2 ug/mL, 5X sample buffer with β-mercaptoethanol was added for a final concentration of 1 ug/mL, and samples were stored at -80°C.

3.8.8 Statistical Analyses

Percentage of the number of positive cells stained over the total DAPI stained cells were calculated. A student's un-paired, nonparametric two-tailed T-test was performed, followed by a Mann-Whitney test to detect significant differences between the stained cells.

3.8.9 Quantification of immunofluorescent microscopy

See section 3.5.4.1

3.9 Primary culture of MLE-12 cells

3.9.1 Culture and passaging of MLE-12 cells

Mouse lung epithelial cells (MLE-12) CRL-2110 (ATCC) cells were kindly provided to us from Dr. Martina Korfei. Cells were cultured as described by ATCC, briefly: 37°C and 5% CO_2 in DMEM/F-12 medium (ATCC) supplemented with 0.005 mg/mL insulin, 0.01 mg/mL transferrin, 10 nM hydrocortisone, 10 nM beta-estradiol, L-glutamine 2 mM, Insulin-Transferrin-Selenium (ITS) solution 1X (PAN Biotech P07-03100), 10 mM HEPES and 2% fetal bovine serum (FBS) and 1% pen-strep. Cells were split every 2 days or at 80% confluence. For treatment with growth factors, cells were deprived of serum for at least 18 hrs prior to treatment.

3.9.2 RNA isolation

See section 3.8.4 for RNA isolation protocol.

3.9.3 Protein isolation and quantification

See section 3.8.7 for RNA isolation protocol.

3.9.4 Western blot

Loading buffer was added to protein samples from cell extracts (5% SDS in bromophenol blue and β-mercaptoethanol) denatured for 5 min at 95°C and cooled on ice. At least 10 ug of sample was loaded on a 10% polyacrylamide gel and run at 120 V for approximately 2 hrs. Samples were then electrically transferred to a polyvinylidene fluoride (PVDF) membrane by semi-dry electro blotting (2 mA/cm2) for 90 min. The membrane was blocked with 3-5% milk in TBS blocking buffer at RT on shaker for 1 h followed by incubation with primary antibody overnight at 4°C. After washing with 1X TBS-T three times for 10 min each, the membrane was incubated with the respective HRP-labeled secondary antibody at RT for 2 hrs followed by three times washing with 1X TBS-T buffer for 10 min each. The protein bands were detected by ECL (Enhanced Chemi-luminescence, Amersham, Germany) treatment, followed by exposure of the membrane.

3.10 Details regarding animal experiments done at JLU (BreAnne MacKenzie: BM, Andreas Gunther: AG) versus those performed at Childrens Hospital Los Angeles (Denise Al Alam: DAA) and the Comprehensive Lung Center in Munich (Melanie Koenigshoff:MK)

The number of animal experiments performed at JLU was limited by a slow approval process, it was decided to take advantage of an ongoing collaboration

with Dr. Denise Al Alam at Children's Hospital Los Angeles (California, USA), Dr. Melanie Koenigshoff (Munich, Germany) and Prof. Andreas Günther (Giessen, Germany).

Collaboration with Denise Al Alam: former postdoc of Dr. Bellusci, inherited Dr. Bellusci's lab when he moved to JLU. All protocols for bleomycin treatment were approved at CHLA and significant experience was in place (Gupta et al., 2009). The animal experiments in Fig 6, 10, 11b, 12 and 15 were done in the US. Bleomycin administration, weight and lung function were carried out at CHLA. Samples were sent to JLU for further analyses by BM.

Collaboration with Melanie Königshoff: Fig 7a. We have obtained cDNA from lungs of mice at different times after bleo exposure. qPCR were done by BM.

Collaboration With Prof. Andreas Günther: Fig 7b. We have obtained protein extracts from lungs of wild type mice at different times after bleomycin exposure. Western blots were done by Dr. Ingrid Henneke from Prof. Dr. Günther's lab. Figure preparation and data analyses were done by BM. The table below summarizes the respective contributions and the protocol

Table 10. Delegation of animal experiment work.

Fig. #	Prot.#	Geno-type	weight meas.	bleo tx	lung function	gross pics	H&E	q-PCR	hydroxy-proline	stain-ing	data
6	CHLA 193-12	WT	DAA	DAA	DAA	-	-		**BM**	**BM**	**BM**
7a	-	WT	-	MK	-	-	-	**BM**	-	-	**BM**
7b	-	WT	-	AG	-	-	-	-	-	AG	**BM**
9	CHLA 193-12	WT	-		DAA	DAA	**BM**	**BM**	-	-	**BM**
10	CHLA 193-12	WT	DAA	DAA	-	-	-	-	-	-	**BM**
11a	JLU 73/2012	DTG	**BM**	**BM**	**BM**	**-**	**BM**	**BM**	**BM**	**-**	**BM**
11b	JLU 73/2012	DTG	DAA	DAA	DAA	-	**BM**	**BM**	**BM**	-	**BM**
12	CHLA 193-12	*Fgfr2b*$^{+/-}$	DAA	DAA	DAA	-	**BM**	**-**	**BM**	-	**BM**
13	JLU 72/2012	*Fgf7*$^{-/-}$	**BM**	**BM**	**BM**	-	**BM**	**BM**	**BM**	-	**BM**
14	JLU 72/2012	*Fgf7*$^{-/-}$	**BM**	**BM**	**BM**	-	**BM**	**BM**	**BM**	-	**BM**
15	CHLA 193-12	*Fgf10*$^{+/-}$	DAA	DAA	DAA	-	**BM**	**BM**	**BM**	**BM**	**BM**

Part 4. Results

4.1 FGF signaling is dysregulated in end-stage IPF lungs

4.1.2 Microarray suggested blunted epithelial FGF signaling in IPF patients

RNA isolated via laser-capture micro-dissection from IPF patients (n=11) and donors (n=11) was reversed transcribed, labeled and competitively hybridized on Agilent whole human genome arrays (Fig 4). Squares indicate comparison between homogenate collected from random areas of IPF lungs with homogenates of random areas collected from donor lungs. Circles represent RNA collected exclusively from fibrotic regions of IPF lungs compared to normal healthy septa of donor lungs. Triangles indicate comparison between normal healthy septa of donor and “normal” appearing septa of IPF patients. When the expression levels of IPF fibrotic septa were compared against normal donor septa (circle symbols), *FGF1* and *FGF7* as well as *FGFR1* were upregulated while *SPRY2* was downregulated. This indicated that while ligands and receptors were present in IPF fibrotic septa, signaling was muted. However, since the Agilent probes were not isoform specific, it could not be determined whether the b or c isoform of the receptors were regulated. When IPF whole lung homogenates were compared to donor whole lung homogenates (square symbols), *FGF1* was not observed to be regulated. However, *FGF7, FGFR1* and *SPRY2* were downregulated while *FGFR2* was upregulated. “Normal” appearing IPF septa were compared to “normal” appearing donor septa (triangle symbols), and the expression pattern was found to be similar to the expression pattern of comparing fibrotic IPF septa with “normal” donor septa (circle symbols); indicating that “normal” appearing septa of IPF lungs may also be molecularly dysregulated. In both normal and fibrotic areas of IPF lungs there was an upregulation of *FGF1* and *FGFR1* while *SPRY2* was downregulated. However, *FGFR2* was also upregulated in “normal” septa of IPF compared to donor controls. In summary, FGF ligands and receptors appeared to be actively expressed in IPF lungs; however, signaling (*SPRY2*) was decreased compared to donor lungs.

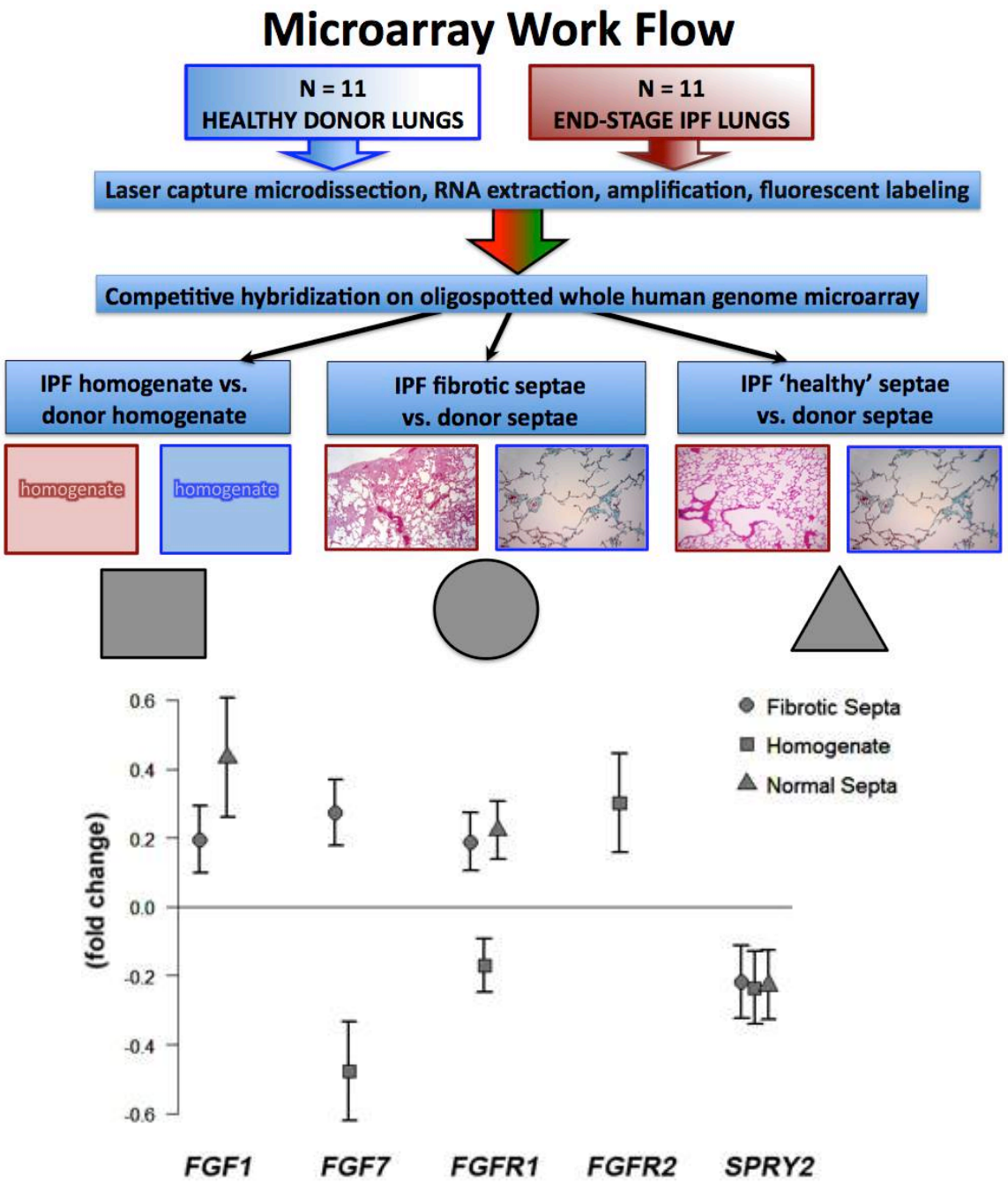

Figure 4. Microarray work flow and profile suggesting decreased FGF signaling in IPF lungs.

Microarray workflow is displayed for (n=11) donor and (n=11) IPF lung samples. Squares indicate comparison between homogenate collected from random areas of IPF lungs with homogenates of random areas collected from donor lungs. Circles represent RNA collected from fibrotic regions of IPF lungs compared to normal

healthy septa of donor lungs. Triangles indicate comparison between normal healthy septa of donor and "normal" appearing septa of IPF patients.

Limitation: isoforms b and c for *FGFR1* and *FGFR2* receptors were not tested. Fibrotic septa of IPF were not compared against "normal" IPF septa. There was no probe for *FGF10.*

Microarray was performed by Dr. Jochen Wilhelm; analyses and presentation by me (BM).

4.1.3 Transcriptome analyses by qPCR of *FGFs* and other genes

In order to identify a transcription signature in IPF whole lung homogenates, qPCR was performed on biopsies from end-stage IPF patients (n=22-30) compared to donors (n=8-15) (Fig 5). Porphobilinogen deaminase (*PGBD*) was selected as a reference gene, as its expression, unlike *HPRT ACTB*, was not regulated in either Donor or IPF lung homogenates as previously published (Tian et al., 2011). Expression is displayed as negative delta delta Ct, so that positive values indicate an increase in expression and negative values, a decrease. First, **mesenchyme specific expression** was analyzed. While *TWIST2,* a basic helix-loop-helix transcription factor, a marker for mesenchyme differentiation, and promoter of EMT (Katoh and Katoh, 2009b) was slightly downregulated, S100 calcium binding protein *S100A4* (Lawson et al., 2005); also known as "fibroblast specific protein" which is involved in cell migration, was slightly upregulated. Next, both as a positive control and to demonstrate upregulation of pathogenic, **markers characteristic of fibrosis**, expression of smooth muscle actin (*ACTA2*), collagen type 1 alpha 1 (*COL1A1*), and fibronectin (*FN*) were assessed (Marmai et al., 2011). While all 3 were highly upregulated, *ACTA2* was the highest, followed by *COL1A1* and then *FN* indicating robust, active fibrosis was occurring in the IPF patient samples. Also highly upregulated was the **cell motility/WNT signaling** ras-related C3 botulinum toxin substrate 1 (rho family, small GTP binding protein Rac1) (*RAC1*) (Akunuru et al., 2011). Next, **epithelial markers** were analyzed. E-cadherin 1 (*ECAD*), a calcium dependent cell-cell adhesion glycoprotein was slightly upregulated, while podoplanin, an epithelial specific marker (*T1-α*) (Ono et al.,

2013) was not regulated. **Epithelial progenitor cell markers** Clara cell secreted protein (*CC10*) was not regulated and surfactant protein C (*SFTPC*) was down-regulated potentially indicating AEC2 cell injury, a decrease in the number of AEC2 cells or dysregulation. Interestingly, **inflammatory markers** transforming growth factor beta 1 (*TGFβ1*), downstream TGFβ1 target *SMAD3,* and potent cytokine interleukin 1 beta (*IL-1β*), were not regulated compared to donor samples; indicating that the inflammatory process in the end-stage IPF samples measured was unlikely to be more active than in donor lungs. **Tumor suppressor** gene phosphatase and tensin homolog (*PTEN*) was only slightly upregulated in IPF samples possibly indicating a lack of epithelial protection. Importantly, **FGF ligands** were also analyzed and observed to be regulated. *FGF1, FGF7*, and *FGF10,* were upregulated, while *FGF2* and *FGF9* were downregulated. **Mesenchymal specific receptor isoforms** *FGFR2c* and *FGFR1c,* the main receptors for *FGF2* and *FGF9* were upregulated possibly indicating an over-abundance of lung mesenchymal cells. *FGFR1b*, expressed in both mesenchymal and epithelial cells, as well as epithelial receptor *FGFR2b,* were downregulated, possibly indicating a lack of epithelial cells or dysregulation of the receptor. Downstream **FGF signaling markers** whether in the epithelium; *SPRY2,* or in the mesenchyme; *SPRY4, ETV4,* were downregulated, as well as **upstream regulators** of FGF signaling *TBX4* and *TBX5.* Only *ETV5* showed a slight trend towards upregulation. **Markers for lipofibroblasts**, adipocyte differentiation related protein (*ADRP*) and CAAT *CEBP/a* were also downregulated indicating a decrease in lipofibroblasts in IPF lungs. Lastly, **eicosanoid expression** was evaluated as it may play an important role in negatively regulating collagen production in the lung (Bozyk and Moore, 2011; Ghosh et al., 2004). Phospholipase A2, an enzyme required for fatty acid synthesis (PLA2) and prostaglandin E2 receptor (EP2) both appeared to be slightly upregulated.

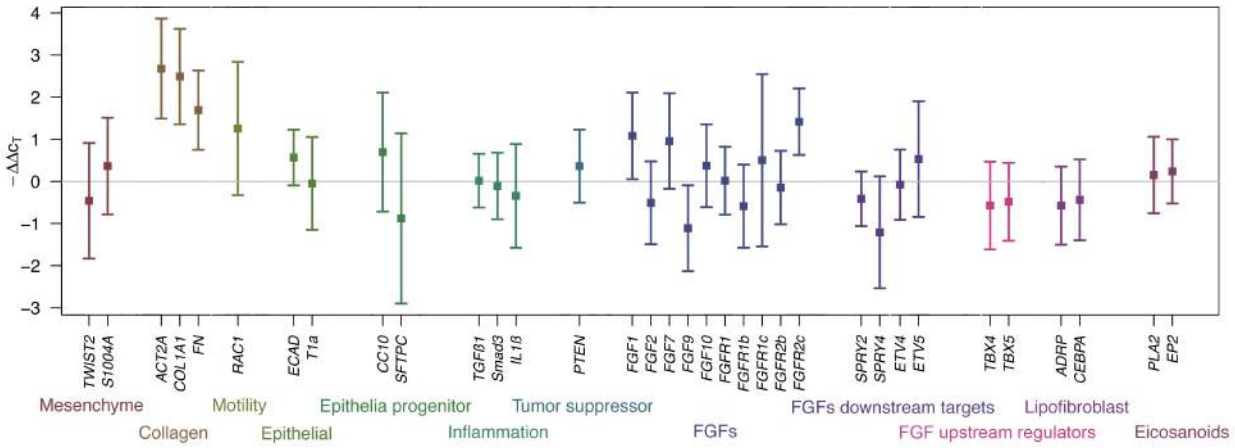

Figure 5. Transcriptome analyses of IPF patients vs. donor by qPCR

qPCR was performed on lung homogenates biopsied from end-stage IPF patients (n=22-30) and compared to donors (n=8-15). Porphobilinogen deaminase (*PGBD*) was used as a reference gene and expression is displayed as negative delta delta C_t, so that positive values indicate an increase in expression and negative values indicate a decrease in expression.

Limitations: no pathological report was provided with donor samples; due to variation in age and sex of donors, patients with emphysema may provide a more homogenous sample pool and serve as a more appropriate control.

qPCR and data analyses by BM, graphic presentation by Dr. Jochen Wilhelm

4.2 Heterogeneity in fibrotic response to bleomycin in C57Bl/6 injured animals (5U/kg i.t.) and limited collagen deposition compared to end-stage IPF

A massive deposition of collagen is characteristic of end-stage IPF patient lung pathology (Fig 6A,B). In order to establish the bleomycin injury model, we first evaluated the level of collagen deposition by Masson's trichrome stain at different time points after injury in order to visualize both the extent of injury and to evaluate homogeneity of response (Fig 6C-Q). We observed, that although

mice from the same background (C57Bl/6) and age (12 weeks) were treated with the same dosage of bleomycin (5U/kg i.t.), some suffered only a moderate injury (MOD INJ), while others suffered severe injury (SEV INJ) as measured by hydroxyproline quantification, weight loss, and lung compliance. This dose, 5U/kg i.t., was chosen since our group previously obtained comparable survival (40%) and a robust fibrotic response with 3U/kg via osmotic mini-pump (Gupte et al., 2009). Notably, whether mice were part of the MOD INJ or SEV INJ group was usually externally apparent, as mice were monitored daily for physiological signs of suffering (see Table 5). Mice suffering from acute lung injury, marked by prolonged periods of abnormal respiration and >20% reduction of initial weight were euthanized and also considered as SEV INJ. At 7 days post injury (dpi) collagen deposition had already begun in SEV INJ mice (Fig. 6E), was accompanied by a robust inflammatory cell influx and an Ashcroft score (AS) of 4 (Fig 6D). A significant decrease in compliance was observed as well at 7 dpi in both groups (Fig 6F), however the MOD INJ group recovered their weight (Fig 6G). By 14 dpi, MOD INJ mice showed an Ashcroft score of 4 (Fig. 6H) while SEV INJ showed an average Ashcroft score of 6 (Fig. 6D). Interestingly, a significant increase in hydroxyproline (Fig 6J) and decrease in weight (Fig 6L) was only detected in SEV INJ mice at 14 dpi, though compliance was significantly decreased in both groups (Fig 6K). Mice that survived to 21 dpi showed less inflammatory cells and more collagen deposition (Fig 6M,N,O) than at 7 and 14 dpi; however, only SEV INJ mice showed a significant decrease in lung compliance (Fig 6P); both groups recovered weight, however SEV INJ mice lost more weight during the earlier stages of injury. Taken together, the results presented in this figure feature important limitations that should temper the conclusions and interpretations drawn from the mouse model of IPF. Thus it is important to consider both the inadequate recapitulation of the human phenotype in the mouse model (AS=8 in end-stage IPF vs. maximum 6 in mice), as well as the disparate responses dependent on sex, age, genetic background, and weight; in addition to the technical expertise required for the administration of bleomycin.

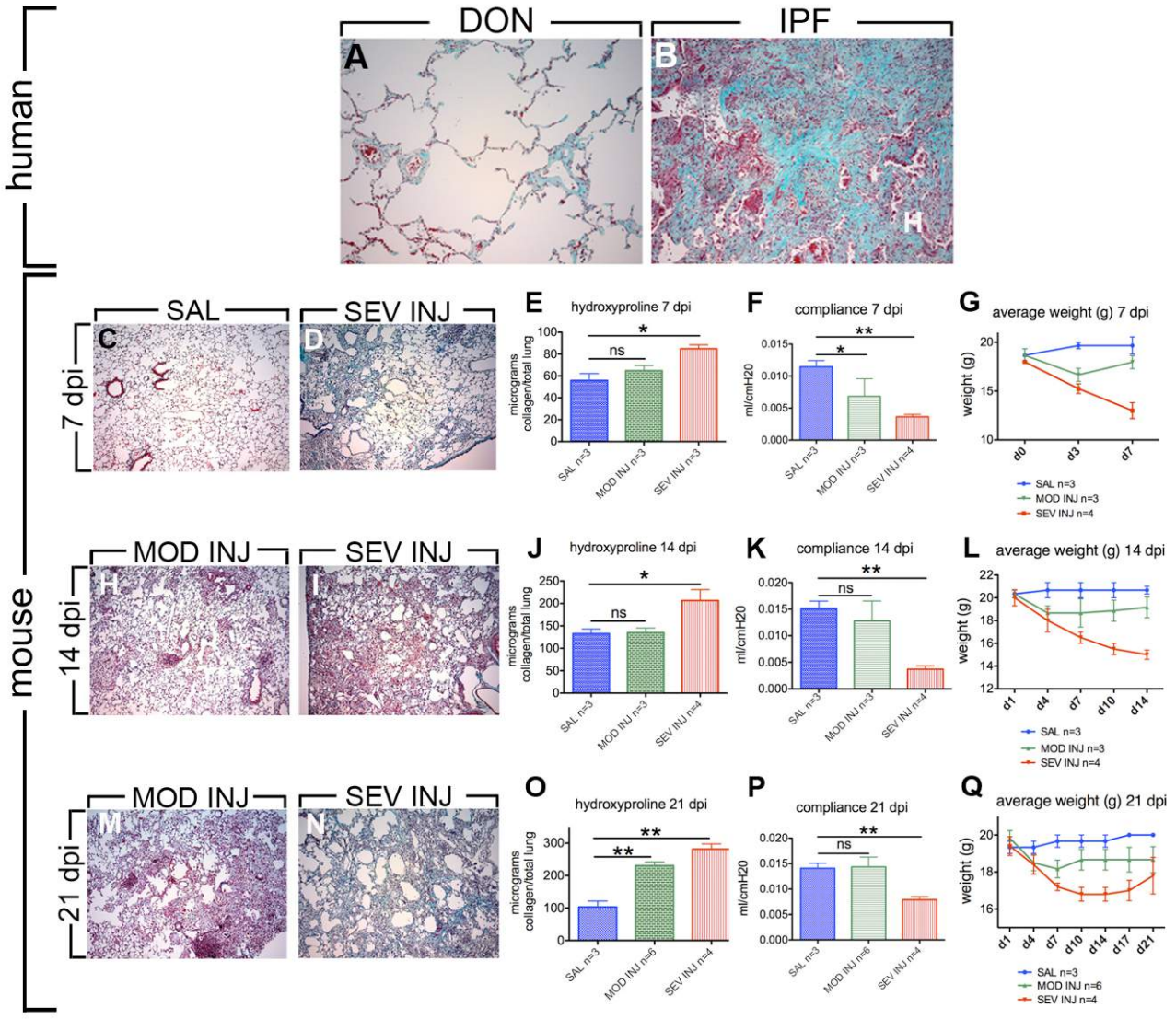

Figure 6. Heterogeneity in response of bleomycin to wild type injured animals (5U/kg i.t.) and limited collagen deposition compared to end-stage IPF

(A,B) Masson's trichrome stain; collagen in green, donor, Ashcroft score Donor (AS)=0 and IPF; AS=8. (C) Masson's trichrome stain at 7 dpi in saline (SAL); AS=0 versus (D) severely injured (SEV INJ) bleomycin-injured lung at 7 dpi; AS=4; comparison at 7 dpi of SAL, versus mice with moderate injury (MOD INJ), and SEV INJ: (E) hydroxyproline, (F) compliance, (G) average weight loss. Masson's trichrome stain at 14 dpi in (H) MOD INJ; AS=4 versus (I) SEV INJ;

AS=6; comparison at 14 dpi SAL, versus mice with MOD INJ and SEV INJ: (J) hydroxyproline, (K) compliance, (L) average weight loss. Masson's trichrome stain at 21 dpi in (M) MOD INJ; AS=5 versus (N) SEV INJ; AS=6 comparison at 21 dpi SAL, versus mice with MOD INJ and SEV INJ: (O) hydroxyproline, (P) compliance, (Q) average weight loss.

Limitations: experimental results may have been confounded by the technical ability to perform i.t. injection efficiently. In addition, only the caudal and medial lobes were assessed for hydroxyproline; other lobes may incur more or less collagen deposition depending on the angle of the sprayer and the anatomy of the mouse. Nonetheless, it should be noted that even with the highest dose of bleomycin injury, collagen deposition in mice never occurred as robustly as in humans with end-stage IPF.

Bleomycin i.t. injury kindly performed by Dr. Denise Al Alam at CHLA, protocol number 193-12; Hydroxyproline measurement, sectioning, and staining, data analyses, performed by me (BM).

4.3 FGF10/FGF7 signaling is blunted in end-stage IPF patients and activated in mice spontaneously recovering from bleomycin-induced lung injury by 14 dpi.

While the lungs of bleomycin-injured mice are demonstrably less damaged than the lungs of human IPF patients, which compromise the conclusions and interpretations drawn from therapies that improve survival and lung function of injured mice, the spontaneous repair response initiated by mice after injury, offer a unique model to evaluate whether FGF signaling is critical for a regulated repair process to occur. Furthermore, comparing the transcriptome signature during the repair response by mice with the end-stage transcriptome signature of IPF, gives insight into whether dysregulation of FGF signaling pathways contributes to IPF in humans.

To determine whether FGF10/FGF7 signaling was dysregulated in IPF lungs, the expression of FGF ligands (*FGF7* and *FGF10*), receptors (*FGFR1b* and *FGFR2b*) and downstream targets (*SPRY2*, *SPRY4* and *ETV5*) in biopsies from end-stage IPF patients (n=22-30) compared to donors (n=8-15) were analyzed (Fig 7a., A-D). Studies in mice have shown that FGFR2b, expressed

primarily in the epithelium, binds to FGF7 and FGF10 while FGFR1b, expressed in both the epithelium and mesenchyme (Beer, 2000) binds FGF10 but not FGF7 (Zhang et al., 2006). While *Spry2* and *Etv4* are epithelial transcriptional targets (Firnberg and Neubüser, 2002; Liu et al., 2003; Zhang et al., 2001) and *Spry4* a mesenchymal target (de Maximy et al., 1999). *Fgfrs* themselves are also downstream targets of FGF signaling (Shu et al., 2005).

IPF lung homogenates showed increased *ACTA2* and *COL1A1* expression indicating an abundance of smooth muscle actin-positive, collagen-producing myofibroblasts (Fig 7a., A). While *FGF7* expression trended towards an increase, *FGF10* expression was significantly increased (Fig 7a., B). A modest decrease in both *FGFR1b* and *FGFR2b* was also observed (Fig 7a., C). Downstream epithelial targets *SPRY2 and ETV4* were also downregulated (Fig 7a., D). Among FGF targets, *SPRY4* was the most decreased.

We performed the same analyses on *WT* mice treated with either saline (n=3) or a single administration of 3.5 U/kg bleomycin (IT) at 7 (n=3-5), 14 (n=4-5) and 21 (n=4-5) days post-bleomycin injury (dpi) (Fig 7a., E-P). By 7 dpi (Fig 7a., E), *Acta2* and *Col1a1* were increased in bleomycin-treated mice. While *Fgf7* and *Fgf10* were not changed (Fig 7a., F), *Fgfr2b*, was downregulated suggesting severe epithelial loss at this stage (Fig 7a., G). *Fgfr1b* was also significantly downregulated. Although no major change in *Spry4* and *Etv4* was detected, a significant reduction in *Spry2* expression was observed (Fig 7a., H). In summary, FGF signaling did not appear to be significantly activated at 7 dpi.

At 14 dpi, (Fig 7a., I-L) *Acta2* and *Col1a1* were significantly increased (Fig 7a., I). Although no change in *Fgf7* expression was observed, *Fgf10* was significantly increased (Fig 7a., J). While *Fgfr1b* expression was upregulated, *Fgfr2b* was still significantly reduced, indicating damaged epithelium (Fig 7a., K). *Spry2* expression was unchanged and *Etv4* expression was increased. Interestingly, the mesenchymal FGF signaling target, *Spry4* was upregulated (Fig 7a., L). Overall, FGF signaling both in the epithelium and mesenchyme appeared to be activated by 14 dpi.

Finally, at 21 dpi (Fig 7a., M-P), fibrosis resolution and epithelial repair

were underway as indicated by *Acta2* expression and *Col1a1*, which although still elevated, were expressed at lower levels than 14 dpi (Fig 7a., M). Though a slight decrease in *Fgf7* expression was observed, *Fgf10* remained upregulated. An increase in *Fgfr1b* expression and maintenance of *Fgfr2b* expression indicated efficient epithelial repair and fibrosis resolution (Fig 7a., O). In addition, *Spry2* expression was not changed, while *Spry4* and *Etv4* remained upregulated (Fig 7a., P). Overall, at 21 dpi, we observed a decrease in mesenchymal FGF signaling associated with maintenance of epithelial FGF signaling.

In summary, our results indicated a dynamic FGF pathway signature after bleomycin injury characterized by strong activation by 14 dpi followed by maintenance of signal during fibrotic resolution. Thus, the decrease in FGF downstream targets in end-stage IPF patients may indicate defective activation of FGF signaling, which may contribute to aberrant repair.

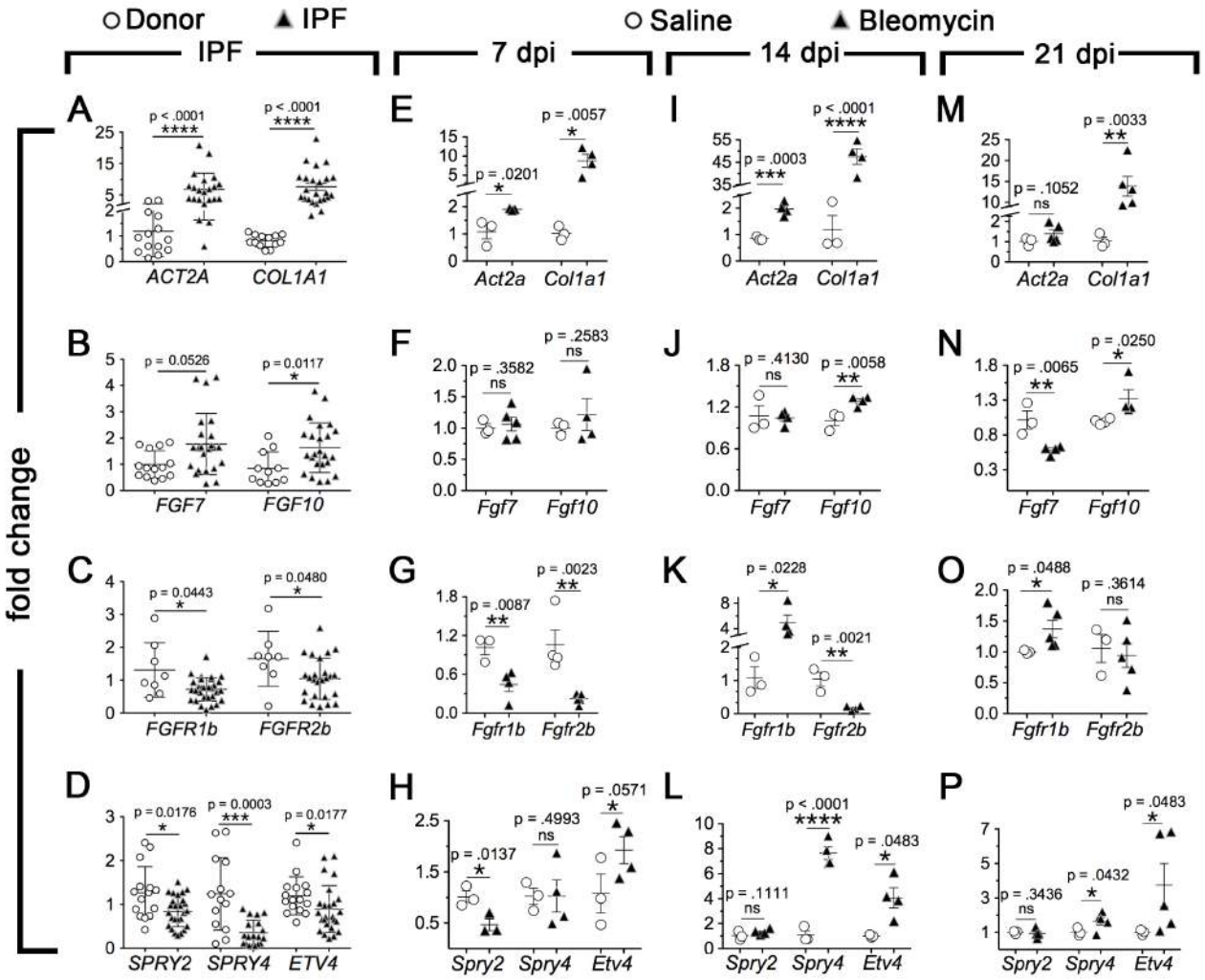

Figure 7a. Transcriptome analysis of members of the FGF7 and 10 signaling pathway in human IPF and bleomycin-treated mice

The expression of *ACTA2* and *COL1A1* was determined to confirm the extent of fibrosis. The expression of the ligands *FGF7* and *FGF10*, the associated receptors *FGFR1b* and *FGFR2b* as well as the downstream targets *SPRY2*, *SPRY4* and *ETV4* was determined in human and WT mice receiving a single, 3.5U/kg bleomycin IT installation or saline. (A-D) End-stage IPF (n=22-30) versus donor (n=8-15). (E-H) Gene expression at day 7; saline (n=3); bleomycin injured (n=3-5). (I-L) Gene expression at day 14; saline (n=3); bleomycin injured (n=4-5). (M-P) Corresponding mouse genes at day 21; saline (n=3); bleomycin

injured (n=4-5).

Limitations: All IPF samples were taken from patients diagnosed with end-stage IPF. While lung donor samples excluded individuals with diagnoses with any IIP diseases, cancers were not excluded thus in order to better standardize analyses, patients with emphysema may be more appropriate controls. While genes may be regulated on a transcriptional level, it is important to also show regulation at the protein level. *cDNA kindly provided by Dr. Melanie Königshoff, München. qPCR and data analyses performed by me (BM).*

4.3.1 p-Akt and p-ERK are activated in patients with IPF and in bleomycin – treated mice; total FGFR2 and FRS are increased in IPF

Levels of growth factor signaling targets, p-ERK and p-Akt were analyzed via western blots in Donor (n=5) and IPF (n=5) lung homogenate. P-ERK and p-Akt was strongly activated in IPF patients compared to donor (Fig 7b, A-C) suggesting increased growth factor signaling in coherence with previous data (Yoshida et al., 2002). In addition these markers were also activated in mice treated with bleomycin (n=5/time point) from 7 dpi (Fig 7b, F-H) compared to saline controls (n=4). Interestingly, total FRS2 and FGFR2 were also found to be upregulated in IPF patients compared to donor (Fig 7b, A). While this may be indicative of an increase in mesenchymal cells in the IPF lung, further experiments are needed to confirm whether FGFs are actively signaling in both IPF and bleomycin-treated mice.

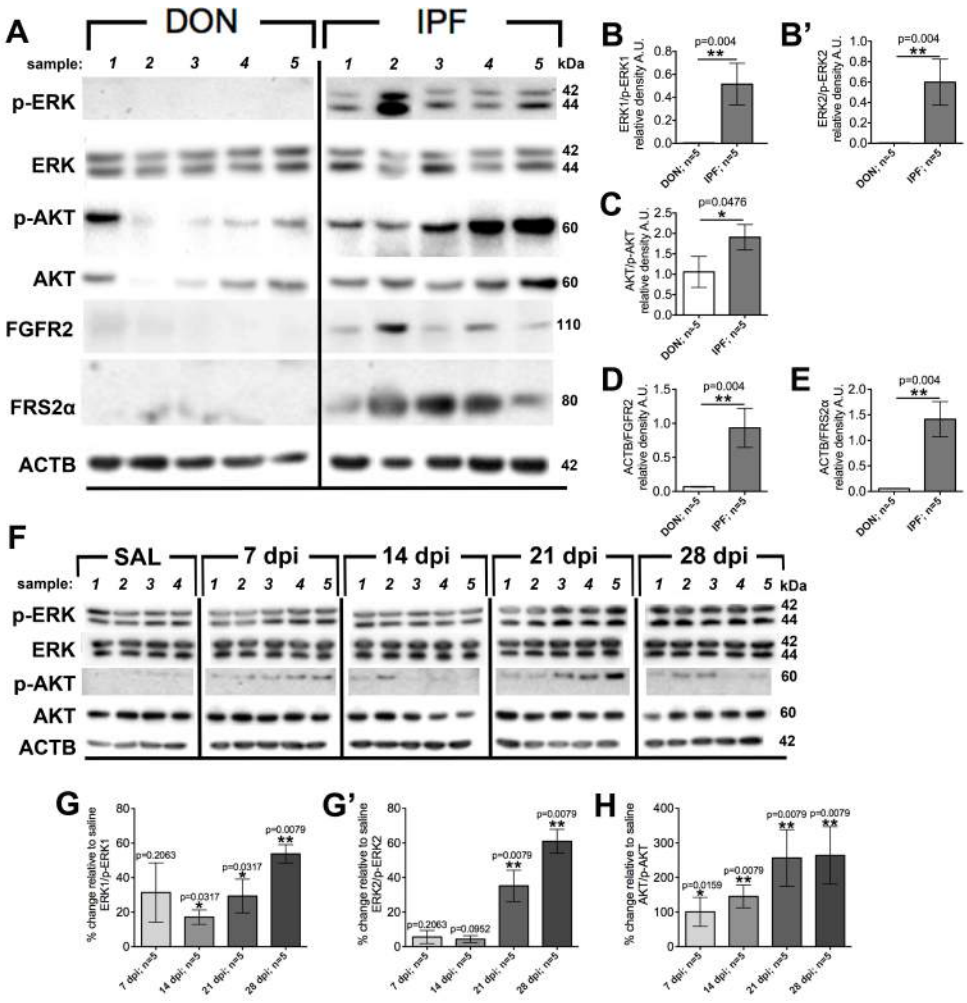

Figure 7b. **p-Akt and p-ERK are activated in patients with IPF and bleomycin treated mice; total FGFR2 and FRS are also increased in IPF**

Limitations: pAkt and pERK are targets of many growth factor signaling cascades including PDGF and VEGF, thus they do not represent an exclusive read-out of FGF signaling. No histological information was available on the donor samples. While total FGFR2 and FRS were increased, whether FGF signaling was actively signaling must be confirmed via p-FGFR2 or p-FRS. *Western blot performed by Dr. Ingrid Henneke; Figure preparation, data analyses performed by me (BM).*

4.4 Bleomycin mouse model experiment schematic

Results from the qPCR transcriptome analyses of bleomycin injured wild type mice suggested that FGF signaling was strongly activated by 14 dpi followed by maintenance of signal during fibrotic resolution (14 – 28+ dpi). Thus, the decrease observed in FGF downstream targets in end-stage IPF patients (*SPRY4, ETV4, ETV5*) may indicate defective activation of FGF signaling during end-stage disease, which may contribute to aberrant repair. Moreover, defective FGF signaling could also contribute to IPF pathogenesis if FGFs are required to activate and sustain an FGF-mediated endogenous repair mechanism in the lung as it is in the case of bleomycin injured mice (Fig 8A). In order to further investigate the hypothesis that deficient endogenous FGF signaling inhibits the lungs repair mechanism after bleomycin injury, mice deficient in FGF signaling: *Rosa26*$^{rtTA+/-}$*;tet(O)solFgfr2b/+* (*DTG*), *Fgfr2b*$^{+/-}$, *Fgf7*$^{-/-}$, and *Fgf10*$^{+/-}$ mice (Fig 8C) were treated with bleomycin and outcome was compared to either littermate or genetic background-matched controls (Fig 8B). Lung function, modified Ashcroft Score (% area confluent fibrosis) and hydroxyproline content or *Col1a1* expression were then performed on injured mice at 28 dpi and compared to corresponding wild types.

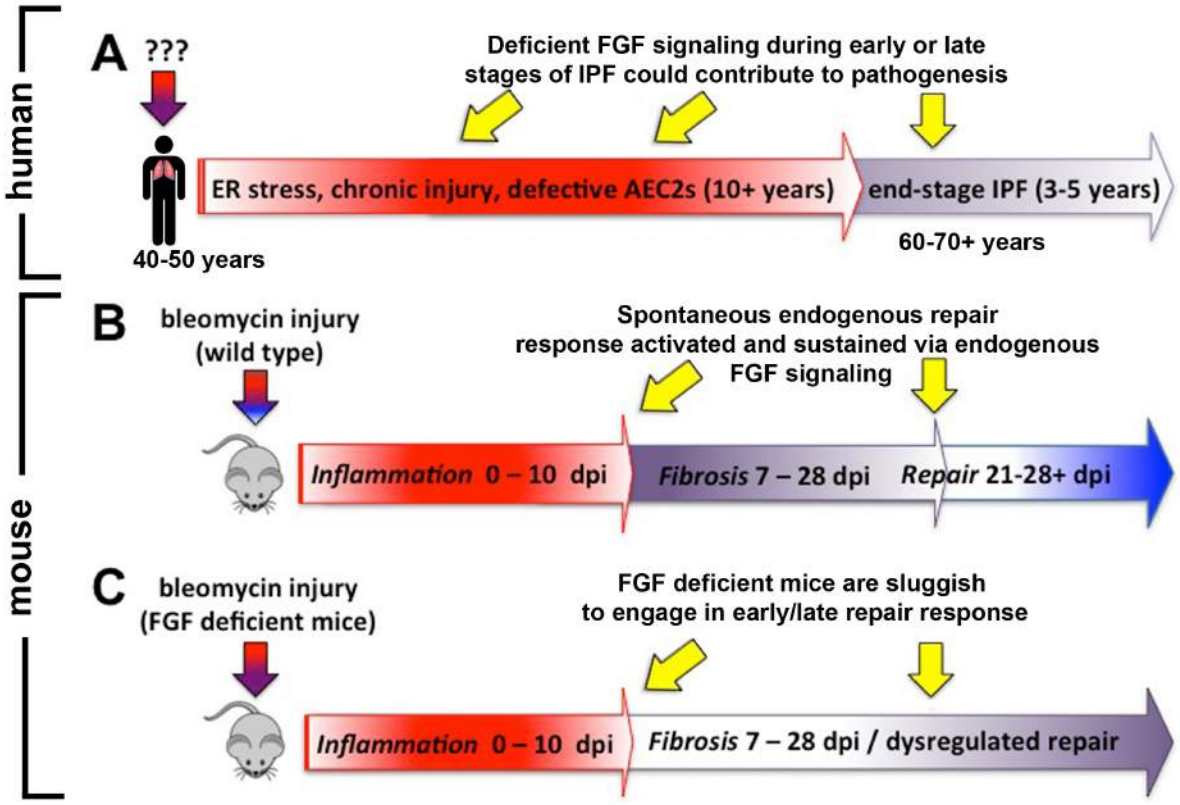

Figure 8. Bleomycin mouse model experiment schematic.

(A) Early pathogenesis of IPF is not well characterized but believed to involve chronic epithelial cell injury, ER stress, and defective AEC2 cells. After presumably many years, patients present with dyspnea, and severely reduced lung function. Thus, once diagnosed, patients are already “end-stage” and live on average 3-5 years due to defective repair mechanisms in the lung. FGF signaling may play a role in both early and late stage IPF, however due to the poor characterization of early disease stages, only the study of FGFs role in end-stage IPF is possible (B) Lungs of wild type mice treated with bleomycin mount and sustain a spontaneous repair response that may be dependent on FGF signaling. (C) Mice deficient in endogenous FGF signaling may also show signs of aberrant repair, thus the hypothesis that FGF signaling is required for the repair after lung injury was tested with using these mice.

4.5 Attenuating FGF1/7/10/22 signaling in mice

4.5.1 Validation of the *Rosa26*$^{rtTA+/-}$;*tet(O)solFgfr2b*/+ construct

In order to attenuate FGF ligand signaling during injury, mice homozygous for reverse tetracycline transactivator (rtTA) (Fig 9A) under the ubiquitous promoter *Rosa26* were crossed with mice carrying a soluble form of the extracellular domain of the endogenous FGFR2-IIIb receptor fused to the Fc domain of the IgG heavy chain and under the control of a tetracycline responsive element, *tet(O)solFgfr2b/*+ (Fig 9B) (Parsa et al., 2010). When mice carrying both constructs are exposed to doxycycline, the soluble, FGFR2b decoy receptor is secreted, trapping all FGFR2b specific ligands (Fig 9C,D). In order to test whether the construct could be activated postnatally, adult *DTG* mice were fed doxycycline food from PN28 to PN88. As previously reported (Parsa et al., 2010), incisors failed to regenerate after extended exposure to doxycyline food (Fig 9E,E'). Pregnant mothers heterozygous for the driver and positive for the *tet(O)solFgfr2b* construct were fed doxycycline food from the date of conception; embryonic (E) day 0 to E12.5 and sacrificed. Embryos deficient in FGF ligand signaling lacked limbs (Fig 9F,F') and lung growth was stunted in *DTG* embryos that were fed dox from E10.5 to E18.5 and analyzed at E18.5 (Fig 9G,G'). These results were expected, as mice homozygous for *Fgfr2b* or *Fgf10* lack both limbs and lungs (De Moerlooze et al., 2000 Ohuchi et al., 2000; Sekine et al., 1999). In an additional postnatal validation, it was observed that mice homozygous for the *Rosa26*^{rtTA} driver, expressed twice as much decoy receptor as mice heterozygous for the driver after one week on doxcycline food (Fig 9H). In a longer study, *DTG* mice fed either normal or doxycyline from PN28 to PN88, showed that lung compliance was observed to be slightly reduced in the *DTG* +DOX group (Fig 9I).

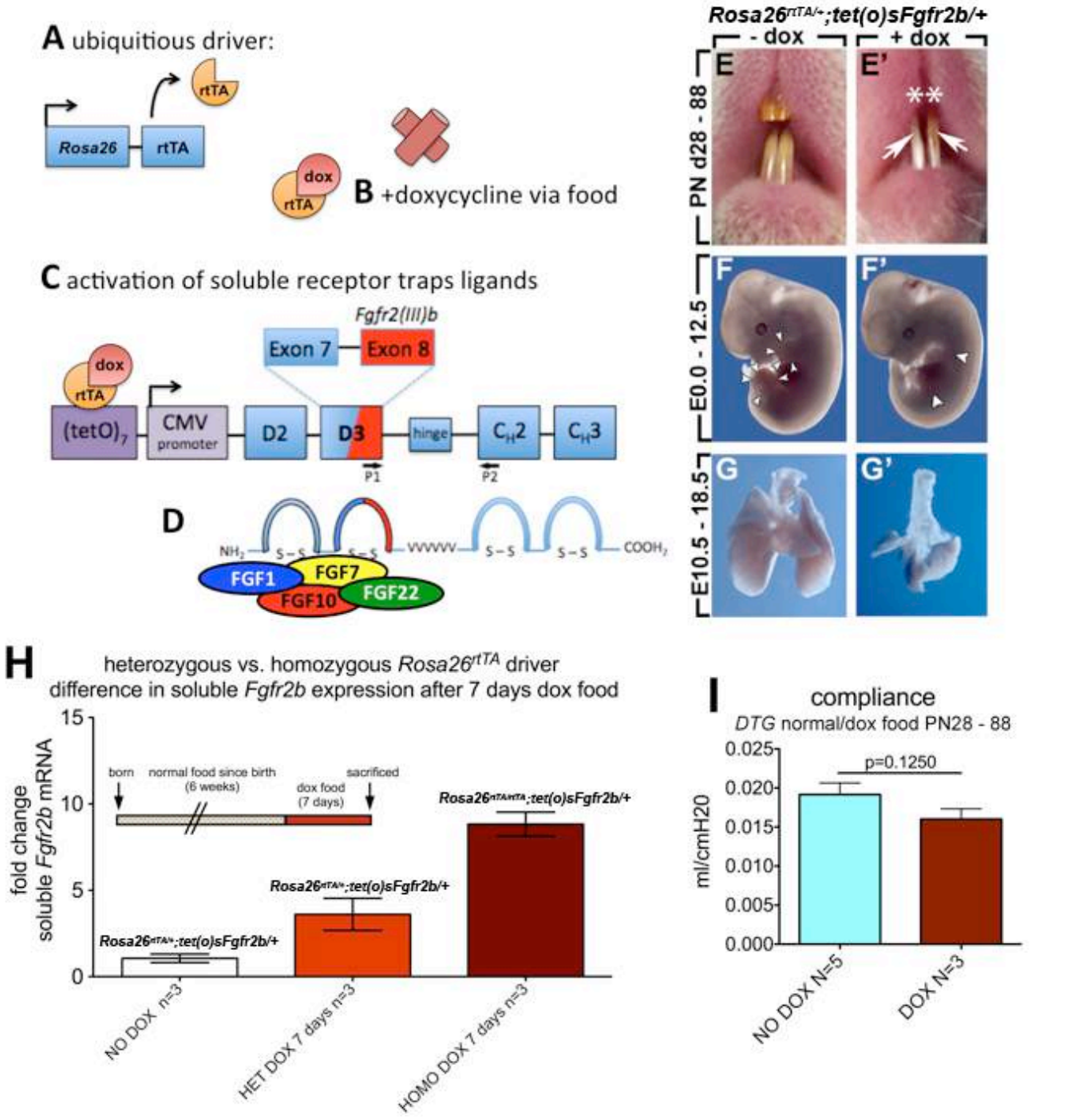

Figure 9. Validation of *Rosa26$^{rtTA/+}$;tet(O)solFgfr2b/+* mice

(A) A reverse tetracycline transactivator is under control of the *Rosa26* promoter, which is expressed in every cell. (B) Doxycycline binds to *rtTA* and (C) binds to the *tet(O)$_7$* response element upstream of the *CMV* promoter, which activates

expression of a soluble decoy *Fgfr2b* receptor. The receptors signaling domain has been replaced with a heavy chain IgG domain, so ligands are sequestered, and signaling is attenuated (D). (E-E') Complete degeneration of maxillary and degradation of mandibular incisors in *DTG* mice fed doxycycline for 60 days postnatally. (F-F') Recapitulation of *Fgf10*$^{-/-}$ and *Fgfr2b*$^{-/-}$ embryonic phenotype E0.5 – E12.5; white arrows indicate limbs (F) and absence of limbs (F'). (G-G') lobes of lung are absent/under-developed; DOX food E10.5 – E18.5. (H) Homozygous driver mice expressed twice as much decoy receptor as heterozygous mice after one week on DOX food. (I) Lung compliance was slightly decreased in mice fed DOX food post-natally from PN28 to PN88.

Limitations: not 100% of ligands are trapped, and residual signaling may occur. Doxycycline administration may interfere with interpretation of animal injury experimental results.

Doxycyline administration kindly provided by Dr. Denise Al Alam, CHLA, protocol number 193-12; Data analyses and presentation performed by me (BM).

4.5.2 Administration of doxycycline food from 7 days post bleomycin-injury had no effect on survival after injury

While some reports have claimed that doxycycline confers resistance to bleomycin delivery (Fujita et al., 2011; Huang et al., 2006), in a pilot study, we found that wild type mice exposed to doxycycline from 7 days post bleomycin injury (3.5U/kg) showed no survival advantage (43%) over wild type mice fed normal chow (63%) (Fig 10A). Moreover, it was noted that mice that did recover from the initial acute lung injury (ALI) stage which occurs during the first week after bleomycin injury, died whether they were fed doxycycline food or not. As illustrated in the figure, changes in endogenous gene expression or administration of potential therapeutics after day 7 may be more relevant for the treatment of IPF than prophylactic treatment of treatment during the first week after injury. Lastly, we found that all survivors recovered weight loss due to injury (Fig 10B).

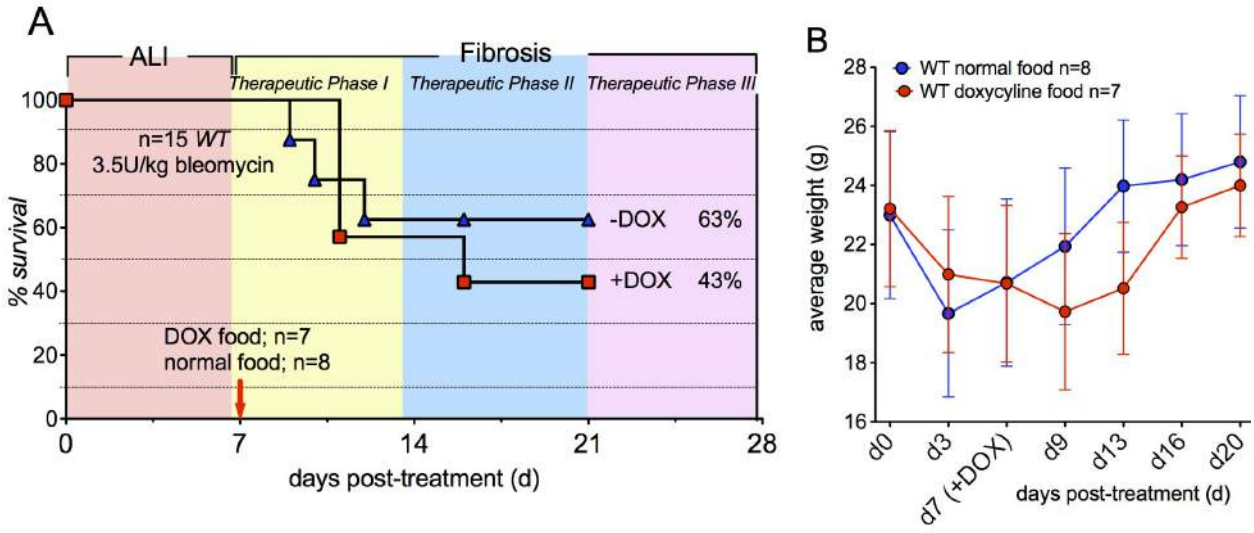

Figure 10. Survival curve for bleomycin-injured wild type mice fed doxycycline chow from 7 dpi.

(A) Mice (n=15) were injured with 3.5U/kg bleomycin. At 7 dpi, mice were divided into two groups. 7 were fed doxycycline food, 8 were not. The group that received plain food had a 63% survival rate, while those from those who received doxycycline food had a 43% survival rate. Survival rate depended on level of injury sustained during the initial phase of bleomycin injury. Mice who showed signs of repair after injury survived while mice that did not, died, regardless of doxycycline food. (B) Survivors in both groups recovered weight loss after injury.

Limitations: while doxycycline did not show a protective effect after 3.5U/kg bleomycin injury, the level of injury resulted in substantial death and was thus too high to discriminate the effect of FGFR2b ligands.

Doxycylcine data kindly provided by Dr. Denise Al Alam at CHLA, protocol number 193-12; data analyses and presentation performed by me (BM).

4.6 Ubiquitous attenuation of FGFR2b ligands activity during bleomycin injury led to moderately increased fibrosis.

To determine whether FGFR2b ligands contribute to spontaneous resolution of bleomycin-induced fibrosis, we globally expressed a soluble decoy receptor upon injury from 7 dpi until 28 dpi. *Rosa26*$^{rtTA/+}$*;tet(O)solFgfr2b/+* (*DTG*) female mice (n=10) and single transgenic age-matched *tet(O)solFgfr2b/+* (*STG)* controls (n=10) were given bleomycin (1.0 U/kg) and fed food containing doxycycline thereafter (Fig 11a., A). This low dose of bleomycin resulted in mild fibrosis and increased survival at 28 dpi. Upon doxycycline administration, the decoy receptor was secreted, trapping endogenous FGF7 and FGF10 ligands in *DTG* mice. While 100% of *DTG* mice survived, one *STG* mouse was sacrificed at 21 dpi due to insufficient respiration and decrease in body weight (90% survival rate) (Fig 11a., A). Surviving *STG*s recovered from injury-induced weight loss significantly better than *DTG*s (Fig 11a., B) suggesting an overall better repair process in *STG*s. Although *DTGs* incurred a uniform increase in fibrosis as visualized by H/E staining (Fig 11a., E-F,E'-F') and quantified by percent area confluent fibrosis (Fig 11a., G), lung function was not statistically different (Fig 11a., D). The decrease in compliance observed indicated very mild lung fibrosis. An increase in hydroxyproline content in either group vs. saline was not observed (Fig 11a., H). The low hydroxyproline content measurement in control groups (60 ug vs. 75-90 ug average in saline groups from other experiments) may be due to an increase in the length of drying time (3 days vs. overnight). In summary, while a homogenous increase in confluent fibrosis was observed in *DTG*s *vs. STG*s, 1U/kg of bleomycin did not cause a significant increase in hydroxyproline content or decrease in lung function in either +DOX or –DOX group.

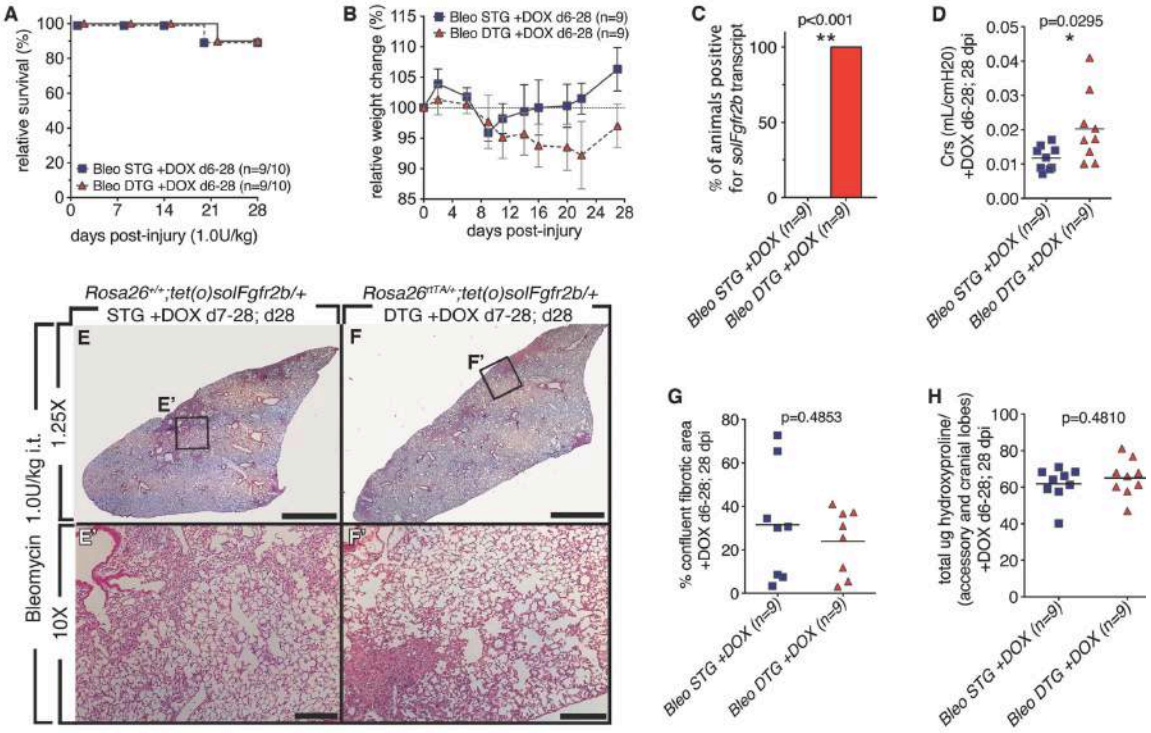

Figure 11a. Impact of FGFR2b signaling attenuation on fibrosis formation in bleomycin-injured mice

(A) *Rosa26$^{rtTA/+}$;tet(O)sFgfr2b/+* (DTG) experimental and *tet(O)sFgfr2b/+* control (WT) mice were treated with bleomycin IT at day 0 and put on doxycycline food from 7 - 28 dpi. (A) Survival curve. (B) Relative weight change. (C) Transcript detected. (D) Compliance in control and experimental lungs at 28 dpi. (E and E') Low and high magnification bleomycin treated WT lungs at 28 dpi. Scale bar F and F': 2 mm; D' and E': 200 µm. Low and high magnification of DTG lungs at 28 dpi. (G) Quantification of percent fibrotic area in control and experimental lungs at 28 dpi (H) Measurement of hydroxyproline content. **Limitations**: low dose of bleomycin resulted in very mild lung phenotype. More extensive injury may be required to detect a difference between mice with intact or attenuated ligand signaling.

JLU Protocol 73/2012

Due to the low level of bleomycin injury sustained by both *WT* and *DTG* mice in the previous experiment, we repeated the experiment using a higher dose of bleomycin (2.0 U/kg) and activated the soluble decoy receptor upon injury from 14 dpi through 28 dpi as our intention was to focus on the role of the FGFR2b receptor *after* the inflammatory response began to subside. *Rosa26*$^{rtTA+/+}$*;tet(O)solFgfr2b/+* (*DTG*) female mice (n=7) and single transgenic age-matched *tet(O)solFgfr2b/+* (*STG)* controls (n=5) were given bleomycin (1.0 U/kg) and fed food containing doxycycline from 14 dpi (Fig 11b). Although the dose of bleomycin used was double the amount used in the previous experiment, 100% of the mice survived (Fig 11b., A) and mice recovered from moderate weight loss by 24 dpi (11b., B). We confirmed that the soluble decoy receptor was expressed exclusively in the *DTG* +DOX mice (Fig 11b., C). *WT* and *DTGs* incurred a similar increase in fibrosis as visualized by H/E staining (Fig 11b., E-F,E'-F') and similar as quantified by percent area confluent fibrosis (Fig 11b., G). Lung compliance was also not statistically different (Fig 11b., D); neither was hydroxyproline content (Fig 11b., H) nor COL1A1 expression (Fig 11b., I). In summary, while a homogenous increase in confluent fibrosis was observed in both *DTG*s *vs. STG*s, a significant difference in fibrotic response was not apparent in either +DOX or –DOX groups indicating that FGFR2b ligands may play a more crucial role in the earlier stages of injury.

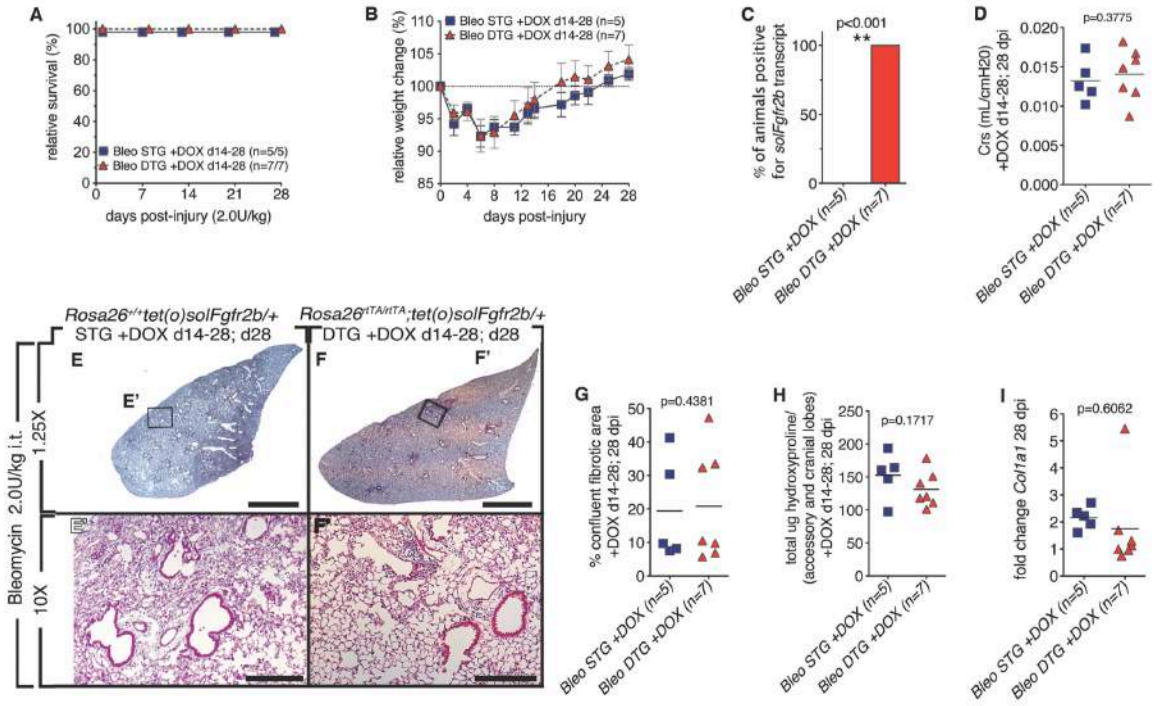

Figure 11b. Impact of FGFR2b signaling attenuation on fibrosis formation in bleomycin-injured mice

(*Rosa26*$^{rtTA/rtTA}$*;tet(O)sFgfr2b/+* (*DTG*) experimental and *tet(O)sFgfr2b/+* control (*WT*) mice were treated with bleomycin IT and fed doxycycline food from 14 dpi and analyzed at 28 dpi. (A) Survival curve. (B) Relative weight change. (c) Detection of soluble Fgfr2b transcript. (D) Compliance in control and experimental lungs at 28 dpi. (E and E') Low and high magnification bleomycin treated WT lungs at 28 dpi. Scale bar F and F': 2 mm; D' and E': 200 μm. Low and high magnification of DTG lungs at 28 dpi. (G) Quantification of percent fibrotic area in control and experimental lungs at 28 dpi. (H) Measurement of hydroxyproline content. (I) *solFgfr2b* expression (J) *Col1a1* expression.

Limitations: despite a moderate dose of bleomycin injury and the use of a homozygous *Rosa26*^{rtTA} driver, a very mild lung phenotype at 28 dpi in these mice resulted which may be due to their CD1 outbred background or inefficiency of this driver in the lung. More extensive injury along with earlier attenuation of ligand signaling may be necessary to detect a function for FGFR2b ligands after

bleomycin injury.

Bleomycin administered by Dr. Denise Al Alam at CHLA, protocol number 193-12; data analyses and presentation, hydroxyproline measurement, qPCR, sectioning, staining and quantification thereof, performed by me (BM).

4.7 *Fgfr2b*$^{+/-}$ mice incurred more bleomycin-induced fibrosis than *WT* mice

We hypothesized that the detrimental effects of attenuating FGFR2b ligand activity during fibrosis resolution may have been diminished due to the low level of bleomycin injury. Therefore, we treated *Fgfr2b*$^{+/-}$ (n=9) and corresponding littermate controls (n=8) with bleomycin (3.5U/kg) and monitored them for 28 days. This higher dose triggered more extensive fibrosis in survivors, and we hypothesized that it engaged endogenous FGF signaling. By 14 dpi, 30% of transgenic and 50% of *WT* mice were sacrificed because of significant weight loss and labored respiration. By day 28, 50% of *WT* mice (n=4) and 60% of *Fgfr2b*$^{+/-}$ mice (n=6) were in stable condition (Fig 3A). No difference was observed between bleomycin groups in terms of weight loss (Fig 12B) and hydroxyproline content (Fig 12G). However, bleomycin-treated *Fgfr2b*$^{+/-}$ mice showed statistically significant increase in fibrosis compared to WT mice as visualized by H/E staining (Fig 12D,E,D',E') and percent area of confluent fibrosis was quantified (Fig 12F). A decrease in lung function as compared to *WT* mice was also observed (Fig 12C). Thus upon a greater degree of injury, epithelial FGFR2b signaling appeared to be required for efficient repair.

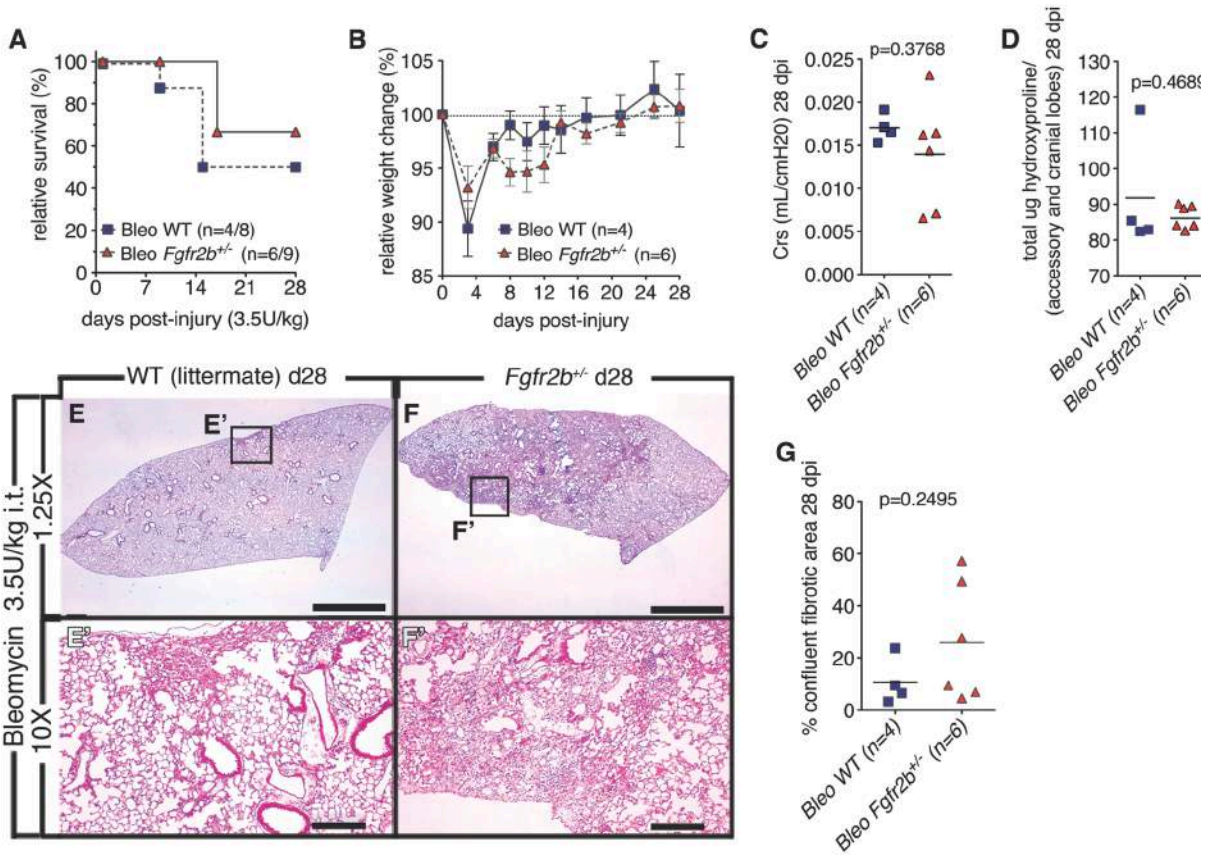

Figure 12. Decrease in endogenous *Fgfr2b* expression leads to increased fibrosis following bleomycin injury

(A) Survival curve. (B) Relative weight change. (C) Compliance in control and experimental lungs at 28 dpi. (D and D') Low and high magnification of control lungs at 28 dpi. (E and E') Low and high magnification of experimental lungs at 28 dpi. Scale bar D and E: 2 mm; D' and E': 200 μm. (F) Quantification of percent area of confluent fibrosis per section in control and experimental lungs at 28 dpi (G) Measurement of hydroxyproline content. *Bleomycin administered by Dr. Denise Al Alam at CHLA, protocol number 193-12; data analyses and presentation, hydroxyproline measurement, qPCR, sectioning, staining and quantification thereof, performed by me (BM).*

4.8 *Fgf7* knockout mice showed no hindrance in repair at 28 dpi

While FGF7, one of the main ligands acting primarily via epithelial FGFR2b, has been shown to protect against acute lung injury, whether it has an effect on fibrotic resolution remains controversial. Therefore, *Fgf7*$^{-/-}$ mice (n=14)

and genetic-background, age, and sex-matched, control mice (n=11) were given (3.5 U/kg) bleomycin and observed for 28 days. After five days, three control mice and three *Fgf7*$^{-/-}$ mice were sacrificed due to acute lung injury. However, at 10 dpi, the remaining seven control mice began to recover from the initial injury (63% survival at d28), while five of the remaining *Fgf7*$^{-/-}$ mice declined in health and were sacrificed at day 14 (43% survival at d28) (Fig 13A). Despite the initial increase in mortality in the bleomycin *Fgf7*$^{-/-}$ group, *Fgf7*$^{-/-}$ survivors (6 out of 14 mice treated initially) showed no difference in their ability to gain weight after injury compared to bleomycin *WT* controls (Fig 13B). In addition, the hydroxyproline content was not significantly different between both bleomycin groups (Fig 13D), and the difference in the amount of confluent fibrosis (Fig 13G) and lung function (Fig 13C) was insignificant suggesting that *Fgf7* may be dispensable for fibrosis resolution.

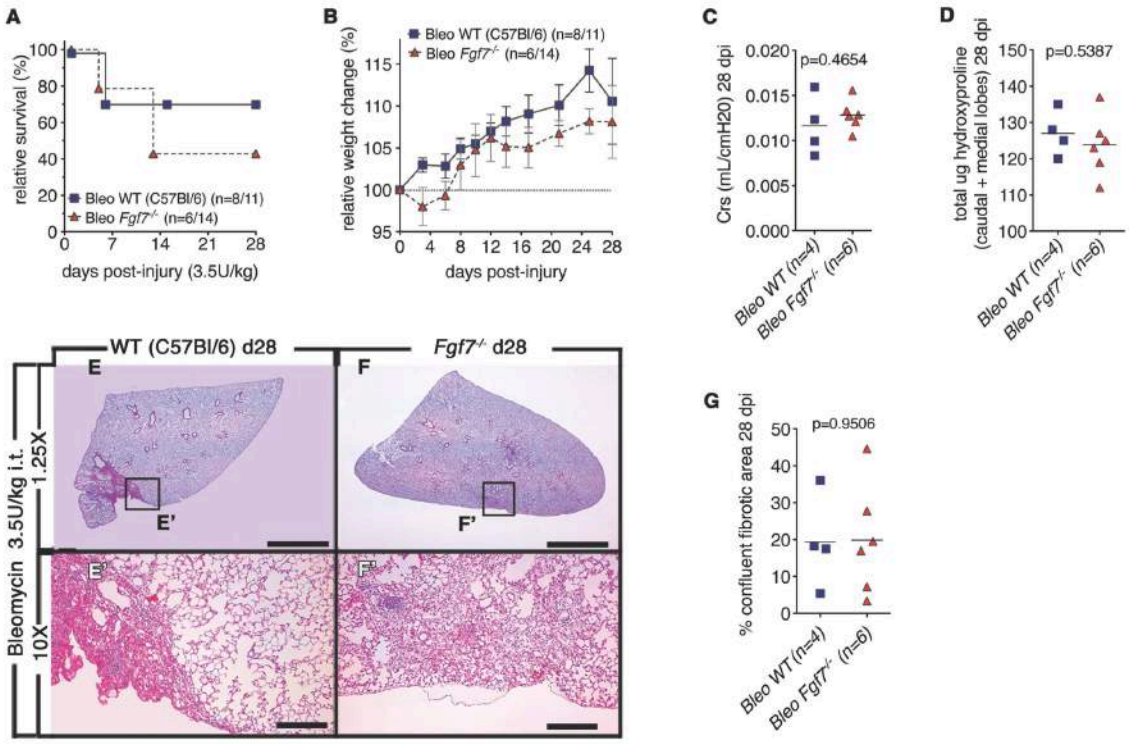

Figure 13. Absence of endogenous *Fgf7* had no significant impact on repair

(A) Survival curve. (B) Relative weight change. (C) Compliance in control and experimental lungs at 28 dpi. (D and D') Low and high magnification of control lungs at 28 dpi. (E and E') Low and high magnification of experimental lungs at 28 dpi. Scale bar D and E: 2 mm ; D' and E': 200 µm. (F) Quantification of percent area of confluent fibrosis in control and experimental lungs at 28 dpi (G) Measurement of hydroxyproline content. **Limitations:** experiment was not performed directly on littermate controls. *JLU Protocol 72/2012*

4.9 *Fgf7* knockout mice were more vulnerable to the acute lung injury phase of bleomycin due to elevated apoptosis

In complement to previous studies showing the beneficial effects of synthetic FGF7 (Palifermin) against a variety of acute lung injuries (Yildirim et al., 2010), we demonstrated that bleomycin treated *Fgf7*$^{-/-}$ mice were much more vulnerable to bleomycin injury than *WT*s. By 10 dpi, 5 of the 11 remaining *Fgf7*$^{-/-}$

bleomycin-treated mice continued to lose weight and showed labored breathing compared to the remaining 7 *WT* mice that began to recover (Fig 14A). By 14 dpi, these 5 mice were removed from the study and 3 of the recovering *WT*s were sacrificed for comparative analyses. The *Fgf7*$^{-/-}$ mice showed a drastic reduction in weight (Fig 14B) and significantly decreased lung function (Fig 14C). Moreover, hydroxyproline content was elevated (Fig 14D) as well as the extent of fibrosis visualized after H/E staining (Fig 14E,F) and quantified (Fig 14K). Interestingly, quantification of TUNEL staining (Fig 14K) indicated an increase in apoptosis not only in bleomycin-treated *Fgf7*$^{-/-}$ compared to bleomycin-treated WT mice (Fig 14I,J) but also in basal level apoptosis in *Fgf7*$^{-/-}$ saline controls as compared to saline treated *WT*s (Fig 14G,H). Our results suggest that while endogenous *Fgf7* expression is required immediately after bleomycin-induced lung injury it appears to be dispensable during fibrosis resolution.

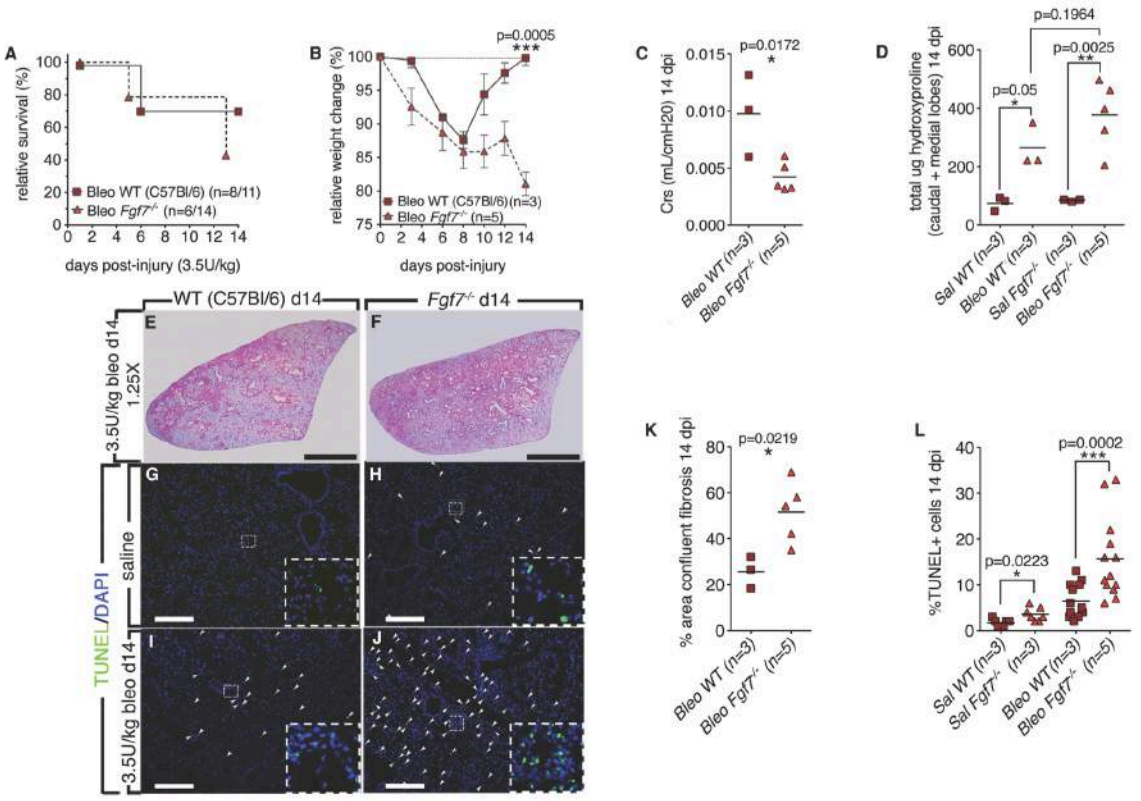

Figure 14. Absence of endogenous *Fgf7* led to increased acute lung injury following bleomycin administration

(A) Survival. (B) Relative weight change. (C) Compliance in control and experimental lungs at 14 dpi. (C) Quantification of percent area of confluent fibrosis in control and experimental lungs at 14 dpi. (D) Measurement of hydroxyproline content. (E) Low magnification of control lungs and (F) experimental lungs at 14 dpi. Scale bar E and F: 2 mm. (G) White arrows indicate TUNEL staining of saline controls, (H) saline *Fgf7*$^{-/-}$ (I) bleomycin-treated WT at d14 and (J) bleomycin-treated *Fgf7*$^{-/-}$ at d14. Scale bar G – J: 100 µm. (K) % area confluent fibrosis. (L) Quantification of TUNEL staining. **Limitations**: experimental controls were performed on C57Bl/6 mice. *Fgf7*$^{-/-}$ mice are 67% C57Bl/6, and 33% 129/Sv.

JLU Protocol 72/2012

4.10 Spontaneous resolution was significantly hindered in *Fgf10*$^{+/-}$ mice

In order to test whether endogenous *Fgf10* deficiency affects spontaneous repair, we treated *Fgf10*$^{+/-}$ (n=10) mice and littermate, *WT* controls (n=5) with bleomycin (3.5 U/kg). *Fgf10*$^{+/-}$ mice survival rate to 28 dpi was poor (60%) compared to *WT* mice (80%) (Fig 15A). However, *Fgf10*$^{+/-}$ survivors recovered their weight to a similar extent as *WT* mice (Fig 15B). Although hydroxyproline accumulation was not significantly different between bleomycin groups (Fig 15D), *Fgf10*$^{+/-}$ mice showed an increase in collagen (*Col1a1*) expression (Fig 15H). Moreover, *Fgf10*$^{+/-}$ survivors showed worse lung function (Fig 15C) and more fibrosis by H/E (Fig 15E,F,E',F') and evaluation of percent area of confluent fibrosis (Fig 15D). Overall, *Fgf10*$^{+/-}$ mice suffered from inefficient repair 28 days after bleomycin injury as demonstrated by decreased lung function and increased fibrosis.

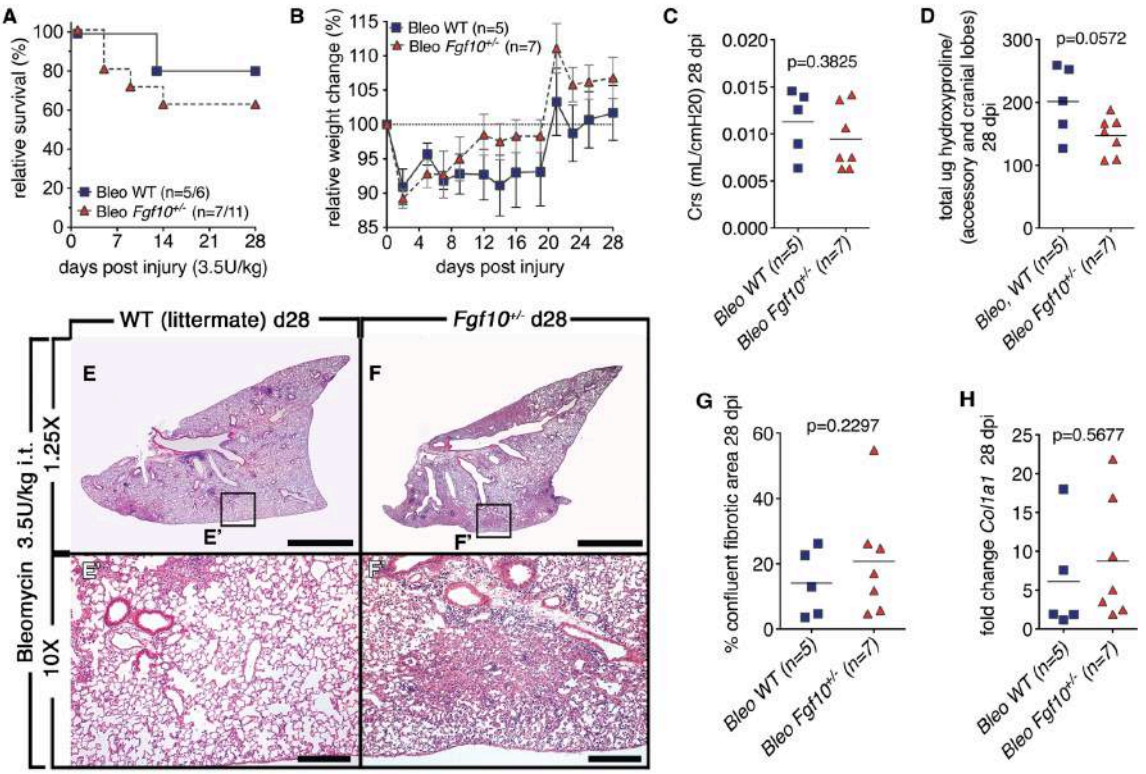

Figure 15. Decrease in endogenous *Fgf10* expression led to increased fibrosis following bleomycin injury

(A) Survival curve. (B) Relative weight change. (C) Compliance in control and experimental lungs at 28 dpi. (D) Measurement of hydroxyproline content. (E and E') Low and high magnification of control lungs at 28 dpi. (F and F') Low and high magnification of experimental lungs at 28 dpi. Scale bar E and F: 2 mm; E' and F': 200 µm. (G) Quantification of percent area of confluent fibrosis in control and experimental lungs at 28 dpi (H) Fold change of *Col1a1* expression. **Limitations**: in order to evaluate whether endogenous FGF10 signaling is critical for repair, an earlier time point between 7 and 14 dpi must be evaluated.

Bleomycin administered by Dr. Denise Al Alam at CHLA, protocol number 193-12; data analyses and presentation, hydroxyproline measurement, qPCR, sectioning, staining and quantification thereof, performed by me (BM).

4.11 Fibrotic foci of bleomycin-injured *Fgf10*$^{+/-}$ mice are more active than corresponding *WT* littermate control lesions

Given that spontaneous resolution of fibrotic lesions was most impaired in *Fgf10*$^{+/-}$ mice, we performed immunohistochemical and gene expression analyses on samples collected at 28 dpi (n=3/group). The fibrotic foci of *Fgf10*$^{+/-}$ bleomycin-treated lungs displayed markedly increased proliferation. 12% of cells in the fibrotic foci of *Fgf10*$^{+/-}$ bleomycin treated lungs were Ki67 positive vs. just 4% in WT fibrotic foci (Fig 16A–C). In addition, cells present in fibrotic foci of *Fgf10*$^{+/-}$ mice also expressed lower levels of the epithelial marker E-Cadherin/Cdh1 (Fig 16D–F) and higher levels of α-Smooth muscle actin (SMA) (Fig 16G–I) suggesting that fibrotic areas of *Fgf10*$^{+/-}$ mice were less resolved than those of bleomycin-treated *WT* littermate controls at 28 dpi. Moreover there was a trend towards increased TGFβ1 signaling in *Fgf10*$^{+/-}$ mouse lungs. Expression of negative regulator *Smad7* was decreased (Fig 16J) while transcriptional target *Smad3* was increased (Fig 16K).

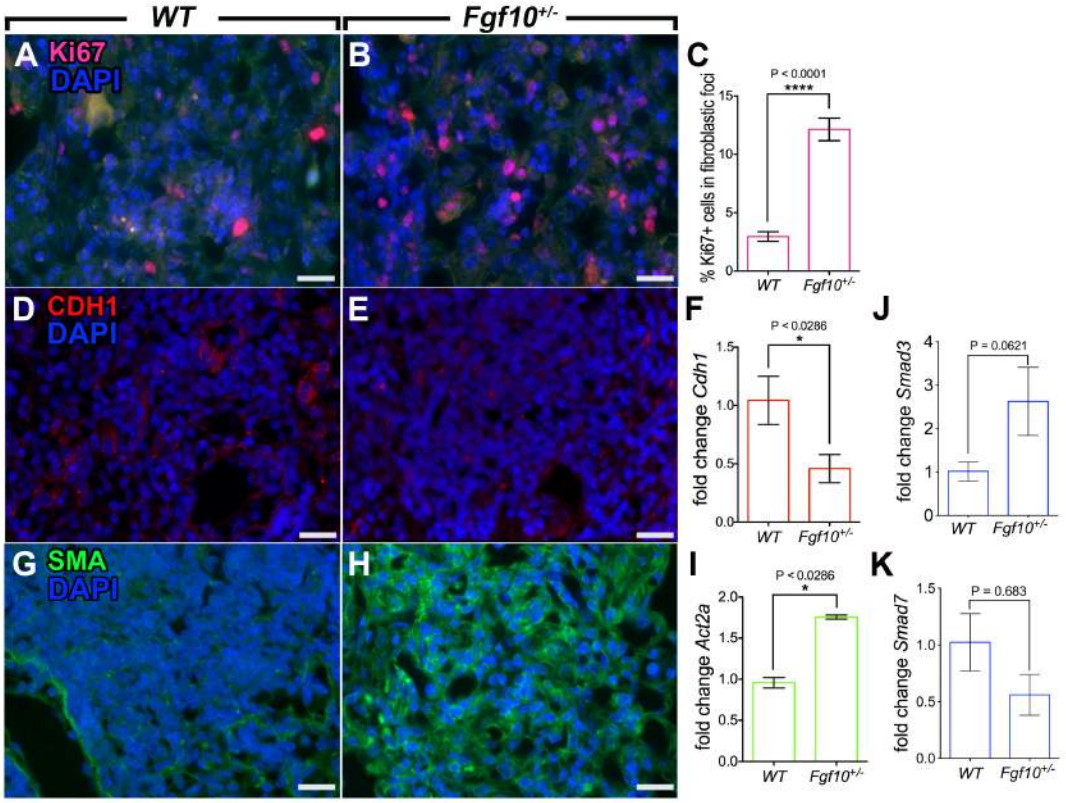

Figure 16. Decreased *Fgf10* expression leads to persistence of fibrotic lesions with increased proliferation, decreased epithelial markers, and increased smooth muscle actin after bleomycin injury.

(A) Immunolocalization of Ki67 in fibrotic areas of WT and (B) *Fgf10*$^{+/-}$ bleomycin-treated mice and (C) quantification (n=3 biological samples/group; 6 fibrotic areas/sample). (D) Immunolocalization of Cadh1 in fibrotic areas of WT and (E) *Fgf10*$^{+/-}$ bleomycin-treated mice and (F) mRNA expression level by qPCR of *Cadh1* (fold change; n = 3/group). (G,H) Immunolocalization of SMA in fibrotic areas of WT and *Fgf10*$^{+/-}$ bleomycin-treated mice. (I) mRNA expression level by qPCR of *Acta2* (*Sma*) (fold change; n = 3/group). mRNA expression of *Smad3* (J) and *Smad7* (K). **Limitations**: qPCR was performed on whole lung homogenates, not particular areas of fibrosis for example via laser-capture microdissection. In addition assays at the protein level for TGFβ1 must be performed. *Bleomycin administration kindly provided by Dr. Denise Al Alam at CHLA, protocol number 193-12*

4.12.1 Primary culture of human lung fibroblasts express FGF ligands and receptors

Relative expression levels were measured by qPCR in donor (n=3) and IPF (n=3) primary culture fibroblasts (Fig 17). Relative to *FGF1* expression, *FGF7* expression was expressed approximately 200-fold more than *FGF1* in donor and 125-fold more than *FGF1* in IPF. *FGF10* was expressed approximately 12-fold for than *FGF1* in donor and 14-fold more than *FGF1* in IPF fibroblasts (Fig 17A,B). In addition, receptor expression was analyzed relative to *FGFR1b* expression in both Donor and IPF fibroblasts (Fig 17A'B'). In donor samples, *FGFR1c* was expressed approximately 70-fold more the *FGFR1b,* while *FGFR2c* expression was minimal (0.1 fold relative to *FGFR1b*) and *FGFR2b* was also very minimally expressed (0.0007 fold). While normally such low expression would be considered background, the receptor was undoubtedly present when compared to e-cadherin (*ECAD*), which was absent in primary cultures (Fig 17A'). In IPF samples, *FGFR1c* was expressed approximately 80-fold more the *FGFR1b,* while *FGFR2c* expression was minimal (0.1 fold relative to *FGFR1b*) and *FGFR2b* was also very minimally expressed (0.0006 fold). *ECAD* was absent (Fig 17B'). Both IPF and Donor fibroblasts exhibited similar expression patterns for these ligands and receptors. No significant difference between gene expression levels in donor and IPF samples were found.

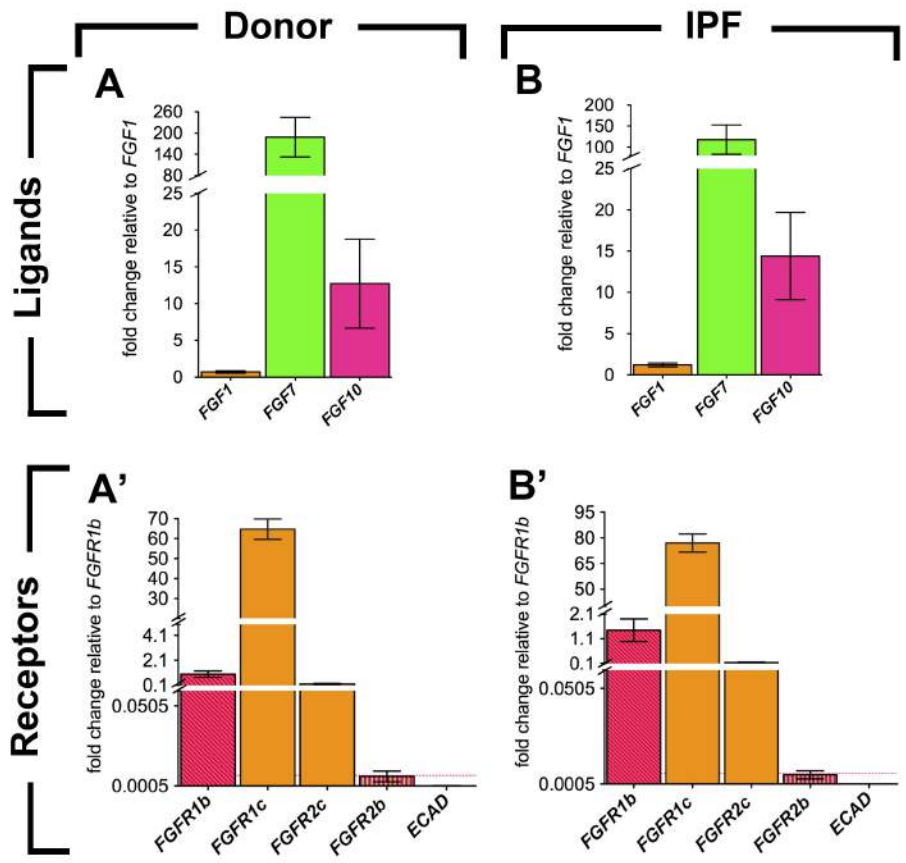

Figure 17. Primary culture of human lung fibroblasts express *FGF* ligands and receptors

(A) *FGF7* and *FGF10* expression relative to *FGF1* in donor samples and (B) IPF; n=3/group. (A') *FGFR1c, FGFR2c, FGFR2b* and *ECAD* expression relative to *FGF1b* in donor samples and (B') IPF; n=3/group. *PGBD* was used as a reference gene for all experiments.

Limitations: fold change calculation were based on an arbitrary calibrator selection of *FGF1* for ligands and *FGFR1b* for receptors.

4.13 Impact of rhFGF10 treatment on donor and IPF fibroblasts

4.13.1 IPF fibroblasts exhibit robust proliferation response to FGF10

In order to investigate whether human fibroblasts respond to FGF10, immunostaining was performed on primary culture of human lung fibroblasts for different markers and results were quantified. Fibroblasts from (n=3) donors and (n=3) IPF patients were counted, seeded and cultured to 50 – 80% confluency on 8 well chamber slides at which point they were serum-starved overnight, and treated with 200 ng/mL rhFGF10 the next day. 18hrs later, cells were stained for Ki67, a marker for cell proliferation (Fig 18a). Both donor and IPF fibroblasts responded by proliferating at an accelerated rate compared to non-treated cells (Fig 18a., A – A'; B – B'). However, donor treated fibroblasts proliferated less than IPF fibroblasts (Fig 18a., C,D). Interestingly, 2.1% (±) 2.53 of serum-starved donor cells were Ki67 positive and 3.13% (±) 2.44 of IPF cells (p=0.0446) (Fig 18a., E). However, after adding FGF10, IPF fibroblasts responded by with an average proliferation rate of 19.7% (±) 13.12 while donors responded with an average of 7.1% (±) 5.53; (p=0.0004) (Fig 18E).

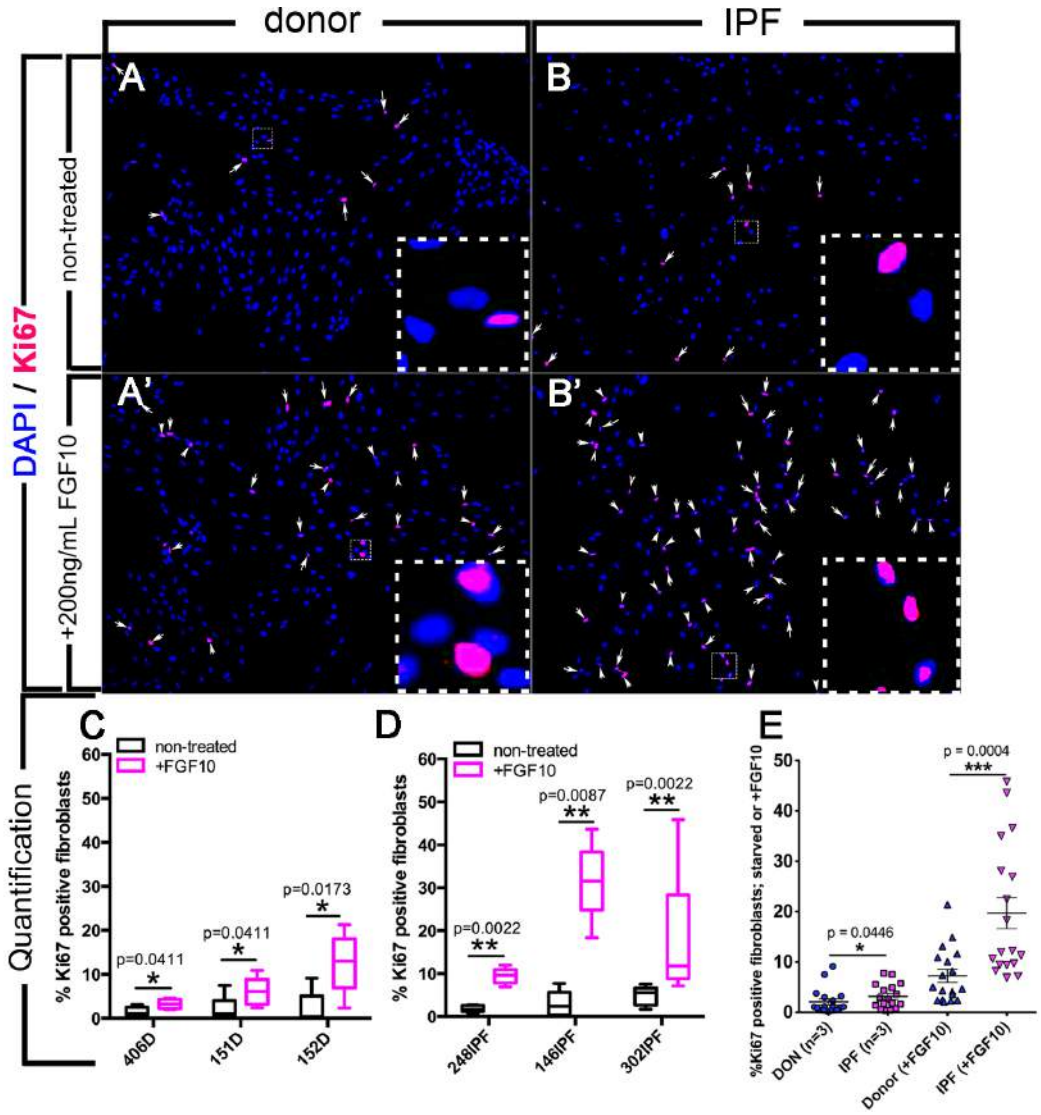

Figure 18a. IPF fibroblasts exhibit robust proliferation response to FGF10 compared to both non-treated IPF and donor treated cells

(A) White arrows indicate immunolocalization of Ki67 (pink), DAPI (blue) in donor fibroblasts and (B) IPF fibroblasts. (A') 200ng/mL rhFGF10 was added to donor and (B') IPF cultures and cells were stained 18 hours later. (C) FGF10 treatment increased the number of Ki67 positive fibroblasts in donor samples (n=3) and (D) IPF (n=3). (E) Average percent of proliferating cells was more robustly increased in FGF10 treated IPF samples than donors. **Limitations:** shorter treatment and

analyses of downstream targets should be performed at the protein level in order show more direct evidence of the cell responding to FGF10.

4.13.1.1 FGF1 or FGF10 treatment results in p-ERK activation in MLE-12 cells

In order to confirm the activity of the growth factors in cell culture experiments, we tested the activity of FGF1 and FGF10 in culture 10, 30, and 60 min after treatment of mouse lung epithelial cells (MLE-12). Compared to untreated, serum starved cells, FGF1 strongly activated p-ERK signaling after just 10 min. FGF10 also activated p-ERK but to a lesser extent than FGF1 (Fig 18b., A).

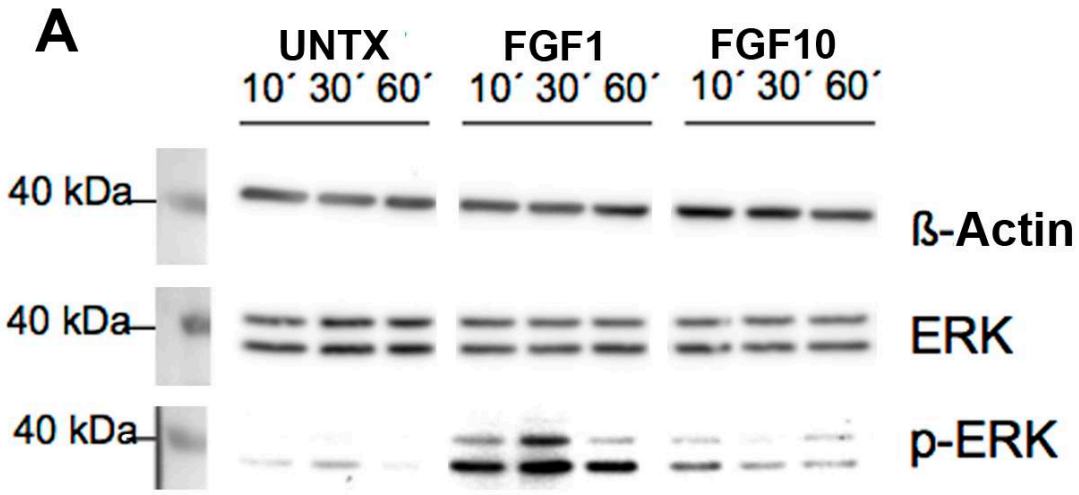

Figure 18b. MLE-12 cells respond to FGF1 and FGF10 treatment

FGF1 and FGF10 (both 200 ng/mL) activated p-ERK in MLE-12 cells compared to serum-starved untreated cells.

Limitations: While this experiment confirms the activity of FGF1 and FGF10 in culture, cell culture experiments with IPF and Donor cells were analyzed either the next day after treatment or after 3 days continuous treatment.

Blot kindly performed by Dr. Ingrid Henneke; experimental design, and data presentation performed by me (BM).

4.13.2 FGF10 treatment of IPF fibroblasts led to increased FGF7 expression

IPF fibroblasts were starved overnight and treated with 200ng/mL FGF10 treatment (n=6) donor and (n=5) IPF patients. 18 hours later, RNA was harvested from cells and expression of *FGF7* was analyzed. While expression of *FGF7* did not change in treated donor cells, there was a trend towards an increase in *FGF7* expression in treated IPF cells (Fig 19A). Immunofluorescence for FGF7 also indicated an increase at the protein level (Fig 19B – C).

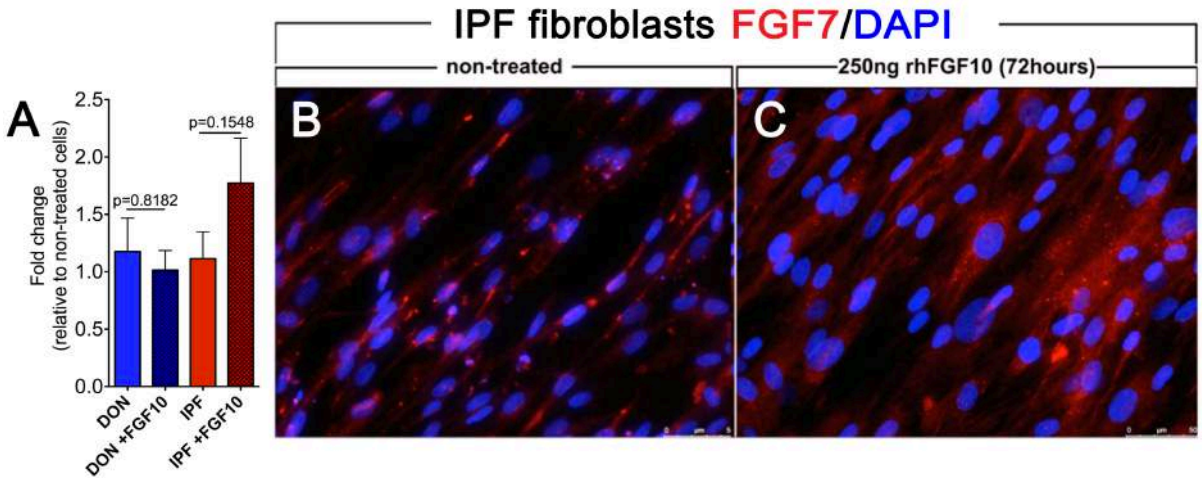

Figure 19. FGF10 treatment resulted in a trend towards an increase in FGF7 expression by IPF fibroblasts

qPCR results show trend towards increase in expression of *FGF7* in IPF fibroblasts 18 hours after 200ng/mL FGF10 treatment (n=6) donor and (n=5) IPF patients (A). Immunofluorescence for FGF7 illustrated increase in staining in IPF fibroblasts treated with 200ng/mL FGF10 (B – C).

4.13.3 Impact of FGF10 treatment of IPF fibroblasts on *FGFR2b* expression

Again, IPF fibroblasts were starved overnight and treated with 200ng/mL FGF10 treatment (n=4) donor and (n=4) IPF patients. 18 hours later, RNA was harvested from cells and expression of *FGFR2b* was analyzed. There was a trend towards an increase in *FGFR2b* expression in both donor and IPF FGF10 treated fibroblasts (Fig 20A). Immunofluorescence for FGFR2 protein, Bek, indicated an increase at the protein level in both donor (Fig 20B – B') and IPF cells 18 hours after FGF10 treatment (Fig 20C – C').

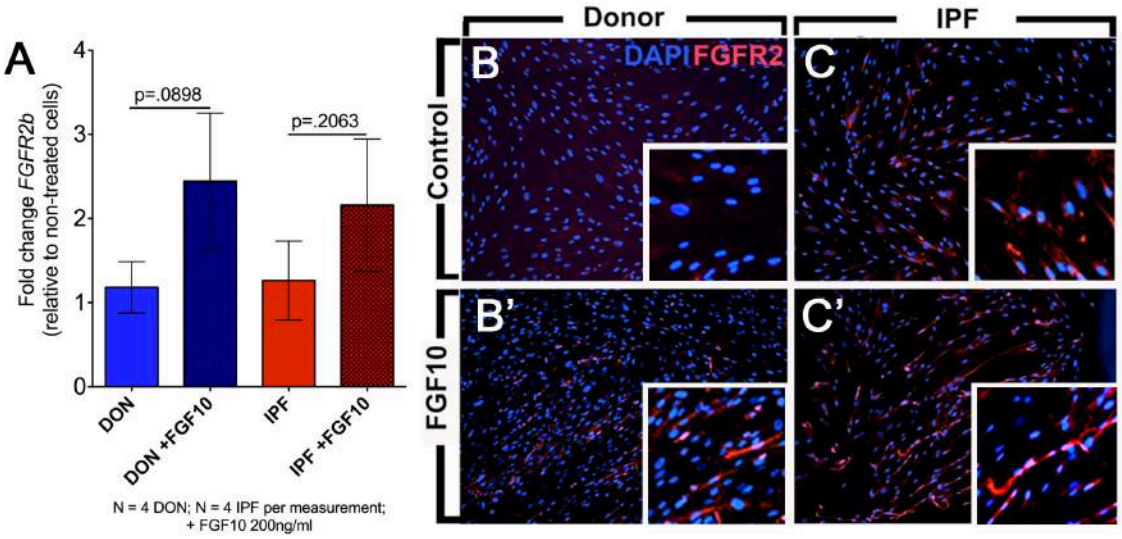

Figure 20. FGF10 treatment results in a trend towards an increase in FGFR1b and FGFR2b expression in IPF fibroblasts

qPCR results show trend towards increase in expression of *FGFR1b* in IPF fibroblasts (A) and *FGFR2b* (B). Immunofluorescence for Bek (FGFR2 antibody) illustrated increase in Bek staining in donor and IPF fibroblasts treated with 200ng/mL FGF10. **Limitations:** Bek antibody is not isoform specific, thus the antibody could be detecting both c and b isoforms of FGFR2.

4.13.4 FGF10 treatment of Donor or IPF lung fibroblasts may result in an increase of lipid droplets

Given the importance of lipofibroblasts in maintaining surfactant homeostasis in the adult lung, Oil Red O staining was performed on IPF and donor primary cultures of lung fibroblasts (Fig 21A – D). 200ng/mL FGF10 treatment resulted in denser lipid droplet formation and possible and increase in lipid droplet formation (Fig 21A' – D').

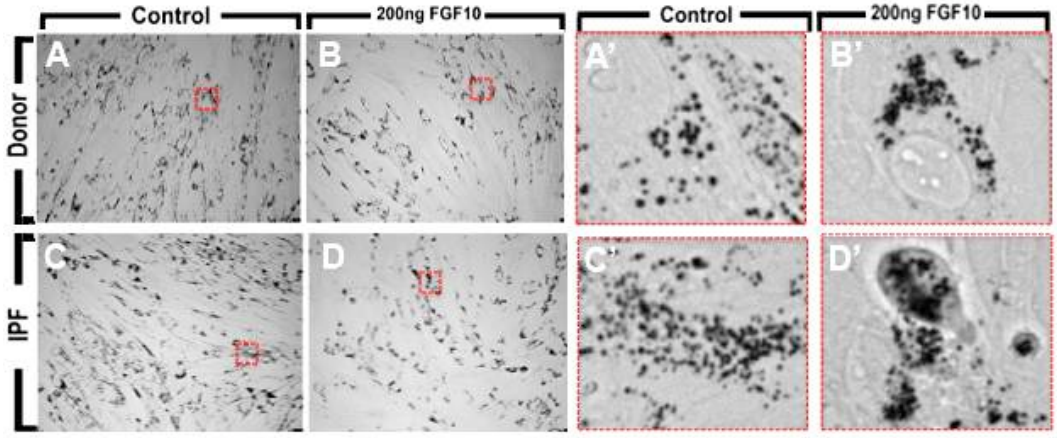

Figure 21. FGF10 treatment of donor or IPF lung fibroblasts may result in an increase and denser localization of lipid droplets

20X Oil Red O stain (black) for lipid droplets in Donor (A) and IPF (C) primary cultures, and 18 hours after 200ng/mL rhFGF10 treatment in Donor (B) and IPF (D'), (A' – D') 40X.

Limitation: results were not quantified; counterstaining with hemotoxylin or collection of dye from cell supernatant and O/D measurement would give a more conclusive result.

4.14 FGF10 and rosiglitazone treatment of IPF cells pushed cells towards a lipofibroblast-like phenotype

Rosiglitazone is a synthetic agonist of the peroxisome proliferator activator receptor gamma (PPARγ), a gene that is known to inhibit profibrotic phenotypes in human lung fibroblasts and bleomycin-induced pulmonary fibrosis (Milam et al., 2008). Human IPF fibroblasts were plated at low density and treated each day for 3 days with either 20 – 100uM Rosiglitazone, 500 or 200ng/mL FGF10, or both. 72 hours later, cells were either immunostained or RNA was harvested for gene expression analyses in order to test whether FGF10 inhibits the profibrotic phenotype of IPF fibroblasts and whether it acts synergistically with PPARγ pathway.

4.14.1 Rosiglitazone and FGF10 treatment decreased the size of SMA+ IPF fibroblasts

Both FGF10 and Rosiglitazone treatment of human IPF lung fibroblasts significantly reduced the size of SMA+ cells (Fig 22). Untreated fibroblasts were displayed many filopodia projections and had an average size of 2000um^2 (Fig 22A – A', E). FGF10 treated SMA+ cells were smaller and rounder (Fig 22B – B') with few projections and reduced to 1000um^2 in size (Fig 22E). Rosiglitazone treated SMA+ cells were also round (Fig 22C – C'), as well as cells treated with both factors (Fig 22D – D'). Rosiglitazone alone, and when added together with FGF10 reduced SMA positive cell size to approximately 200um^2 (Fig 22E). While size was reduced, neither the average fluorescence intensity of the SMA staining (Fig 22F) nor the number of SMA+ cells (Fig 22G) was significantly reduced in any of the treated groups compared to the untreated group. Interestingly, FGF10 treatment resulted in a trend towards a decrease in SMA expression while Rosiglitazone had no effect (Fig 22H). When cells were treated with both, no change was observed (Fig 22H).

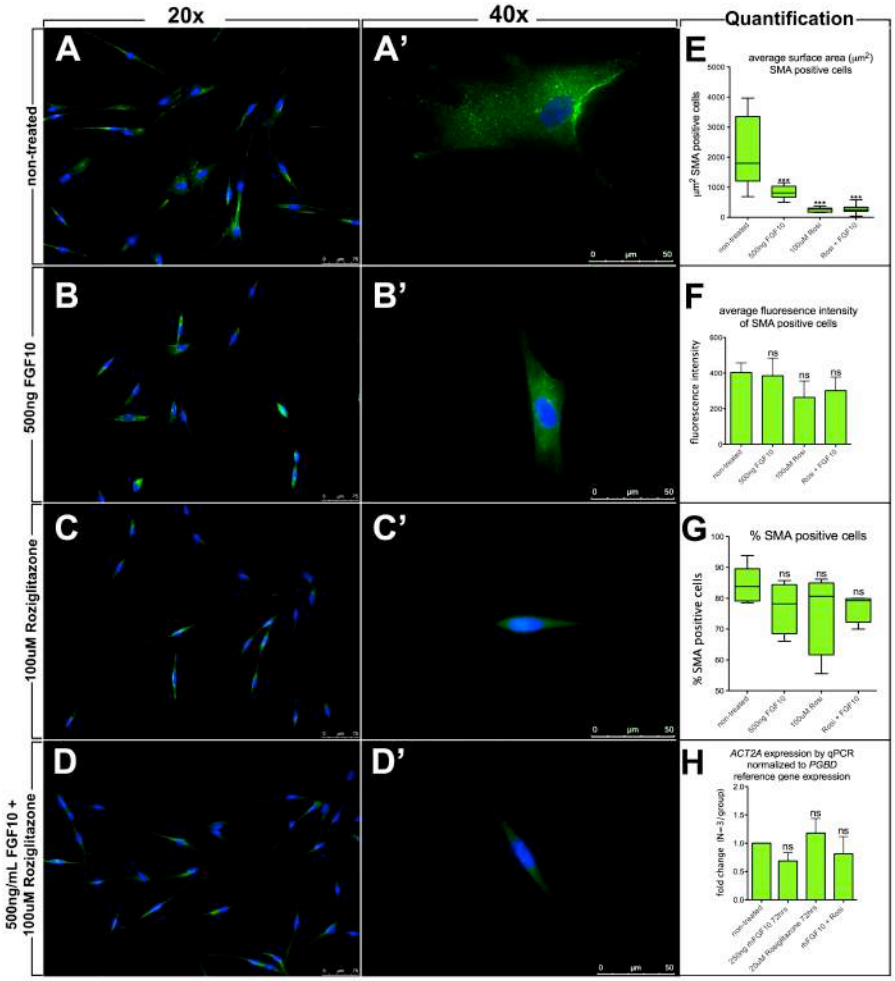

Figure 22. Rosiglitazone and FGF10 treatment decreased the size of SMA+ IPF fibroblasts

(A – A') Untreated IPF fibroblasts at 20 and 40X, (B – B') 500ng/mL FGF10 treated (C – C') 100uM Rosiglitazone treated (D – D') 500ng/mL FGF10 and 100uM Rosiglitazone treated cells. (E) Average surface area of SMA+ cells, (F) fluorescence intensity of SMA+ cells, (G) percent of cells SMA+, (F) *ACT2A* (SMA) expression fold change normalized to non-treated cells with *PGBD* as a reference gene. **Limitations:** results were only observed when cells were cultured at low density. A shorter time period after treatment followed by protein analyses is necessary.

4.14.2 Rosiglitazone and FGF10 treatment increased *C/EBPα* expression

IPF fibroblasts were treated with either 250ng/mL of rhFGF10 or 20uM of Rosiglitazone, or both for 3 days to test whether treatment could induce the expression of adipogenesis marker, *C/EBPα* (Martis et al., 2006; Rehan et al., 2006). *C/EBPα* was induced by FGF10 (Fig 23E), however the percent of *C/EBPα*+ cells did not change (Fig 23F). Rosiglitazone also induced the expression of *C/EBPα* (Fig 23E), and the number of *C/EBPα* positive cells (Fig 23F). Interestingly, treatment with both Rosiglitazone and FGF10 resulted in a significant increase in *C/EBPα* cells (Fig 23F).

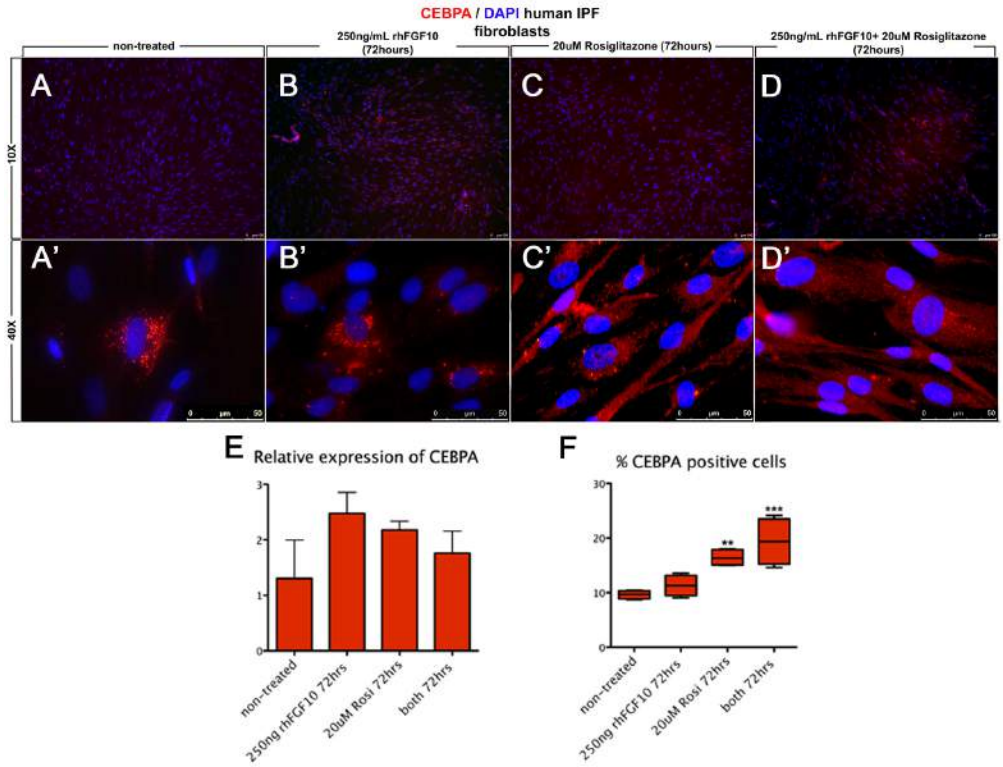

Figure 23. Rosiglitazone and FGF10 treatment increased *C/EBPα* expression

Immunofluorescence of *C/EBPα* (red) and DAPI (blue) on human IPF fibroblasts at 10X and 40X magnification on (A – A') untreated (B – B') 250ng/mL rhFGF10, (C - C') 20uM Rosiglitazone (D – D') both. Quantification of *C/EBPα* expression at the RNA level (E) and percent *C/EBPα*+ cells (F). While *C/EBPα* mRNA was not significantly increased in IPF cells treated with FGF10 and/or Rosiglitazone, the percent of *C/EBPα*+ cells as measured by immunofluorescence was significantly increased.

4.14.3 Impact of Rosiglitazone and FGF10 on *FGFR1b* expression

Human IPF fibroblasts were treated with either 250 ng/mL of rhFGF10 or 20 uM of Rosiglitazone for 3 days to test whether FGF10 or rosiglitazone could induce the expression of *FGFR1*-IIIb. Cells treated with FGF10 showed a slight reduction in *FGFR1*-IIIb (Fig 24E) and *FGFR1*-IIIc (Fig 24F) after treatment at the RNA level. However, immunostaining suggested increased FGFR1 receptor at the protein level (Fig 24B – B') compared to non-treated controls. Rosiglitazone treatment resulted in a slight increase in *FGFR1*-IIIb (Fig 24E) and *FGFR1*-IIIc (Fig 24F) at the RNA level, however immunostaining, revealed less FGFR1 (Fig 24C – C') at than untreated cells or cells treated with FGF10. Lastly, cells treated with both, also revealed in a slight increase in *FGFR1*-IIIb (Fig 24E) and no change in *FGFR1*-IIIc (Fig 24F) at the RNA level, and also an increase in FGFR1 at the protein level (Fig 24D – D').

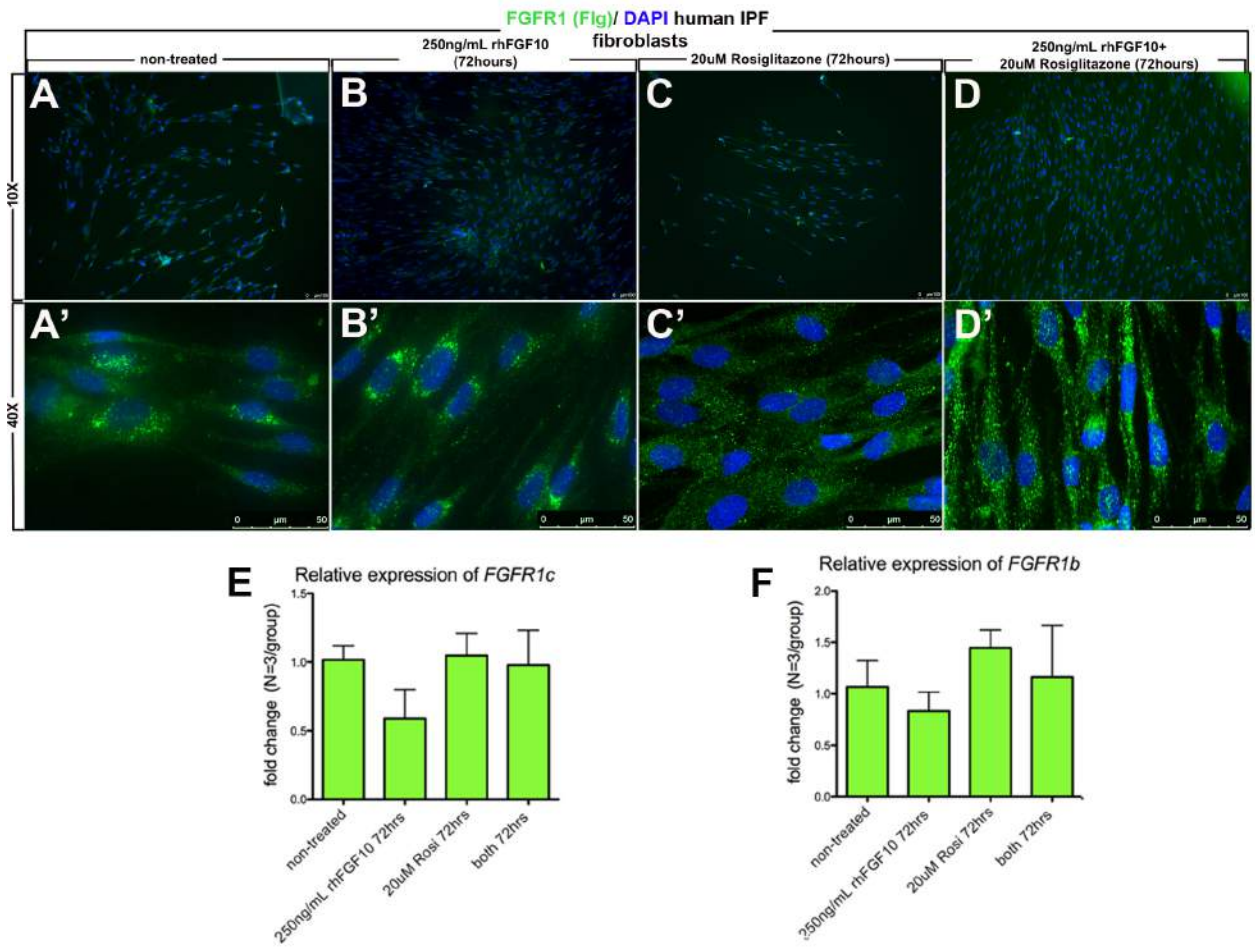

Figure 24. Rosiglitazone resulted in trend towards increased *FGFR1* expression.

Immunofluorescence of FGFR1/Flg (green) and DAPI (blue) on human IPF fibroblasts at 10X and 40X magnification on (A – A') untreated (B – B') 250ng/mL rhFGF10, (C - C') 20uM Rosiglitazone (D – D') both. Quantification of *FGFR1*-IIIb expression (E) and *FGFR1*-IIIc expression at the RNA level (F).

Limitation: Immunofluorescence study is limited since Flg antibody detects both c and b isoforms of FGFR1.

4.15 FGF10 hinders TGF-β signaling in primary cultures of human lung fibroblasts

Given that TGF-β signaling is involved in the transition of lung fibroblasts to become activated collagen and ECM secreting 'myofibroblasts'; a cell type strongly implicated in the formation of UIP lesions in IPF, we tested whether FGF10 treatment of human lung fibroblasts could alter TGF-β signaling and the level of SMA expression.

4.15.1 FGF10 treatment decreased TGF-β signaling

Pre-treatment of IPF human fibroblasts (n=3) with 250 ng/mL rhFGF10 one hour before 4 ng/mL TGF-β treatment resulted in significantly reduced TGF-β signaling as indicated by reduction of pSMAD3 staining (Fig 25A-B). pSMAD3, a downstream target of TGF-β was slightly reduced in FGF10 treated cells compared to untreated cells as well as by approximately 80% when administered one hour before TGF-β stimulation (Fig 25C).

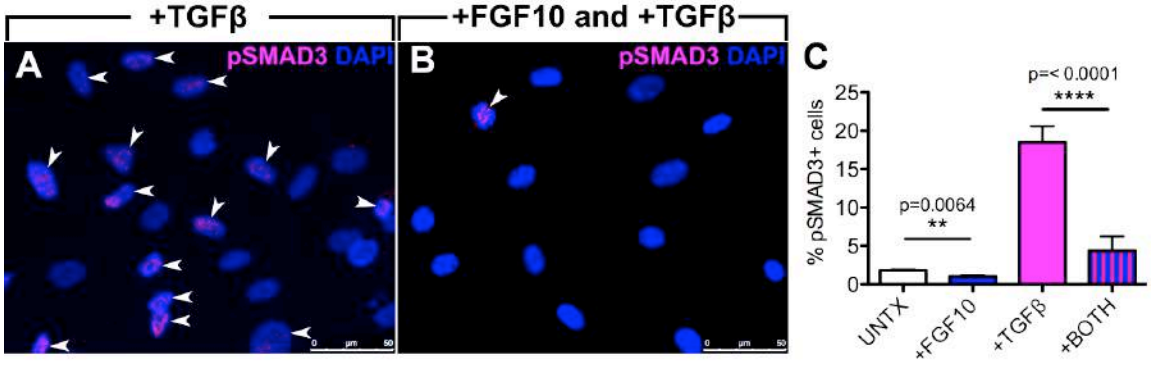

Figure 25. FGF10 treatment decreased TGF-β signaling

Immunofluorescence for pSMAD3 (pink) and DAPI (blue) on human IPF fibroblasts at 40X magnification one hour after (A) 4 ng/mL TGF-β treatment and (B) 250 ng/mL rhFGF10 followed by 4ng/mL TGF-β. (C) pSMAD signal in FGF10 pre-treated cells was slightly reduced FGF10 treated cells compared to untreated cells and by approximately 80% when administered one hour before TGF-β stimulation.

4.15.2 FGF10 treatment decreases number of high SMA+ cells

IPF fibroblasts expressing ‘high’ levels of SMA constituted approximately 5% of the total number of DAPI stained cells in culture (Fig 26A,E). When 250 ng/mL of FGF10 was added and SMA staining was performed one hour later, FGF10 treatment reduced the number of “high” SMA positive cells to approximately 3% (Fig 26B,E). This finding corresponded to a 30% reduction in the overall intensity measured by mean gray values on the red channel using Leica software (Fig 26F). Adding 4 ng/mL TGF-β to culture medium increased the percentage of ‘high’ SMA+ cells to approximately 9% (Fig 26C,E). Pre-treating cells with FGF10 reduced the number of high positive SMA cells to around 5% or the level of the untreated (Fig 26D,E). This result also corresponded to the measured mean gray values, as pretreatment reduces intensity of SMA staining by approximately 27% (Fig 26F).

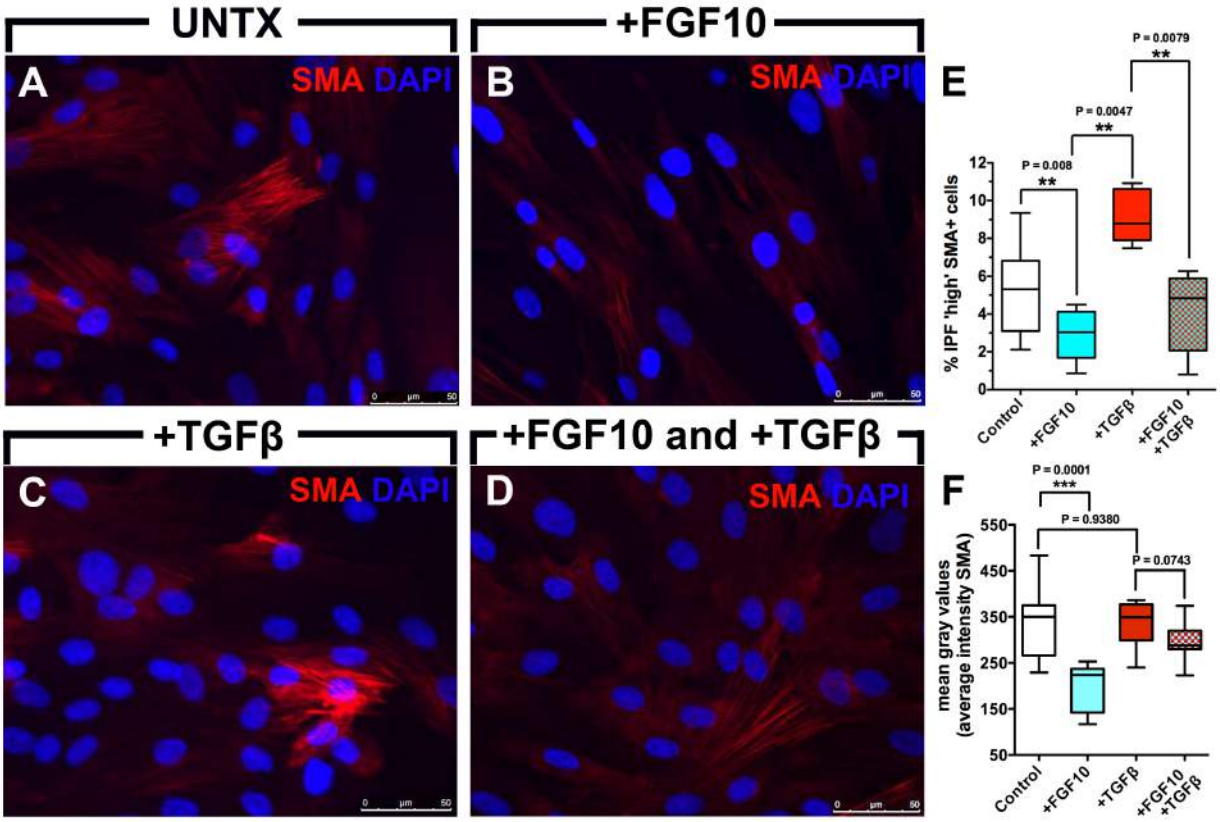

Figure 26. FGF10 treatment decreases number of SMA+ fibroblasts

Immunofluorescence for SMA (red) and DAPI (blue) on human IPF fibroblasts at 40X magnification (A) without treatment (B) one hour after FGF10 treatment (C) one hour after 4ng/mL TGF-β treatment and (D) 250ng/mL rhFGF10 pre-treatment followed by 4ng/mL TGF-β. (E) Quantification of 'high' SMA+ cells in immunofluorescent samples. (F) Quantification of red channel staining intensity

Part 5. Discussion

5.1 Analyzing the resolution of bleomycin-induced fibrosis in mice may be more relevant to IPF than analyses at earlier stages

Bleomycin-induced lung injury in rodents is the most used and best characterized model for IPF; however, just as a cure for IPF is still lacking, relevant translational conclusions generated by this model are also scarce; perhaps partly due to the heterogeneity of the animals in response to the drug (Fig 6). While animal studies have traditionally focused on either prophylactic or early effects of drugs, the focus has recently shifted to analyses at later stages. Bleomycin-mediated DNA destruction results in AEC1 and 2 cell death and a subsequent acute inflammatory response that continues until approximately 14 dpi. Thereafter, inflammation wanes and peribronchial fibrotic lesions form, contributing to mortality after 14 dpi. Unlike UIP lesions, bleomycin-induced lesions resolve spontaneously at 21-28 dpi (Moeller et al., 2008). Therefore, comparing the effect of endogenous gene dosages or drugs on the resolution of UIP-like lesions in mice may be more clinically relevant than identifying targets that have a positive impact when administered before 14 dpi. However, given that the height of injury is occurs between 7 and 14 dpi, it may be useful to compare experimental groups at two given time points (i.e. 14 and 28 dpi) in order to more accurately assess the extent of injury and recovery especially since it is not currently possible to measure the extent of injury without sacrificing the animal. Although the molecular mechanism of spontaneous resolution after bleomycin injury in mice is unknown, we showed that endogenous *Fgf10* is critical for bleomycin-induced fibrotic repair and that recovery was not perturbed in *Fgf7*$^{-/-}$ animals surviving until 28 dpi. However, additional analyses at an earlier time point (7 and 14 dpi) will provide more conclusively whether FGF10 is involved in the active repair of bleomycin-induced lesions.

5.2 FGF signaling is activated in bleomycin-treated mice and attenuated in end-stage IPF patients.

Microarray gene expression analyses of IPF fibrotic septa compared against normal donor septa showed that *FGF7* was upregulated while *SPRY2* was downregulated (Fig 4). This indicated that while ligands were likely expressed in IPF fibrotic septa, downstream signaling was muted. While *FGF10* but not *FGF7* was upregulated in end-stage IPF whole lung homogenates, a downregulation in both the receptors and downstream targets of *FGF7* and *10* including: *FGFR1b, FGFR2b, SPRY2, SPRY4* and *ETV4* were detected, suggesting that expression of FGF signaling genes; critical for lung repair, were diminished in IPF patients (Figs 5,7a). Interestingly, downregulation of ligands *FGF2* and *FGF9* and upregulation of their main receptors *FGFR2c* and *FGFR1c* were observed. Copy number increases as well as mutations leading to gain of function of c-isoforms have been implicated in the progression of tumorgenesis in many different cancers, with FGFR1c specifically implicated in lung cancer (Katoh and Katoh, 2009a; Katoh and Nakagama, 2013). Furthermore, an isoform switch from FGFR2-IIIb to IIIc in epithelial cells have has also been observed in lung cancers (Dutt et al., 2011). Therefore, a gain of c-isoform expression in IPF lungs along with a loss of b-isoform expression may contribute to the persistence of UIP lesions. Moreover, reduced FGF signaling could be due to several factors including distorted extracellular matrix architecture due to UIP lesions, aberrant expression of HSPGs (Yue et al., 2013), as well as diminished expression of both *FGFR2-IIIb* on hyperplastic AEC2 cells and *FGFR1-IIIb* on activated myofibroblasts. Taken together, an imbalance of FGF signaling could play an important role in the pathogenesis of IPF.

To further explore the potential role of FGF signaling on fibrotic resolution, we examined the expression of the same ligands, receptors and targets in bleomycin-treated wild type mice at different stages after injury. While FGF signaling was not activated at 7 dpi, the transcriptomic signature at 14 dpi suggested a significant upregulation of FGF signaling in both the epithelium and mesenchyme. By 21 dpi, a decrease in mesenchymal FGF signaling associated

with maintenance of epithelial FGF signaling is observed. Interestingly, the increase in FGF signaling (at 14 dpi) is not concomitant, but rather precedes the fibrosis resolution phase (21 dpi onwards) suggesting that FGF signaling is a driving force in fibrotic resolution. Further analyses of FGF hypomorphs at 14 dpi will be needed in order to determine whether these mice incur greater injury than controls as well as additional analyses at the protein level.

Interestingly, p-ERK and p-Akt were activated in IPF samples as well as in bleomycin-treated mice from 7 dpi and sustained through 28 dpi (Fig 7b). While these markers are known downstream targets of FGF signaling, they are also the targets of many other growth factor signaling pathways. While some clinical studies aimed to block tyrosine kinase activity with anti-RTK agents, none have shown a clear, significant beneficial clinical outcome and treatment comes at the cost of reduced quality of life due to side effects (Daniels et al., 2010; Günther et al., 2012). The results of these studies may support the role of particular RTK signaling in lung repair. More specific downstream targets for FGF signaling such as p-FRS2, p-FGFR1 and p-FGFR2 should be analyzed at the protein level. While total FGFR2 and FRS2 was increased in IPF patients, it is unclear whether this is due to an accumulation of mesenchymal derived cells or indicative of active FGF signaling. In addition to phosphorylated FGF specific protein analyses, a bleomycin experiment using a transgenic mouse to induce FRS2 silencing (as knockouts are not viable) may be necessary in order to uncouple the role of FGF signaling in the mouse response to bleomycin.

5.3 Exogenous FGF7 may protect the epithelium from acute lung injury but is unlikely to promote fibrotic lesion resolution

FGF7 is an established survival factor for AEC2 cells. It has been shown to protect against lung injury by increasing surfactant protein production and enhancing barrier integrity. While many *in vivo* studies have focused on either prophylactic or therapeutic application of FGF7 (KGF or Palifermin) in chemical-, mechanical- or radiation-mediated, as well as bleomycin and other drug-induced lung epithelial injuries (Guo et al., 1998; Hu et al., 2010; Li et al., 2010; Liu et al.,

2011; Yildirim et al., 2008), none have studied the long-term effects of bleomycin-induced lung injury in *Fgf7* deficient mice. However, a recent study challenged this idea: mice that received adenoviral-vector FGF7 at 7 dpi after an initial bleomycin mini-pump injury followed by a second 7-day bleomycin mini-pump instillation at d29, showed increased survival and recovery. The limitation, however is that it was not clear whether the observed effect was due to attenuation of inflammation or enhanced fibrotic resolution (Sakamoto et al., 2011). Thus this result supports the idea that FGF7 acts as a potent epithelial survival factor during lung injury rather than a driving force in fibrotic resolution. We are the first to show that *Fgf7*$^{-/-}$ animals are susceptible specifically to the acute phase of bleomycin-induced lung fibrosis yet dispensable for long-term repair. Consequently, while Palifermin may promote survival of lung epithelium, it is unlikely to promote the resolution of UIP lesions. On the contrary, our data using our previously published *Fgf10* gain- (Gupte et al., 2009) and loss-of-function (this study) suggest that FGF10, unlike FGF7, could effectively drive fibrotic resolution, thus presenting a potential therapeutic option.

5.4 Importance of FGFR2b-independent FGF10 signaling for fibrosis resolution in mice

Surprisingly, attenuating FGF ligand signaling either, 6 – 28 dpi (Fig 11a) or 14 – 28 (Fig 11b) had little effect on the ability of the mouse lung to repair after bleomycin injury. While the first experiment (Fig 11a) resulted in very subtle increases in injury in animals expressing the soluble decoy receptor, we concluded that the lack of difference could be related to the low level of injury (1.0U/kg bleomycin i.t.). However, upon repeating the experiment with double the dose of bleomycin (2.0U/kg) and inducing expression of the soluble receptor starting from 14 dpi in order to focus on the resolution of bleomycin induced lesions, we did not find a significant difference between wild types and those expressing the soluble decoy (Fig 11b). Although we confirmed the expression of the soluble receptor via qPCR, (Fig 11b., I), it could be that the *Rosa26* driver is not highly expressed in the adult lung. In addition, the mice were bred on a

CD1 outbred background, which may render them more resistant to bleomycin injury than other inbred strains such as C57bl/6. Lastly, since the soluble decoy receptor traps all ligands, it may be possible that the negative effects of a lack of FGF7 or FGF10 signaling are muted by the lack of FGF1 signaling which is able to signal to both c and b isoforms of FGFR1 and FGFR2 as expession of a soluble decoy receptor for FGFR2c was shown to be beneficial in the bleomycin model (Yu et al., 2012)

Despite the lack of phenotype incurred by bleomycin treated mice expressing soluble FGFR2b, we found, complementary to our previous study which showed that overexpression of FGF10 enhances fibrotic resolution (Gupte et al., 2009), that bleomycin-induced fibrotic lesions of *Fgf10*$^{+/-}$ animals were less resolved and lung function was significantly attenuated at 28 dpi (Fig 15). Interestingly, *Fgf10*$^{+/-}$ lungs were impaired not only relative to *WT*s, but also compared to mice with attenuated epithelial FGFR2b signaling (*Fgfr2b*$^{+/-}$ mice and *Fgf7*$^{-/-}$ mice). Therefore we hypothesize that FGF10 may drive fibrotic resolution in an epithelial, FGFR2b-independent manner, possibly via FGFR1b. FGFR1b, expressed in the epithelium and mesenchyme (*unpublished data*), is upregulated at 14 dpi in mice and may be important in fibrosis resolution. Supporting this possibility, we observed an increase in *Spry4* expression (an FGF transcriptional target expressed mostly in the mesenchyme) at 14 dpi. In the future, bleomycin studies performed on mice genetically deficient in *Fgfr1b* could determine the significance of this receptor in the resolution of fibrosis. Moreover, additional studies should be performed to determine the differential effect of FGF10 on the epithelium versus mesenchyme. Finally, given the trend towards increased TGFß1 activity in *Fgf10*$^{+/-}$ bleomycin-induced lesions, which correlates with the decreased TGFß1 signaling (and expression of *Tgfß1* itself at the transcriptional level) upon FGF10 overexpression (Gupte et al., 2009), more studies are needed to investigate the molecular and cellular bases underlying the inhibition of TGFß1 signaling by FGF10 *in vivo*.

5.5 FGF10 pushed IPF fibroblasts towards a lipofibroblast-like phenotype

Lipofibroblasts are important for alveologenesis and later assist AEC2 cells in the production of lipids and thus help to maintain surface tension and epithelial barrier integrity. While the presence of lipofibroblasts have been described in the adult lung (Vaccaro and Brody, 1978), they have recently emerged in the literature as cell types requiring further investigation and characterization. Lipid homeostasis, and thus barrier function is compromised in IPF lungs due to damaged AEC2 cells and the activation of myofibroblasts. Recently, it was shown that growth and differentiation of the AEC2 cells occurred most readily when co-cultured with primary PDGFRα+ lung stromal cells and lipofibroblasts (Barkauskas et al., 2013a); thus suggesting not only that that mesenchymal-epithelial cross-talk is essential for repair, but also that lipofibroblasts form part of a lung stem cell niche. However the signals required for clonal expansion, and differentiation of AEC2s are yet to be defined. Thus targeting myofibroblasts for transdifferentiation into lipofibroblasts may be a potential therapeutic approach.

Though the progenitors of lipofibroblasts have not yet been thoroughly described, lineage tracing studies performed by our lab using the *FGF10^{iCre};Tomato^{flox}* mouse, have shown that FGF10 is a marker for a subset of lipofibroblasts progenitors (El Agha et. al., 2013, Development, *in press*) which become SMA positive 14 days after bleomycin injury (*unpublished data*). In addition, Thy-1, a glycosylphosphytidylinositol-linked cell-surface glycoprotein signals via peroxisome proliferator-activated receptor-gamma (PPARγ) and is critical for the differentiation of lipofibroblasts during alveologenesis and is thus also considered a marker of lipofibroblasts (Varisco et al., 2012). Interestingly, the PPARγ signaling pathway has also been targeted in therapeutic approaches for IPF, as its actions are not only limited to lipid metabolism and homeostasis but also in the regulation of inflammatory responses and cellular proliferation and differentiation and apoptosis (Corton et al., 2000; Escher and Wahli, 2000). For example, PPARγ-agonist rosiglitazone significantly reduced bleomycin-induced lung injury in mice (Genovese et al., 2005).

In order to assess whether FGF10 stimulation of IPF cells triggered a similar response as PPARγ-agonists, IPF fibroblasts were treated with either Rosiglitazone or FGF10. Both treatments induced expression of *C/EBP*α, a marker of adipogenesis (Fig 20) as well as *PPARγ* (*data not shown*). Furthermore, treatment with both factors seemed to have a synergistic effect on FGFR1-IIIb expression (Fig 21), a receptor implicated as both a tumor-suppressor (Ricol et al., 1999) and in adipocyte formation (Asaki et al., 2004a; Sakaue et al., 2002). Interestingly, FGF10 treatment also seemed to correlate with an increase in the aggregation of lipid droplets in both IPF and donor fibroblasts (Fig 18). Whether FGF10 promotes lipogenesis in adult human lung fibroblasts must be further investigated.

5.6 FGF10 tempers TGFß1 signaling in IPF fibroblasts

Though the origin of activated myofibroblasts in IPF is disputed, they are nonetheless conspicuously involved in the formation of UIP lesions. While resident lung fibroblasts, epithelial to mesenchymal transition of AEC1 and AEC2 cells, bone marrow–derived fibrocytes, pericytes of the lung interstitium, and endothelial cells have all been implicated (Patel et al., 2013; Scotton and Chambers, 2007) (Fig 27). Thus although the origin of the myofibroblasts remains undefined, the damage they cause to the alveolar epithelium due to the secretion of exorbitant amounts of matrix is clearly lethal.

Many studies propose that the master switch of fibrogenic mediators, TGF-β is responsible for the activation of cells to become myofibroblasts. Damaged AEC2 cells express TGF-β, which in turn activates other cells in the milieu, thus propagating a fibrotic response. Cleavage of latent TGF-β into its active form is mediated by matrix metalloproteinases (Dancer et al., 2011), changes in pH (acidic conditions), reactive oxygen species (Bargagli et al., 2009), thrombospondin-1 (Crawford et al., 1998), tissue stiffness (Hinz, 2009), as well as by integrins αVβ3, αVβ5, αVβ8, and αVβ6, which have also been implicated in fibrotic disorders (Margadant and Sonnenberg, 2010). In the lung, TGF-β is produced by alveolar macrophages, neutrophils, activated alveolar epithelial

cells, endothelial cells, fibroblasts, and myofibroblasts. Once activated, not only does it induce macrophage and fibroblast recruitment as well as fibroblast proliferation via platelet-derived growth factor (PDGF) expression, it also stimulates expression of a number of pro-inflammatory and fibrogenic cytokines, such as TNF-α, PDGF, IL-1β, or IL-13, thereby amplifying and perpetuating the fibrotic response (Fernandez and Eickelberg, 2012). In the mouse model of bleomycin-induced fibrosis, epithelial specific reduction of TGF-β receptor has also been found to attenuate the fibrotic response (Li et al., 2011). Thus targeting TGF-β has been the goal of ongoing clinical studies. While Pirfenidone has demonstrated anti-fibrotic and anti-inflammatory effects by attenuating TGF-β production and action (Hisatomi et al., 2012) the clinical efficacy is on one hand celebrated, but also extremely limited and additionally mitigated by its side effects (Günther et al., 2012; Jenkins, 2013; Raghu and Thickett, 2013).

Interestingly, our preliminary results showed that FGF10 treatment of IPF fibroblasts also limits TGF-β signaling. Pre-treatment of cells one hour prior to TGF-β treatment decreased the percentage of cells positive for pSMAD3 staining by approximately 80% (Fig 25). While the basal level of pSMAD3 staining was not particularly high in untreated cells (less than 5%), treatment with only FGF10 also slightly reduced pSMAD3 staining. Further evidence for the attenuation of TGF-β signaling by FGF10 was demonstrated by a 40% reduction of “high” SMA staining (Fig 26E) and 34% reduction in overall SMA staining intensity following pre-treatment of FGF10 (Fig 26F). Pre-treatment of cells with FGF10 one hour prior to TGF-β treatment resulted in a 44% decrease in high SMA staining compared to TGF-β treatment alone (Fig 26E) and a 27% reduction in the overall intensity of SMA staining (Fig 26E).

We have shown that FGF10 inhibits TGF-β signaling in IPF fibroblasts as well as that reduction in endogenous signaling can have a detrimental effect on lung repair in the bleomycin mouse model. Likewise, overexpression of FGF10 enhanced fibrotic resolution in accordance with attenuation of TGF-β signaling (Gupte et al., 2009). Taken together, we hypothesize that FGF10 contributes to reducing active TGF-β signaling in the fibrotic milieu thus preventing trans-

differentiation of resident fibroblasts and lipofibroblast cells into activated myofibroblasts (Fig 27). Our model predicts that the recruitment of resident lung cells into the fibrotic milieu involves a step in which they lose their original markers; such as a reduction of lipid droplets in lipofibroblasts, followed by the acquisition of a “synthetic” phenotype characterized by high proliferation, low production of ECM and lack of SMA expression. Due to continued exposure to TGF-β and other profibrotic cytokines, these cells eventually acquire a “contractile” phenotype characterized by low proliferation, high SMA expression and excessive ECM production and eventually the formation of UIP lesions; a lesion that FGF10 may be able to inhibit. Interestingly, both FGF10 and Rosiglitazone treatments resulted in a reduction in cell size and filopodia projections, as well as a decrease in the intensity in SMA staining (Fig 19) possibly indicating a transdifferentiation out of a myofibroblast phenotype and possibly towards a more “synthetic” phenotype (Rensen et al., 2007), which may characterize an earlier stage of IPF. Our results thus implicate a role for FGF10 in the transdifferentiation of UIP cells back into a SMA negative cell type via the inhibition of TGF-β signaling. Whether FGF10 can push cells that have acquired a “contractile” phenotype all the way back to normal lipofibroblasts however, remains to be studied.

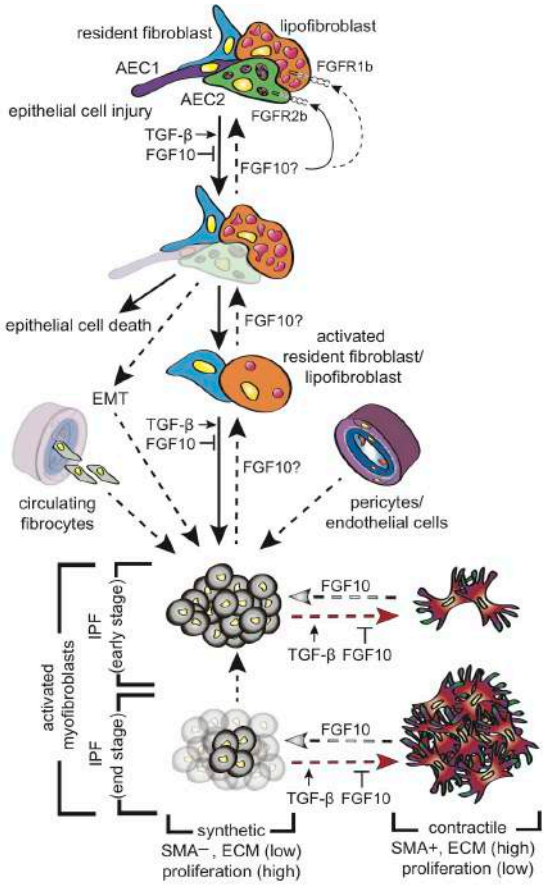

Figure 27. Model of the inhibition of TGF-β signaling by FGF10 in IPF

Epithelial cell injury results in the production of TGF-β which results in EMT, epithelial cell death and/or the "activation" of resident fibroblasts and lipofibroblasts characterized by the loss of markers such as lipid droplets. In IPF, we hypothesize that these activated cells undergo a transition towards a "synthetic" phenotype characterized by high proliferation. Due to continued exposure to TGF-β, synthetic cells then acquire a "contractile" phenotype characterized by high SMA expression and ECM production, and low proliferation. Thus we hypothesize that FGF10; via inhibition of TGF-β signaling, not only blocks the activation of myofibroblasts, but also inhibits the acquisition of a "contractile" phenotype. Whether FGF10 can push contractile cells back to a synthetic phenotype, and/or synthetic cells back to a resident or lipofibroblast cells phenotype remains to be studied.

5.7 Therapeutic potential of FGF10 for end-stage IPF patients

FGF10 may have potential therapeutic effects on end-stage IPF patients. These include: 1) the amplification of lung progenitor cells (Fig 28D); 2) the trans-differentiation of myofibroblasts to lipofibroblasts (Fig 28E) and 3) and like FGF7, the protection of intact epithelium (Fig 28D,E).

Given that *Fgf10* and *Fgfr2b* knockout mice fail to form both limbs and lungs indicating the importance of this signaling pathway in organ branching morphogenesis and of course lung development (Arman et al., 1999; Bellusci et al., 1997) and thus may be essential for human lung repair after injury as FGF10 has been already to be enhance repair in mice after bleomycin (Gupte et al., 2009) and FGFR2b ligands have been shown to be critical for lung epithelial repair after naphthalene injury (Volckaert et al., 2011). While earlier studies have found that FGF10 specifies smooth muscle cell progenitors in the lung during development (Ramasamy et al., 2007), our group recently showed that FGF10 marks lung lipofibroblast progenitors in adults mice both before and after bleomycin challenge (El Agha et. al., Development*, in press*). This data suggests that exogenous FGF10 may play a role in the transdifferentiation of myofibroblasts to lipofibroblasts possible through the attenuation of TGF-β signaling. Studies further characterizing FGF10 cells in the adult mouse lung must be completed in order to attain a better understanding of the role of endogenous FGF10 in the adult lung. Moreover, additional studies are needed in order to characterize adult lung cell types in general as there is a dire need for specific markers of differentiated cells in the lung.

FGF ligands are also known to be critical for the maintenance of transit-amplifying ameloblast progenitor cells of the mouse incisors (Parsa et al., 2010). Additional studies should be performed by expressing the soluble decoy FGFR2b receptor in the lung over a long period of time and analyzing not only the status of AEC2 cells but also of putative lung epithelial and mesenchymal progenitor cells by FACS analyses (McQualter et al., 2010).

Taken together, we have provided evidence to support the role of FGF10 as a potential therapy for IPF patients. Additional experiments however are critical to define the role of endogenous FGF10 signaling in the lung.

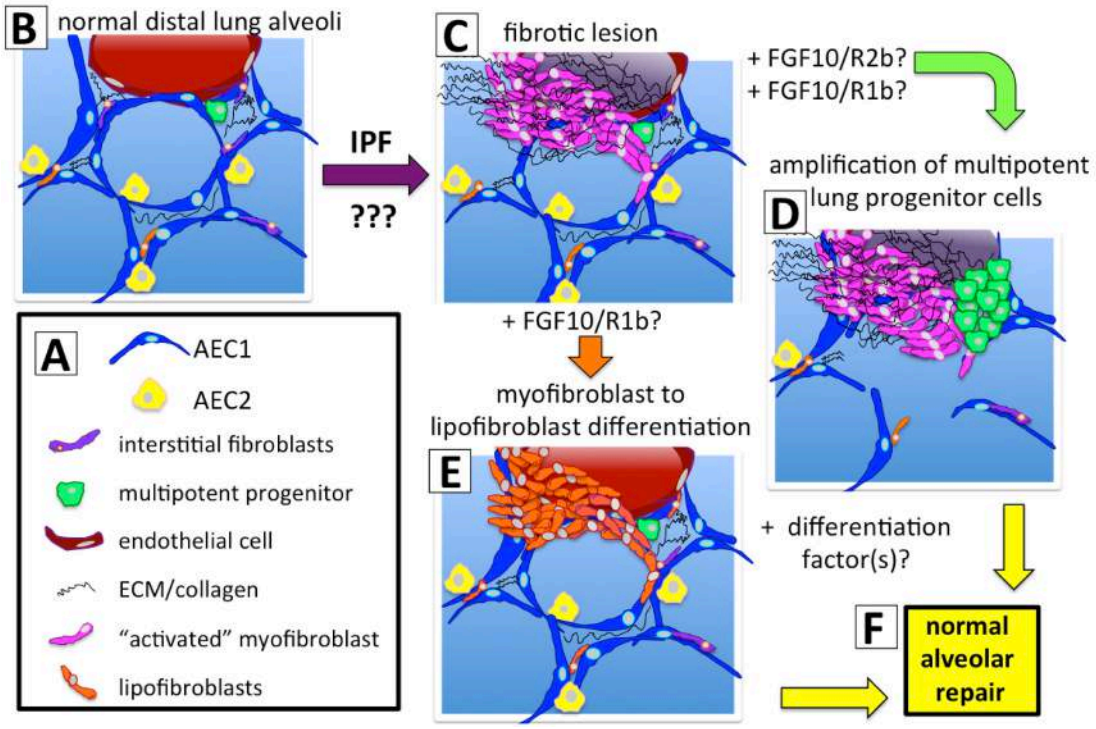

Figure 28. Model for therapeutic effects of FGF10 in end-stage fibrosis

A) Legend. B) Normal distal lung epithelium of healthy person featuring AEC1 and 2 cells, interstitial fibroblasts, lipofibroblasts, endothelial cells, multipotent progenitor cell, and ECM. C) end-stage IPF involves the activation of cells of unknown origin which become "myofibroblasts" characterized excessive of matrix secretion resulting in a respiratory blockade. D) Exposure of UIP lesions to FGF10 results in signaling via FGFR1b or FGFR2b leading to the amplification of lung progenitor cells. E) Signaling via FGFR1b, possibly expressed on cells of mesenchymal origin could result in cell type switch from pathogenic myofibroblast to lipofibroblasts, possibly via inhibition of TGFβ. F) Additional differentiation factors may be necessary to promote differentiation of multipotent progenitors.

5.8 Future analyses of the role of FGF10 in lung progenitor cells are critical

While AEC2s were initially described as being the main distal lung progenitor cell, recent experiments using mouse genetics and cell lineage tracing in mouse lung injury models suggest the recruitment of diverse populations of progenitors that not only self-renew but also repopulate and repair the lung after injury (Fig 29). Using the bleomycin model of lung injury and an SPC-driven inducible cre mouse to fate-map AECs, the majority of AEC2s in fibrotic areas were found to derive not from preexisting AEC2s, but rather from SPC negative, α6β4+ epithelial progenitor cells (Chapman et al., 2011). These progenitor cells were also able gave rise to Scgb1a1+ cells indicating their ability to differentiate into both distal and proximal epithelium. In addition to epithelial progenitor cells, distal airway stem cells that were keratin 5 and p63 double positive were demonstrated to form “pods” or solid spheres of cells after H1N1 influenza injury (Kumar et al., 2011). The pods developed lumen and expanded in size over 10 days and formed alveoli-like structures. Interestingly, while they expressed AEC1 markers and markers for angiogenesis, SPC expression was absent. In addition, SPC negative, Clara (Scgb1a1+) cells have also been shown to contribute to repopulating the epithelium with SPC+ cells after bleomycin injury (Barkauskas et al., 2013b; Rock et al., 2011) and variant Clara cells have been shown to give rise to both Clara and ciliated cell populations after naphthalene injury (Volckaert et al., 2011). Interestingly, in this study, FGF10 was implicated as an important mediator for inducing re-epithelialization after naphthalene injury. Furthermore, FGF10 expression was found to correlate with the capacity of stromal cells to support lung epithelial stem cell growth in vitro (McQualter et al., 2013). Given the importance of FGF10/R2b signaling for lung development and the aforementioned studies, it will be important for future studies using mouse injury models to address the role of FGF10 in

the self-renewal and or differentiation of lung progenitor cells during lung injury and repair.

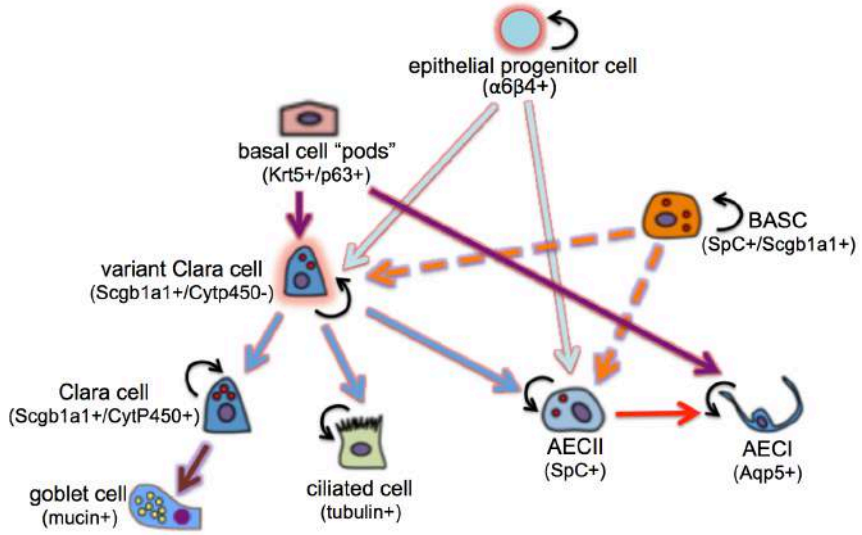

Figure 29. Model of lung progenitor cells are recruited during injury/repair

Distal lung epithelial progenitor cells (α6β4+) were demonstrated to differentiate into variant Clara cells and AEC2 cells. The putative broncho-alveolar stem cell or BASC is thought to be present at the broncho-alveolar duct junction and differentiate into AEC2s or variant Clara cells, however recently their existence and the proportion of their contribution to repair is disputed. Basal cells form "pods" after H1N1, bleomycin and naphthalene injury and express markers for both Clara cells and AEC1 cells. Variant Clara cells repopulate both the broncho-alveolar epithelium and the distal epithelium. Clara cells can also give rise to mucin secreting goblet cells. AEC2s give rise to AEC1 cells after hyperoxia and other injuries that damage the distal lung.

Part 6. Conclusion

The aim of this project was to investigate the role of FGFR2b ligands in IPF. We demonstrated that endogenous FGFR2b ligand signaling may be dysregulated in end-stage IPF patients and that FGF10 may drive repair of bleomycin-induced lesions in mice.

Despite increased expression of *FGF7* and *FGF10* in end-stage IPF patient lungs, receptors as well as downstream targets of these ligands were significantly decreased. In contrast, wild type mice undergoing spontaneous repair after bleomycin injury, expressed *Fgf10* and downstream targets from 14 days post injury, suggesting recruitment of the pathway during repair. While mice deficient in endogenous Fgfr2b ligand signaling were not significantly more injured than wild type animals, the possibility that the soluble Fgfr2b receptor bound mesenchymal Fgf ligands as well, may have masked the contribution of epithelial Fgfr2b signaling in balancing the spontaneous repair equation. Nevertheless, the lack of FGF7/10/FGFR2b and FGF10/FGFR1b signaling observed in end-stage IPF lungs and the recruitment of Fgf10/Fgfr1b during the peak of bleomycin injury of wild type mice both indicate the potential therapeutic use of exogenous growth factors to promote lung repair. Likewise the ability of FGF10 to reduce cell size and inhibit TGF-β signaling in IPF fibroblasts, suggests that it could effectively mediate a contractile to synthetic-like phenotype, which may be an important step towards UIP lesion repair.

Effective treatment of IPF may be a matter of efficiently targeting which cells in the lung should survive and which cells should die. While a global blockade of tyrosine kinase activity may eventually lead to the abolishment of activated fibroblasts, intact lung epithelial cells as well as progenitor cells in both epithelial and stromal cell compartments, are also likely to suffer when they are deprived of survival signals over an extended period of time. Likewise, globally inhibiting a master inflammatory regulator such as TGF-β may result in both positive and negative outcomes for IPF patients. Thus if a cell type exclusive therapeutic is not possible, combining an auspicious regimen of cytoprotective, exogenous FGF10 ligand in conjunction with a global tyrosine kinase blocker or TGF-β inhibitor may preserve the remaining epithelial integrity as well as progenitor cell populations, possibly resulting in a better outcome in terms of fibrosis progression and/or resolution.

Conclusion

I joined the Molecular Biology and Medicine of the Lung Program in Giessen, Germany because I was attracted to the “translational” component of research projects offered to PhD students in Giessen. Though I did not succeed in curing IPF, while investigating the aim of this project I learned the limitations of translational models and the importance of using multiple experimental approaches and designs to investigate a clearly defined hypothesis. Ideally, both etiology; the causes of a disease; and pathogenesis; the mechanisms by which the disease develops, causes tissue damage and spreads within the body are understood before therapeutic approaches are investigated. However, while even the most transparent disease pathogenesis allows specific targeting to slow, stop, or even reverse the disease both *in vitro* and *in vivo* (animal models), translation of a potential therapy to humans is not guaranteed; several thousand diseases distress us, but fewer than 500 can be treated. Moreover, the average length of time from target discovery to new drug approval is 13 years. The failure rate exceeds 95%, and the cost per successful drug exceeds $1-2 billion, after adjusting for all of the failures (Munos, 2009; Paul et al., 2010). Intense interdisciplinary cooperation is essential to successful “translation” of experimental results at the bench to medicines in the clinic. Moreover, understanding the limitations of animal models as well as their unique, innate response to drugs and treatments will help researchers to streamline translational research.

IPF remains a rare, idiopathic disease; the clinical manifestations are variable as there are variations in the age of on-set, rate of progression, and histological phenotype, rendering it intrinsically very difficult to model in an animal. The bleomycin mouse model seeks to recapitulate the general phenotype of IPF (UIP lesions) using a DNA damaging substance that results in lung scarring. While hundreds of studies report agents that ‘attenuate bleomycin induced fibrosis in mice’, repairing this *UIP-like* phenotype has led neither to an effective treatment nor a cure for IPF. Thus, it is imperative that researchers not only understand the limitations, assumptions and caveats embedded in animal models, but also explore further experimental approaches when attempting to solve the mystery of this terrible disease.

References

Aaroson, S. A., Bottaro, D. P., Miki, T., Ron, D., Finch, P. W., Fleming, T. P., Ahn, J., Taylor, W. G. and Rubin, J. S. (1991). Keratinocyte Growth Factor: A Fibroblast Growth Factor Family Member with Unusual Target Cell Specificity. *Annals of the New York Academy of Sciences* **638**, 62–77.

Abler, L. L., Mansour, S. L. and Sun, X. (2009). Conditional gene inactivation reveals roles for Fgf10 and Fgfr2 in establishing a normal pattern of epithelial branching in the mouse lung. *Developmental dynamics : an official publication of the American Association of Anatomists* **238**, 1999–2013.

Adams, A. C., Coskun, T., Rovira, A. R. I., Schneider, M. A., Raches, D. W., Micanovic, R., Bina, H. A., Dunbar, J. D. and Kharitonenkov, A. (2012). Fundamentals of FGF19 & FGF21 action in vitro and in vivo. *PloS one* **7**, e38438.

Akunuru, S., Palumbo, J., Zhai, Q. J. and Zheng, Y. (2011). Rac1 targeting suppresses human non-small cell lung adenocarcinoma cancer stem cell activity. *PloS one* **6**, e16951.

Alberts, D. S., Chen, H. S., Liu, R., Himmelstein, K. J., Mayersohn, M., Perrier, D., Gross, J., Moon, T., Broughton, A. and Salmon, S. E. (1978). Bleomycin pharmacokinetics in man. I. Intravenous administration. *Cancer chemotherapy and pharmacology* **1**, 177–81.

Albuisson, J., Pêcheux, C., Carel, J.-C., Lacombe, D., Leheup, B., Lapuzina, P., Bouchard, P., Legius, E., Matthijs, G., Wasniewska, M., et al. (2005). Kallmann syndrome: 14 novel mutations in KAL1 and FGFR1 (KAL2). *Human mutation* **25**, 98–9.

American Thoracic Society/European Respiratory Society International Multidisciplinary Consensus Thoracic Society (ATS), and the European Respiratory Society (E (2002). *American journal of* **Classification of the Idiopathic Interstitial Pneumonias. This joint statement of the American** *respiratory and critical care medicine* **165**, 277–304.

Arman, E., Haffner-Krausz, R., Gorivodsky, M. and Lonai, P. (1999). Fgfr2 is required for limb outgrowth and lung-branching morphogenesis. *Proceedings of the National Academy of Sciences of the United States of America* **96**, 11895–9.

Asaki, T., Konishi, M., Miyake, A., Kato, S., Tomizawa, M. and Itoh, N. (2004a). Roles of fibroblast growth factor 10 (Fgf10) in adipogenesis in vivo. *Molecular and cellular endocrinology* **218**, 119–28.

Asaki, T., Konishi, M., Miyake, A., Kato, S., Tomizawa, M. and Itoh, N. (2004b). Roles of fibroblast growth factor 10 (Fgf10) in adipogenesis in vivo. *Molecular and cellular endocrinology* **218**, 119–28.

Bargagli, E., Olivieri, C., Bennett, D., Prasse, A., Muller-Quernheim, J. and Rottoli, P. (2009). Oxidative stress in the pathogenesis of diffuse lung diseases: a review. *Respiratory medicine* **103**, 1245–56.

Barkauskas, C. E., Cronce, M. J., Rackley, C. R., Bowie, E. J., Keene, D. R., Stripp, B. R., Randell, S. H., Noble, P. W. and Hogan, B. L. M. (2013). Type 2 alveolar cells are stem cells in adult lung. *The Journal of clinical investigation*.

Beer, H.-D. (2000). Fibroblast Growth Factor (FGF) Receptor 1-IIIb Is a Naturally Occurring Functional Receptor for FGFs That Is Preferentially Expressed in the Skin and the Brain. *Journal of Biological Chemistry* **275**, 16091–16097.

References

Beer, H. D., Vindevoghel, L., Gait, M. J., Revest, J. M., Duan, D. R., Mason, I., Dickson, C. and Werner, S. (2000). Fibroblast growth factor (FGF) receptor 1-IIIb is a naturally occurring functional receptor for FGFs that is preferentially expressed in the skin and the brain. *The Journal of biological chemistry* **275**, 16091–7.

Belleudi, F., Purpura, V. and Torrisi, M. R. (2011). The receptor tyrosine kinase FGFR2b/KGFR controls early differentiation of human keratinocytes. *PloS one* **6**, e24194.

Bellusci, S., Grindley, J., Emoto, H., Itoh, N. and Hogan, B. (1997). Fibroblast growth factor 10 (FGF10) and branching morphogenesis in the embryonic mouse lung. *Development* **124**, 4867–4878.

Belteki, G., Haigh, J., Kabacs, N., Haigh, K., Sison, K., Costantini, F., Whitsett, J., Quaggin, S. E. and Nagy, A. (2005). Conditional and inducible transgene expression in mice through the combinatorial use of Cre-mediated recombination and tetracycline induction. *Nucleic acids research* **33**, e51.

Bernard-Pierrot, I., Ricol, D., Cassidy, A., Graham, A., Elvin, P., Caillault, A., Lair, S., Broët, P., Thiery, J.-P. and Radvanyi, F. (2004). Inhibition of human bladder tumour cell growth by fibroblast growth factor receptor 2b is independent of its kinase activity. Involvement of the carboxy-terminal region of the receptor. *Oncogene* **23**, 9201–11.

Bérubé, K., Prytherch, Z., Job, C. and Hughes, T. (2010). Human primary bronchial lung cell constructs: the new respiratory models. *Toxicology* **278**, 311–8.

Böhlen, P., Esch, F., Baird, A. and Gospodarowicz, D. (1985). Acidic fibroblast growth factor (FGF) from bovine brain: amino-terminal sequence and comparison with basic FGF. *The EMBO journal* **4**, 1951–6.

Borzone, G., Moreno, R., Urrea, R., Meneses, M., Oyarzún, M. and Lisboa, C. (2001). Bleomycin-induced chronic lung damage does not resemble human idiopathic pulmonary fibrosis. *American journal of respiratory and critical care medicine* **163**, 1648–53.

Bozyk, P. D. and Moore, B. B. (2011). Prostaglandin E 2 and the Pathogenesis of Pulmonary Fibrosis. *American Journal of Respiratory Cell and Molecular Biology* **45**, 445–452.

Brehm, J. M., Hagiwara, K., Tesfaigzi, Y., Bruse, S., Mariani, T. J., Bhattacharya, S., Boutaoui, N., Ziniti, J. P., Soto-Quiros, M. E., Avila, L., et al. (2011). Identification of FGF7 as a novel susceptibility locus for chronic obstructive pulmonary disease. *Thorax* **66**, 1085–90.

Burdine, R. D., Branda, C. S. and Stern, M. J. (1998). EGL-17(FGF) expression coordinates the attraction of the migrating sex myoblasts with vulval induction in C. elegans. *Development (Cambridge, England)* **125**, 1083–93.

Carrel, A. (1913). Artificial activation of the growth on vitro of connective tissue. *Journal of Experimental Medicine* **17**, 14–19.

Chedid, M., Rubin, J. S., Csaky, K. G. and Aaronson, S. A. (1994). Regulation of keratinocyte growth factor gene expression by interleukin 1. *The Journal of biological chemistry* **269**, 10753–7.

Cheon, H. G., LaRochelle, W. J., Bottaro, D. P., Burgess, W. H. and Aaronson, S. a (1994). High-affinity binding sites for related fibroblast growth factor ligands reside within different receptor immunoglobulin-like domains. *Proceedings of the National Academy of Sciences of the United States of America* **91**, 989–93.

Cohen, M. B., Austin, J. H., Smith-Vaniz, A., Lutzky, J. and Grimes, M. M. (1989). Nodular bleomycin toxicity. *American journal of clinical pathology* **92**, 101–4.

Collard, H. R., Ryu, J. H., Douglas, W. W., Schwarz, M. I., Curran-Everett, D., King, T. E. and Brown, K. K. (2004). Combined corticosteroid and cyclophosphamide therapy does not alter survival in idiopathic pulmonary fibrosis. *Chest* **125**, 2169–74.

Coppens, J. T., Van Winkle, L. S., Pinkerton, K. and Plopper, C. G. (2007). Distribution of Clara cell secretory protein expression in the tracheobronchial airways of rhesus monkeys. *American journal of physiology. Lung cellular and molecular physiology* **292**, L1155–62.

Corton, J. C., Anderson, S. P. and Stauber, A. (2000). Central role of peroxisome proliferator-activated receptors in the actions of peroxisome proliferators. *Annual review of pharmacology and toxicology* **40**, 491–518.

Crawford, S. E., Stellmach, V., Murphy-Ullrich, J. E., Ribeiro, S. M., Lawler, J., Hynes, R. O., Boivin, G. P. and Bouck, N. (1998). Thrombospondin-1 is a major activator of TGF-beta1 in vivo. *Cell* **93**, 1159–70.

D'Andrea, A. D. and Haseltine, W. A. (1978). Sequence specific cleavage of DNA by the antitumor antibiotics neocarzinostatin and bleomycin. *Proceedings of the National Academy of Sciences of the United States of America* **75**, 3608–12.

Dancer, R. C. A., Wood, A. M. and Thickett, D. R. (2011). Metalloproteinases in idiopathic pulmonary fibrosis. *The European respiratory journal* **38**, 1461–7.

De Langhe, S. P., Carraro, G., Warburton, D., Hajihosseini, M. K. and Bellusci, S. (2006). Levels of mesenchymal FGFR2 signaling modulate smooth muscle progenitor cell commitment in the lung. *Developmental biology* **299**, 52–62.

De Maximy, A. A., Nakatake, Y., Moncada, S., Itoh, N., Thiery, J. P. and Bellusci, S. (1999). Cloning and expression pattern of a mouse homologue of drosophila sprouty in the mouse embryo. *Mechanisms of development* **81**, 213–6.

De Moerlooze, L., Spencer-Dene, B., Revest, J. M., Hajihosseini, M., Rosewell, I. and Dickson, C. (2000). An important role for the IIIb isoform of fibroblast growth factor receptor 2 (FGFR2) in mesenchymal-epithelial signalling during mouse organogenesis. *Development (Cambridge, England)* **127**, 483–92.

De Roos, A. D. G. (2007). Conserved intron positions in ancient protein modules. *Biology direct* **2**, 7.

Del Moral, P.-M., De Langhe, S. P., Sala, F. G., Veltmaat, J. M., Tefft, D., Wang, K., Warburton, D. and Bellusci, S. (2006). Differential role of FGF9 on epithelium and mesenchyme in mouse embryonic lung. *Developmental biology* **293**, 77–89.

Deterding, R. R., Jacoby, C. R. and Shannon, J. M. (1996). Acidic fibroblast growth factor and keratinocyte growth factor stimulate fetal rat pulmonary epithelial growth. *The American journal of physiology* **271**, L495–505.

Deterding, R. R., Havill, A. M., Yano, T., Middleton, S. C., Jacoby, C. R., Shannon, J. M., Simonet, W. S. and Mason, R. J. (1997). Prevention of bleomycin-induced lung injury in rats by keratinocyte growth factor. *Proceedings of the Association of American Physicians* **109**, 254–68.

Ding, W., Bellusci, S., Shi, W. and Warburton, D. (2003). Functional analysis of the human Sprouty2 gene promoter. *Gene* **322**, 175–85.

Drugan, C. S., Paterson, I. C. and Prime, S. S. (1998). Fibroblast growth factor receptor expression reflects cellular differentiation in human oral squamous carcinoma cell lines. *Carcinogenesis* **19**, 1153–6.

Dutt, A., Ramos, A. H., Hammerman, P. S., Mermel, C., Cho, J., Sharifnia, T., Chande, A., Tanaka, K. E., Stransky, N., Greulich, H., et al. (2011). Inhibitor-sensitive FGFR1 amplification in human non-small cell lung cancer. *PloS one* **6**, e20351.

Entesarian, M., Dahlqvist, J., Shashi, V., Stanley, C. S., Falahat, B., Reardon, W. and Dahl, N. (2007). FGF10 missense mutations in aplasia of lacrimal and salivary glands (ALSG). *European journal of human genetics : EJHG* **15**, 379–82.

Escher, P. and Wahli, W. (2000). Peroxisome proliferator-activated receptors: insight into multiple cellular functions. *Mutation research* **448**, 121–38.

Evans, M. J., Cabral, L. J., Stephens, R. J. and Freeman, G. (1973). Renewal of alveolar epithelium in the rat following exposure to NO2. *The American journal of pathology* **70**, 175–98.

Fernandez, I. E. and Eickelberg, O. (2012). The Impact of TGF-β on Lung Fibrosis.

Finch, P. W. and Rubin, J. S. (2006). Keratinocyte growth factor expression and activity in cancer: implications for use in patients with solid tumors. *Journal of the National Cancer Institute* **98**, 812–24.

Finch, P. W., Rubin, J. S., Miki, T., Ron, D. and Aaronson, S. A. (1989). Human KGF is FGF-related with properties of a paracrine effector of epithelial cell growth. *Science (New York, N.Y.)* **245**, 752–5.

Firnberg, N. and Neubüser, A. (2002). FGF signaling regulates expression of Tbx2, Erm, Pea3, and Pax3 in the early nasal region. *Developmental biology* **247**, 237–50.

Francannet, C., Vanlieferinghen, P., Dechelotte, P., Urbain, M. F., Campagne, D. and Malpuech, G. (1994). LADD syndrome in five members of a three-generation family and prenatal diagnosis. *Genetic counseling (Geneva, Switzerland)* **5**, 85–91.

Froudarakis, M., Hatzimichael, E., Kyriazopoulou, L., Lagos, K., Pappas, P., Tzakos, A. G., Karavasilis, V., Daliani, D., Papandreou, C. and Briasoulis, E. (2013). Revisiting bleomycin from pathophysiology to safe clinical use. *Critical reviews in oncology/hematology*.

Fujita, H., Sakamoto, N., Ishimatsu, Y., Kakugawa, T., Hara, S., Hara, A., Amenomori, M., Ishimoto, H., Nagata, T., Mukae, H., et al. (2011). Effects of doxycycline on production of growth factors and matrix metalloproteinases in pulmonary fibrosis. *Respiration; international review of thoracic diseases* **81**, 420–30.

Gahl, W. A., Brantly, M., Troendle, J., Avila, N. A., Padua, A., Montalvo, C., Cardona, H., Calis, K. A. and Gochuico, B. (2002). Effect of pirfenidone on the pulmonary fibrosis of Hermansky-Pudlak syndrome. *Molecular genetics and metabolism* **76**, 234–42.

Gazdhar, A., Temuri, A., Knudsen, L., Gugger, M., Schmid, R. A., Ochs, M. and Geiser, T. (2013). Targeted gene transfer of hepatocyte growth factor to alveolar type II epithelial cells reduces lung fibrosis in rats. *Human gene therapy* **24**, 105–16.

Genovese, T., Cuzzocrea, S., Di Paola, R., Mazzon, E., Mastruzzo, C., Catalano, P., Sortino, M., Crimi, N., Caputi, A. P., Thiemermann, C., et al. (2005). Effect of rosiglitazone and 15-deoxy-Delta12,14-prostaglandin J2 on bleomycin-induced lung injury. *The European respiratory journal* **25**, 225–34.

Ghosh, M., Stewart, A., Tucker, D. E., Bonventre, J. V, Murphy, R. C. and Leslie, C. C. (2004). Role of cytosolic phospholipase A(2) in prostaglandin E(2) production by lung fibroblasts. *American journal of respiratory cell and molecular biology* **30**, 91–100.

Gospodarowicz, D. (1975). Purification of a fibroblast growth factor from bovine pituitary. *The Journal of biological chemistry* **250**, 2515–20.

Goss, A. M., Tian, Y., Cheng, L., Yang, J., Zhou, D., Cohen, E. D. and Morrisey, E. E. (2011). Wnt2 signaling is necessary and sufficient to activate the airway smooth muscle program in the lung by regulating myocardin/Mrtf-B and Fgf10 expression. *Developmental biology* **356**, 541–52.

Gossen, M. and Bujard, H. (1992). Tight control of gene expression in mammalian cells by tetracycline-responsive promoters. *Proceedings of the National Academy of Sciences of the United States of America* **89**, 5547–51.

Gotoh, N. (2008). Regulation of growth factor signaling by FRS2 family docking/scaffold adaptor proteins. *Cancer science* **99**, 1319–25.

Gribbin, J., Hubbard, R. B., Le Jeune, I., Smith, C. J. P., West, J. and Tata, L. J. (2006). Incidence and mortality of idiopathic pulmonary fibrosis and sarcoidosis in the UK. *Thorax* **61**, 980–5.

Günther, A., Korfei, M., Mahavadi, P., von der Beck, D., Ruppert, C. and Markart, P. (2012). Unravelling the progressive pathophysiology of idiopathic pulmonary fibrosis. *European respiratory review : an official journal of the European Respiratory Society* **21**, 152–60.

Guo, L., Degenstein, L. and Fuchs, E. (1996). Keratinocyte growth factor is required for hair development but not for wound healing. *Genes & development* **10**, 165–75.

Guo, J., Yi, E. S., Havill, A. M., Sarosi, I., Whitcomb, L., Yin, S., Middleton, S. C., Piguet, P. and Ulich, T. R. (1998). Intravenous keratinocyte growth factor protects against experimental pulmonary injury. *The American journal of physiology* **275**, L800–5.

Gupte, V. V, Ramasamy, S. K., Reddy, R., Lee, J., Weinreb, P. H., Violette, S. M., Guenther, A., Warburton, D., Driscoll, B., Minoo, P., et al. (2009). Overexpression of fibroblast growth factor-10 during both inflammatory and fibrotic phases attenuates bleomycin-induced pulmonary fibrosis in mice. *American journal of respiratory and critical care medicine* **180**, 424–36.

Hadari, Y. R., Gotoh, N., Kouhara, H., Lax, I. and Schlessinger, J. (2001). Critical role for the docking-protein FRS2 alpha in FGF receptor-mediated signal transduction pathways. *Proceedings of the National Academy of Sciences of the United States of America* **98**, 8578–83.

Hajihosseini, M. K., Wilson, S., De Moerlooze, L. and Dickson, C. (2001). A splicing switch and gain-of-function mutation in FgfR2-IIIc hemizygotes causes Apert/Pfeiffer-syndrome-like phenotypes. *Proceedings of the National Academy of Sciences of the United States of America* **98**, 3855–60.

Hajihosseini, M. K., Duarte, R., Pegrum, J., Donjacour, A., Lana-Elola, E., Rice, D. P., Sharpe, J. and Dickson, C. (2009). Evidence that Fgf10 contributes to the skeletal and visceral defects of an Apert syndrome mouse model. *Developmental dynamics : an official publication of the American Association of Anatomists* **238**, 376–85.

Haston, C. K., Wang, M., Dejournett, R. E., Zhou, X., Ni, D., Gu, X., King, T. M., Weil, M. M., Newman, R. A., Amos, C. I., et al. (2002). Bleomycin hydrolase and a genetic locus within the MHC affect risk for pulmonary fibrosis in mice. *Human molecular genetics* **11**, 1855–63.

Hinz, B. (2009). Tissue stiffness, latent TGF-beta1 activation, and mechanical signal transduction: implications for the pathogenesis and treatment of fibrosis. *Current rheumatology reports* **11**, 120–6.

Hisatomi, K., Mukae, H., Sakamoto, N., Ishimatsu, Y., Kakugawa, T., Hara, S., Fujita, H., Nakamichi, S., Oku, H., Urata, Y., et al. (2012). Pirfenidone inhibits TGF-β1-induced over-expression of collagen type I and heat shock protein 47 in A549 cells. *BMC pulmonary medicine* **12**, 24.

Hochberg, Y. and Benjamini, Y. (1990). More powerful procedures for multiple significance testing. *Statistics in medicine* **9**, 811–8.

Hokuto, I., Perl, A.-K. T. and Whitsett, J. A. (2003). Prenatal, but not postnatal, inhibition of fibroblast growth factor receptor signaling causes emphysema. *The Journal of biological chemistry* **278**, 415–21.

Hu, X., Zhang, X., Li, B., Zhang, J. and Wang, Y. (2010). [The protective effect of keratinocyte growth factor on lipopolysaccharide-induced acute lung injury in rat]. *Zhongguo wei zhong bing ji jiu yi xue = Chinese critical care medicine = Zhongguo weizhongbing jijiuyixue* **22**, 486–9.

Huang, Y., Li, Y., Shang, Y., Ouyang, Z. and Zhen, Y. (2006). [Inhibition of pulmonary fibrosis by doxycycline: an experiment with mice]. *Zhonghua yi xue za zhi* **86**, 182–6.

Hübner, R.-H., Gitter, W., El Mokhtari, N. E., Mathiak, M., Both, M., Bolte, H., Freitag-Wolf, S. and Bewig, B. (2008). Standardized quantification of pulmonary fibrosis in histological samples. *BioTechniques* **44**, 507–11, 514–7.

Ibrahimi, O. A., Zhang, F., Eliseenkova, A. V, Itoh, N., Linhardt, R. J. and Mohammadi, M. (2004). Biochemical analysis of pathogenic ligand-dependent FGFR2 mutations suggests distinct pathophysiological mechanisms for craniofacial and limb abnormalities. *Human molecular genetics* **13**, 2313–24.

Igarashi, M. (1998). Characterization of Recombinant Human Fibroblast Growth Factor (FGF)-10 Reveals Functional Similarities with Keratinocyte Growth Factor (FGF-7). *Journal of Biological Chemistry* **273**, 13230–13235.

Itoh, N. and Ornitz, D. M. (2008). Functional evolutionary history of the mouse Fgf gene family. *Developmental dynamics : an official publication of the American Association of Anatomists* **237**, 18–27.

Itoh, N. and Ornitz, D. M. (2011). Fibroblast growth factors: from molecular evolution to roles in development, metabolism and disease. *Journal of biochemistry* **149**, 121–30.

Izvolsky, K. I., Shoykhet, D., Yang, Y., Yu, Q., Nugent, M. A. and Cardoso, W. V (2003). Heparan sulfate-FGF10 interactions during lung morphogenesis. *Developmental biology* **258**, 185–200.

Jenkins, G. (2013). Pirfenidone should be prescribed for patients with idiopathic pulmonary fibrosis. *Thorax*.

Jin, C., McKeehan, K., Guo, W., Jauma, S., Ittmann, M. M., Foster, B., Greenberg, N. M., McKeehan, W. L. and Wang, F. (2003). Cooperation between ectopic FGFR1 and depression of FGFR2 in induction of prostatic intraepithelial neoplasia in the mouse prostate. *Cancer research* **63**, 8784–90.

Johnson, D. E. and Williams, L. T. (1993). Structural and functional diversity in the FGF receptor multigene family. *Advances in cancer research* **60**, 1–41.

Kathuria, H., Cao, Y., Hinds, A., Ramirez, M. I. and Williams, M. C. (2007). ERM is expressed by alveolar epithelial cells in adult mouse lung and regulates caveolin-1 transcription in mouse lung epithelial cell lines. *Journal of cellular biochemistry* **102**, 13–27.

Katoh, M. (2008). Cancer genomics and genetics of FGFR2 (Review). *International journal of oncology* **33**, 233–7.

Katoh, Y. and Katoh, M. (2009a). FGFR2-related pathogenesis and FGFR2-targeted therapeutics (Review). 307–311.

Katoh, Y. and Katoh, M. (2009b). Hedgehog target genes: mechanisms of carcinogenesis induced by aberrant hedgehog signaling activation. *Current molecular medicine* **9**, 873–86.

Katoh, M. and Nakagama, H. (2013). FGF Receptors: Cancer Biology and Therapeutics. *Medicinal research reviews*.

Khatri, P., Voichita, C., Kattan, K., Ansari, N., Khatri, A., Georgescu, C., Tarca, A. L. and Draghici, S. (2007). Onto-Tools: new additions and improvements in 2006. *Nucleic acids research* **35**, W206–11.

Klar, J., Blomstrand, P., Brunmark, C., Badhai, J., Håkansson, H. F., Brange, C. S., Bergendal, B. and Dahl, N. (2011). Fibroblast growth factor 10 haploinsufficiency causes chronic obstructive pulmonary disease. *Journal of medical genetics* **48**, 705–9.

Kolb, M., Margetts, P. J., Anthony, D. C., Pitossi, F. and Gauldie, J. (2001). Transient expression of IL-1beta induces acute lung injury and chronic repair leading to pulmonary fibrosis. *The Journal of clinical investigation* **107**, 1529–36.

Korfei, M., Ruppert, C., Mahavadi, P., Henneke, I., Markart, P., Koch, M., Lang, G., Fink, L., Bohle, R.-M., Seeger, W., et al. (2008). Epithelial endoplasmic reticulum stress and apoptosis in sporadic idiopathic pulmonary fibrosis. *American journal of respiratory and critical care medicine* **178**, 838–46.

Kropski, J. A., Lawson, W. E., Young, L. R. and Blackwell, T. S. (2013). Genetic studies provide clues on the pathogenesis of idiopathic pulmonary fibrosis. *Disease models & mechanisms* **6**, 9–17.

Kuro-o, M. (2008). Endocrine FGFs and Klothos: emerging concepts. *Trends in endocrinology and metabolism: TEM* **19**, 239–45.

Kwapiszewska, G., Wilhelm, J., Wolff, S., Laumanns, I., Koenig, I. R., Ziegler, A., Seeger, W., Bohle, R. M., Weissmann, N. and Fink, L. (2005). Expression profiling of laser-microdissected intrapulmonary arteries in hypoxia-induced pulmonary hypertension. *Respiratory research* **6**, 109.

Lawson, W. E., Polosukhin, V. V, Zoia, O., Stathopoulos, G. T., Han, W., Plieth, D., Loyd, J. E., Neilson, E. G. and Blackwell, T. S. (2005). Characterization of fibroblast-specific protein 1 in pulmonary fibrosis. *American journal of respiratory and critical care medicine* **171**, 899–907.

Lazo, J. S. and Humphreys, C. J. (1983). Lack of metabolism as the biochemical basis of bleomycin-induced pulmonary toxicity. *Proceedings of the National Academy of Sciences of the United States of America* **80**, 3064–8.

Lazo, J. S., Boland, C. J. and Schwartz, P. E. (1982). Bleomycin hydrolase activity and cytotoxicity in human tumors. *Cancer research* **42**, 4026–31.

Lebeche, D., Malpel, S. and Cardoso, W. V (1999). Fibroblast growth factor interactions in the developing lung. *Mechanisms of development* **86**, 125–36.

Lewis, D. and Scullion, J. (2012). Palliative and end-of-life care for patients with idiopathic pulmonary fibrosis: challenges and dilemmas. *International journal of palliative nursing* **18**, 331–7.

Li, D. Q. and Tseng, S. C. (1997). Differential regulation of keratinocyte growth factor and hepatocyte growth factor/scatter factor by different cytokines in human corneal and limbal fibroblasts. *Journal of cellular physiology* **172**, 361–72.

Li, X., Brunton, V. G., Burgar, H. R., Wheldon, L. M. and Heath, J. K. (2004). FRS2-dependent SRC activation is required for fibroblast growth factor receptor-induced phosphorylation of Sprouty and suppression of ERK activity. *Journal of cell science* **117**, 6007–17.

Li, X., Li, S., Zhang, M., Li, X., Zhang, X., Zhang, W. and Li, C. (2010). Protective effects of a bacterially expressed NIF-KGF fusion protein against bleomycin-induced acute lung injury in mice. *Acta biochimica et biophysica Sinica* **42**, 548–57.

Li, M., Krishnaveni, M. S., Li, C., Zhou, B., Xing, Y., Banfalvi, A., Li, A., Lombardi, V., Akbari, O., Borok, Z., et al. (2011). Epithelium-specific deletion of TGF-β receptor type II protects mice from bleomycin-induced pulmonary fibrosis. *The Journal of clinical investigation* **121**, 277–87.

Limper, A. H. (2004). Chemotherapy-induced lung disease. *Clinics in chest medicine* **25**, 53–64.

Liu, J. Y., Sime, P. J., Wu, T., Warshamana, G. S., Pociask, D., Tsai, S. Y. and Brody, A. R. (2001). Transforming growth factor-beta(1) overexpression in tumor necrosis factor-alpha receptor knockout mice induces fibroproliferative lung disease. *American journal of respiratory cell and molecular biology* **25**, 3–7.

Liu, Y., Jiang, H., Crawford, H. C. and Hogan, B. L. M. (2003). Role for ETS domain transcription factors Pea3/Erm in mouse lung development. *Developmental biology* **261**, 10–24.

Liu, Z., Neiss, N., Zhou, S., Henne-Bruns, D., Korc, M., Bachem, M. and Kornmann, M. (2007a). Identification of a fibroblast growth factor receptor 1 splice variant that inhibits pancreatic cancer cell growth. *Cancer research* **67**, 2712–9.

Liu, Z., Ishiwata, T., Zhou, S., Maier, S., Henne-Bruns, D., Korc, M., Bachem, M. and Kornmann, M. (2007b). Human fibroblast growth factor receptor 1-IIIb is a functional fibroblast growth factor receptor expressed in the pancreas and involved in proliferation and movement of pancreatic ductal cells. *Pancreas* **35**, 147–57.

Liu, C.-J., Ha, X.-Q., Jiang, J.-J., Lv, T.-D. and Wu, C. (2011). Keratinocyte growth factor (KGF) gene therapy mediated by an attenuated form of Salmonella typhimurium ameliorates radiation induced pulmonary injury in rats. *Journal of radiation research* **52**, 176–84.

Loomis-King, H., Flaherty, K. R. and Moore, B. B. (2013). Pathogenesis, current treatments and future directions for idiopathic pulmonary fibrosis. *Current opinion in pharmacology* **13**, 377–85.

Lü, J., Izvolsky, K. I., Qian, J. and Cardoso, W. V (2005). Identification of FGF10 targets in the embryonic lung epithelium during bud morphogenesis. *The Journal of biological chemistry* **280**, 4834–41.

Luo, Y., Lu, W., Mohamedali, K. A., Jang, J. H., Jones, R. B., Gabriel, J. L., Kan, M. and McKeehan, W. L. (1998). The glycine box: a determinant of specificity for fibroblast growth factor. *Biochemistry* **37**, 16506–15.

Luo, Y., Ye, S., Kan, M. and McKeehan, W. L. (2006a). Structural specificity in a FGF7-affinity purified heparin octasaccharide required for formation of a complex with FGF7 and FGFR2IIIb. *Journal of cellular biochemistry* **97**, 1241–58.

Luo, Y., Ye, S., Kan, M. and McKeehan, W. L. (2006b). Control of fibroblast growth factor (FGF) 7- and FGF1-induced mitogenesis and downstream signaling by distinct heparin octasaccharide motifs. *The Journal of biological chemistry* **281**, 21052–61.

Luo, Y., Yang, C., Jin, C., Xie, R., Wang, F. and McKeehan, W. L. (2009). Novel phosphotyrosine targets of FGFR2IIIb signaling. *Cellular signalling* **21**, 1370–8.

Maina, J. N. and West, J. B. (2005). Thin and strong! The bioengineering dilemma in the structural and functional design of the blood-gas barrier. *Physiological reviews* **85**, 811–44.

Marchand-Adam, S., Plantier, L., Bernuau, D., Legrand, A., Cohen, M., Marchal, J., Soler, P., Lesèche, G., Mal, H., Aubier, M., et al. (2005). Keratinocyte growth factor expression by fibroblasts in pulmonary fibrosis: poor response to interleukin-1beta. *American journal of respiratory cell and molecular biology* **32**, 470–7.

Margadant, C. and Sonnenberg, A. (2010). Integrin-TGF-beta crosstalk in fibrosis, cancer and wound healing. *EMBO reports* **11**, 97–105.

Marmai, C., Sutherland, R. E., Kim, K. K., Dolganov, G. M., Fang, X., Kim, S. S., Jiang, S., Golden, J. A., Hoopes, C. W., Matthay, M. A., et al. (2011). Alveolar epithelial cells express mesenchymal proteins in patients with idiopathic pulmonary fibrosis. *American journal of physiology. Lung cellular and molecular physiology* **301**, L71–8.

Martis, P. C., Whitsett, J. A., Xu, Y., Perl, A.-K. T., Wan, H. and Ikegami, M. (2006). C/EBPalpha is required for lung maturation at birth. *Development (Cambridge, England)* **133**, 1155–64.

Mason, I. J., Fuller-Pace, F., Smith, R. and Dickson, C. (1994). FGF-7 (keratinocyte growth factor) expression during mouse development suggests roles in myogenesis, forebrain regionalisation and epithelial-mesenchymal interactions. *Mechanisms of development* **45**, 15–30.

Mason, R. J., Pan, T., Edeen, K. E., Nielsen, L. D., Zhang, F., Longphre, M., Eckart, M. R. and Neben, S. (2003). Keratinocyte growth factor and the transcription factors C/EBP alpha, C/EBP delta, and SREBP-1c regulate fatty acid synthesis in alveolar type II cells. *The Journal of clinical investigation* **112**, 244–55.

Mason, J. M., Morrison, D. J., Bassit, B., Dimri, M., Band, H., Licht, J. D. and Gross, I. (2004). Tyrosine phosphorylation of Sprouty proteins regulates their ability to inhibit growth factor signaling: a dual feedback loop. *Molecular biology of the cell* **15**, 2176–88.

Matsubara, A., Kan, M., Feng, S. and McKeehan, W. L. (1998). Inhibition of growth of malignant rat prostate tumor cells by restoration of fibroblast growth factor receptor 2. *Cancer research* **58**, 1509–14.

McLaughlin, J. S. and Shafritz, A. B. (2011). Cutaneous warts. *The Journal of hand surgery* **36**, 343–4.

McLeod, B. F., Lawrence, H. J., Smith, D. W., Vogt, P. J. and Gandara, D. R. (1987). Fatal bleomycin toxicity from a low cumulative dose in a patient with renal insufficiency. *Cancer* **60**, 2617–20.

McQualter, J. L., Yuen, K., Williams, B. and Bertoncello, I. (2010). Evidence of an epithelial stem/progenitor cell hierarchy in the adult mouse lung. *Proceedings of the National Academy of Sciences of the United States of America* **107**, 1414–9.

Meyers, G. A., Day, D., Goldberg, R., Daentl, D. L., Przylepa, K. A., Abrams, L. J., Graham, J. M., Feingold, M., Moeschler, J. B., Rawnsley, E., et al. (1996). FGFR2 exon IIIa and IIIc mutations in Crouzon, Jackson-Weiss, and Pfeiffer syndromes: evidence for missense changes, insertions, and a deletion due to alternative RNA splicing. *American journal of human genetics* **58**, 491–8.

Milam, J. E., Keshamouni, V. G., Phan, S. H., Hu, B., Gangireddy, S. R., Hogaboam, C. M., Standiford, T. J., Thannickal, V. J. and Reddy, R. C. (2008). PPAR-gamma agonists inhibit profibrotic phenotypes in human lung fibroblasts and bleomycin-induced pulmonary fibrosis. *American journal of physiology. Lung cellular and molecular physiology* **294**, L891–901.

Moeller, A., Ask, K., Warburton, D., Gauldie, J. and Kolb, M. (2008). The bleomycin animal model: a useful tool to investigate treatment options for idiopathic pulmonary fibrosis? *The international journal of biochemistry & cell biology* **40**, 362–82.

Munos, B. (2009). Lessons from 60 years of pharmaceutical innovation. *Nature reviews. Drug discovery* **8**, 959–68.

O'Brien, K., Troendle, J., Gochuico, B. R., Markello, T. C., Salas, J., Cardona, H., Yao, J., Bernardini, I., Hess, R. and Gahl, W. A. (2011). Pirfenidone for the treatment of Hermansky-Pudlak syndrome pulmonary fibrosis. *Molecular genetics and metabolism* **103**, 128–34.

Ohkoshi, M. and Oka, T. (1984). Age-related changes in drug concentration in skin and lungs of mice. *The Journal of dermatology* **11**, 438–42.

Olson, A. L., Swigris, J. J., Lezotte, D. C., Norris, J. M., Wilson, C. G. and Brown, K. K. (2007). Mortality from pulmonary fibrosis increased in the United States from 1992 to 2003. *American journal of respiratory and critical care medicine* **176**, 277–84.

Ono, S., Ishii, G., Nagai, K., Takuwa, T., Yoshida, J., Nishimura, M., Hishida, T., Aokage, K., Fujii, S., Ikeda, N., et al. (2013). Podoplanin-positive cancer-associated fibroblasts could have prognostic value independent of cancer cell phenotype in stage I lung squamous cell carcinoma: usefulness of combining analysis of both cancer cell phenotype and cancer-associated fibroblast phe. *Chest* **143**, 963–70.

Parsa, S., Kuremoto, K.-I., Seidel, K., Tabatabai, R., Mackenzie, B., Yamaza, T., Akiyama, K., Branch, J., Koh, C. J., Al Alam, D., et al. (2010). Signaling by FGFR2b controls the regenerative capacity of adult mouse incisors. *Development (Cambridge, England)* **137**, 3743–52.

Partanen, J., Schwartz, L. and Rossant, J. (1998). Opposite phenotypes of hypomorphic and Y766 phosphorylation site mutations reveal a function for Fgfr1 in anteroposterior patterning of mouse embryos. *Genes & Development* **12**, 2332–2344.

Patel, N. M., Kawut, S. M., Jelic, S., Arcasoy, S. M., Lederer, D. J. and Borczuk, A. C. (2013). Pulmonary arteriole gene expression signature in idiopathic pulmonary fibrosis. *The European respiratory journal* **41**, 1324–30.

Paul, S. M., Mytelka, D. S., Dunwiddie, C. T., Persinger, C. C., Munos, B. H., Lindborg, S. R. and Schacht, A. L. (2010). How to improve R&D productivity: the pharmaceutical industry's grand challenge. *Nature reviews. Drug discovery* **9**, 203–14.

Peng, R., Sridhar, S., Tyagi, G., Phillips, J. E., Garrido, R., Harris, P., Burns, L., Renteria, L., Woods, J., Chen, L., et al. (2013). Bleomycin induces molecular changes directly relevant to idiopathic pulmonary fibrosis: a model for "active" disease. *PloS one* **8**, e59348.

Popovici, C., Roubin, R., Coulier, F. and Birnbaum, D. (2005). An evolutionary history of the FGF superfamily. *BioEssays : news and reviews in molecular, cellular and developmental biology* **27**, 849–57.

R Development Core Team (2009). R: A language and environment for statistical computing. R Foundation for Statistical Computing, Vienna, Austria.

Raghu, G. and Thickett, D. R. (2013). Pirfenidone for IPF: pro/con debate; the "con" viewpoint. *Thorax*.

Ramasamy, S. K., Mailleux, A. a, Gupte, V. V, Mata, F., Sala, F. G., Veltmaat, J. M., Del Moral, P. M., De Langhe, S., Parsa, S., Kelly, L. K., et al. (2007). Fgf10 dosage is critical for the amplification of epithelial cell progenitors and for the formation of multiple mesenchymal lineages during lung development. *Developmental biology* **307**, 237–47.

Rehan, V. K., Sugano, S., Wang, Y., Santos, J., Romero, S., Dasgupta, C., Keane, M. P., Stahlman, M. T. and Torday, J. S. (2006). Evidence for the presence of lipofibroblasts in human lung. *Experimental lung research* **32**, 379–93.

Ricol, D., Cappellen, D., El Marjou, A., Gil-Diez-de-Medina, S., Girault, J. M., Yoshida, T., Ferry, G., Tucker, G., Poupon, M. F., Chopin, D., et al. (1999). Tumour suppressive properties of fibroblast growth factor receptor 2-IIIb in human bladder cancer. *Oncogene* **18**, 7234–43.

Riley, B. M., Mansilla, M. A., Ma, J., Daack-Hirsch, S., Maher, B. S., Raffensperger, L. M., Russo, E. T., Vieira, A. R., Dodé, C., Mohammadi, M., et al. (2007). Impaired FGF signaling contributes to cleft lip and palate. *Proceedings of the National Academy of Sciences of the United States of America* **104**, 4512–7.

Rogozin, I. B., Sverdlov, A. V, Babenko, V. N. and Koonin, E. V (2005). Analysis of evolution of exon-intron structure of eukaryotic genes. *Briefings in bioinformatics* **6**, 118–34.

Rubin, C., Zwang, Y., Vaisman, N., Ron, D. and Yarden, Y. (2005). Phosphorylation of carboxyl-terminal tyrosines modulates the specificity of Sprouty-2 inhibition of different signaling pathways. *The Journal of biological chemistry* **280**, 9735–44.

Sakamoto, S., Yazawa, T., Baba, Y., Sato, H., Kanegae, Y., Hirai, T., Saito, I., Goto, T. and Kurahashi, K. (2011). Keratinocyte growth factor gene transduction ameliorates pulmonary fibrosis induced by bleomycin in mice. *American journal of respiratory cell and molecular biology* **45**, 489–97.

Sakaue, H., Konishi, M., Ogawa, W., Asaki, T., Mori, T., Yamasaki, M., Takata, M., Ueno, H., Kato, S., Kasuga, M., et al. (2002). Requirement of fibroblast growth factor 10 in development of white adipose tissue. *Genes & development* **16**, 908–12.

Sandilands, E., Akbarzadeh, S., Vecchione, A., McEwan, D. G., Frame, M. C. and Heath, J. K. (2007). Src kinase modulates the activation, transport and signalling dynamics of fibroblast growth factor receptors. *EMBO reports* **8**, 1162–9.

Santrach, P. J., Askin, F. B., Wells, R. J., Azizkhan, R. G. and Merten, D. F. (1989). Nodular form of bleomycin-related pulmonary injury in patients with osteogenic sarcoma. *Cancer* **64**, 806–11.

Sauer, B. (1998). Inducible gene targeting in mice using the Cre/lox system. *Methods (San Diego, Calif.)* **14**, 381–92.

Schwenk, F., Baron, U. and Rajewsky, K. (1995). A cre-transgenic mouse strain for the ubiquitous deletion of loxP-flanked gene segments including deletion in germ cells. *Nucleic acids research* **23**, 5080–1.

Scotton, C. J. and Chambers, R. C. (2007). Molecular targets in pulmonary fibrosis: the myofibroblast in focus. *Chest* **132**, 1311–21.

Sekine, K., Ohuchi, H., Fujiwara, M., Yamasaki, M., Yoshizawa, T., Sato, T., Yagishita, N., Matsui, D., Koga, Y., Itoh, N., et al. (1999). Fgf10 is essential for limb and lung formation. *Nature genetics* **21**, 138–41.

Seo, J.-S., Ju, Y. S., Lee, W.-C., Shin, J.-Y., Lee, J. K., Bleazard, T., Lee, J., Jung, Y. J., Kim, J.-O., Shin, J.-Y., et al. (2012). The transcriptional landscape and mutational profile of lung adenocarcinoma. *Genome research* **22**, 2109–19.

Shu, W., Guttentag, S., Wang, Z., Andl, T., Ballard, P., Lu, M. M., Piccolo, S., Birchmeier, W., Whitsett, J. A., Millar, S. E., et al. (2005). Wnt/beta-catenin signaling acts upstream of N-myc, BMP4, and FGF signaling to regulate proximal-distal patterning in the lung. *Developmental biology* **283**, 226–39.

Smyth, G. K. (2004). Linear models and empirical bayes methods for assessing differential expression in microarray experiments. *Statistical applications in genetics and molecular biology* **3**, Article3.

Snyder-Warwick, A. K., Perlyn, C. A., Pan, J., Yu, K., Zhang, L. and Ornitz, D. M. (2010). Analysis of a gain-of-function FGFR2 Crouzon mutation provides evidence of loss of function activity in the etiology of cleft palate. *Proceedings of the National Academy of Sciences of the United States of America* **107**, 2515–20.

Study of the clinical efficiency of bleomycin in human cancer. (1970). *British medical journal* **2**, 643–5.

Sugahara, K., Rubin, J. S., Mason, R. J., Aronsen, E. L. and Shannon, J. M. (1995). Keratinocyte growth factor increases mRNAs for SP-A and SP-B in adult rat alveolar type II cells in culture. *Am J Physiol Lung Cell Mol Physiol* **269**, L344–350.

Sugahara, K., Iyama, K., Kuroda, M. J. and Sano, K. (1998). Double intratracheal instillation of keratinocyte growth factor prevents bleomycin-induced lung fibrosis in rats. *The Journal of pathology* **186**, 90–8.

Thannickal, V. J., Toews, G. B., White, E. S., Lynch, J. P. and Martinez, F. J. (2004). Mechanisms of pulmonary fibrosis. *Annual review of medicine* **55**, 395–417.

Tian, X., Vroom, C., Ghofrani, H. A., Weissmann, N., Bieniek, E., Grimminger, F., Seeger, W., Schermuly, R. T. and Pullamsetti, S. S. (2011). Phosphodiesterase 10A upregulation contributes to pulmonary vascular remodeling. *PloS one* **6**, e18136.

Tichelaar, J. W. (2000). Conditional Expression of Fibroblast Growth Factor-7 in the Developing and Mature Lung. *Journal of Biological Chemistry* **275**, 11858–11864.

Tiozzo, C., De Langhe, S., Carraro, G., Alam, D. Al, Nagy, A., Wigfall, C., Hajihosseini, M. K., Warburton, D., Minoo, P. and Bellusci, S. (2009). Fibroblast growth factor 10 plays a causative role in the tracheal cartilage defects in a mouse model of Apert syndrome. *Pediatric research* **66**, 386–90.

Trowell, O. A. and Willmer, E. N. (1939). Studies on the growth of tissues in vitro. *Journal of Experimental Biology* **16**, 60–70, 193.

Umezawa, H., Ishizuki, M., Hori, S., Chimura, H. and Takeuchi, T. (1968). The distribution of 3H-bleomycin in mouse tissue. *The Journal of antibiotics* **21**, 638–42.

Umezawa, H., Takeuchi, T., Hori, S., Sawa, T. and Ishizuka, M. (1972). Studies on the mechanism of antitumor effect of bleomycin of squamous cell carcinoma. *The Journal of antibiotics* **25**, 409–20.

Umezawa, H., Hori, S., Sawa, T., Yoshioka, T. and Takeuchi, T. (1974). A bleomycin-inactivating enzyme in mouse liver. *The Journal of antibiotics* **27**, 419–24.

Urness, L. D., Paxton, C. N., Wang, X., Schoenwolf, G. C. and Mansour, S. L. (2010). FGF signaling regulates otic placode induction and refinement by controlling both ectodermal target genes and hindbrain Wnt8a. *Developmental biology* **340**, 595–604.

Vaccaro, C. and Brody, J. S. (1978). Ultrastructure of developing alveoli. I. The role of the interstitial fibroblast. *The Anatomical record* **192**, 467–79.

Vargas, R. A. P., Maegawa, G. H. B., Taucher, S. C., Leite, J. C. L., Sanz, P., Cifuentes, J., Parra, M., Muñoz, H., Maranduba, C. M. and Passos-Bueno, M. R. (2003). Beare-Stevenson syndrome: Two South American patients with FGFR2 analysis. *American journal of medical genetics. Part A* **121A**, 41–6.

Varisco, B. M., Ambalavanan, N., Whitsett, J. A. and Hagood, J. S. (2012). Thy-1 signals through PPARγ to promote lipofibroblast differentiation in the developing lung. *American journal of respiratory cell and molecular biology* **46**, 765–72.

Volckaert, T., Dill, E., Campbell, A., Tiozzo, C., Majka, S., Bellusci, S. and De Langhe, S. P. (2011). Parabronchial smooth muscle constitutes an airway epithelial stem cell niche in the mouse lung after injury. *The Journal of clinical investigation* **121**, 4409–19.

Wagner, M. and Siddiqui, M. A. Q. (2007). Signal transduction in early heart development (I): cardiogenic induction and heart tube formation. *Experimental biology and medicine (Maywood, N.J.)* **232**, 852–65.

Wang, F., McKeehan, K., Yu, C., Ittmann, M. and McKeehan, W. L. (2004). Chronic activity of ectopic type 1 fibroblast growth factor receptor tyrosine kinase in prostate epithelium results in hyperplasia accompanied by intraepithelial neoplasia. *The Prostate* **58**, 1–12.

Wang, J., Wang, S., Manzer, R., McConville, G. and Mason, R. J. (2006). Ozone induces oxidative stress in rat alveolar type II and type I-like cells. *Free radical biology & medicine* **40**, 1914–28.

Wang, C., Wang, C., Hoch, E. G. and Pitt, G. S. (2011). Identification of novel interaction sites that determine specificity between fibroblast growth factor homologous factors and voltage-gated sodium channels. *The Journal of biological chemistry* **286**, 24253–63.

Weaver, M., Dunn, N. R. and Hogan, B. L. (2000). Bmp4 and Fgf10 play opposing roles during lung bud morphogenesis. *Development (Cambridge, England)* **127**, 2695–704.

Wilkie, A. O., Slaney, S. F., Oldridge, M., Poole, M. D., Ashworth, G. J., Hockley, A. D., Hayward, R. D., David, D. J., Pulleyn, L. J. and Rutland, P. (1995). Apert syndrome results from localized mutations of FGFR2 and is allelic with Crouzon syndrome. *Nature genetics* **9**, 165–72.

Xu, S., Kuang, J., Liu, J., Ma, C., Feng, Y. and Su, Z. (2012). Association between fibroblast growth factor 7 and the risk of chronic obstructive pulmonary disease. *Acta pharmacologica Sinica* **33**, 998–1003.

Yan, G., Fukabori, Y., McBride, G., Nikolaropolous, S. and McKeehan, W. L. (1993). Exon switching and activation of stromal and embryonic fibroblast growth factor (FGF)-FGF receptor genes in prostate epithelial cells accompany stromal independence and malignancy. *Molecular and cellular biology* **13**, 4513–22.

Yi, E. S., Williams, S. T., Lee, H., Malicki, D. M., Chin, E. M., Yin, S., Tarpley, J. and Ulich, T. R. (1996). Keratinocyte growth factor ameliorates radiation- and bleomycin-induced lung injury and mortality. *The American journal of pathology* **149**, 1963–70.

Yildirim, A. O., Veith, M., Rausch, T., Müller, B., Kilb, P., Van Winkle, L. S. and Fehrenbach, H. (2008). Keratinocyte growth factor protects against Clara cell injury induced by naphthalene. *The European respiratory journal : official journal of the European Society for Clinical Respiratory Physiology* **32**, 694–704.

Yildirim, A. O., Muyal, V., John, G., Müller, B., Seifart, C., Kasper, M. and Fehrenbach, H. (2010). Palifermin induces alveolar maintenance programs in emphysematous mice. *American journal of respiratory and critical care medicine* **181**, 705–17.

Yoshida, K., Kuwano, K., Hagimoto, N., Watanabe, K., Matsuba, T., Fujita, M., Inoshima, I. and Hara, N. (2002). MAP kinase activation and apoptosis in lung tissues from patients with idiopathic pulmonary fibrosis. *The Journal of pathology* **198**, 388–96.

Yue, X., Lu, J., Auduong, L., Sides, M. D. and Lasky, J. A. (2013). Overexpression of Sulf2 in idiopathic pulmonary fibrosis. *Glycobiology* **23**, 709–19.

Zhang, S., Lin, Y., Itäranta, P., Yagi, A. and Vainio, S. (2001). Expression of Sprouty genes 1, 2 and 4 during mouse organogenesis. *Mechanisms of development* **109**, 367–70.

Zhang, X., Ibrahimi, O. A., Olsen, S. K., Umemori, H., Mohammadi, M. and Ornitz, D. M. (2006). Receptor specificity of the fibroblast growth factor family. The complete mammalian FGF family. *The Journal of biological chemistry* **281**, 15694–700.

Zhang, Y., McKeehan, K., Lin, Y., Zhang, J. and Wang, F. (2008). Fibroblast growth factor receptor 1 (FGFR1) tyrosine phosphorylation regulates binding of FGFR substrate 2alpha (FRS2alpha) but not FRS2 to the receptor. *Molecular endocrinology (Baltimore, Md.)* **22**, 167–75.

Zhou, L., Graeff, R. W., McCray, P. B., Simonet, W. S. and Whitsett, J. A. (1996). Keratinocyte growth factor stimulates CFTR-independent fluid secretion in the fetal lung in vitro. *Am J Physiol Lung Cell Mol Physiol* **271**, L987–994.

Acknowledgements

First and foremost, I would like to sincerely thank Prof. Dr. Saverio Bellusci for his excellent mentorship and insight into this project, and for giving me the special opportunity to continue my research training in a brand new, state-of-the-art laboratory in Germany. I greatly appreciated his enthusiasm and guidance during the last four years and I am especially grateful for his open-mindedness and constructive feedback.

Secondly, I am exceptionally thankful to the Bellusci laboratory manager and technical expert, Kerstin Goth for her invaluable technical support and resourcefulness. Her hard work and dedication to students enabled the lab to run efficiently and her vigilance and attention to detail brought order and structure to our work environment.

Thirdly, this project is immensely indebted to the hard work and dedication of Dr. Denise Al Alam. Without her expertise and her technical assistants at Children's Hospital Los Angeles this work would not have been possible. I am especially thankful for her invaluable mentorship and critical feedback regarding manuscripts and results.

I am especially thankful to Heike Habermann for the skillful translation of animal protocols and to Jana Rostkovius for excellent technical assistance.

Acknowledgements

I am especially thankful to Matt Jones for the genotyping of the mice used in this project, as well as for his refreshing comic relief and his serious philosophical insights into life.

I am also thankful to Susanne Ziegler and Gabi Dahlem for technical assistance in the culturing of human cells and the gathering of human samples that allowed me to bring human relevance to this work.

I am very grateful to Dr. Ingrid Henneke and Stephanie Hezel for their patience, dedication, and expertise in their assistance with the establishment of new experimental protocols in our lab. In addition, I am thankful to Prof. Dr. Andreas Günther for his guidance and critical feedback of my work; and also for recognizing me as an artist.

My PhD experience would not have been complete without the Molecular Biology and Medicine of the Lung Program (MBML) organized and administrated by Dr. Rory Morty and founded by Prof. Dr. Werner Seeger who regularly facilitated fascinating lectures on the lung and organized outstanding international meetings. Rory's dedication to students and his innate outgoingness brought people from all over the world closer to each other and fostered new working collaborations. In addition to organizers of the MBML, I would like to thank Dr. Lorna Lück from the Giessen Graduate School for Life Sciences (GGL) and Prof.

Dr. Eveline Baumgart-Vogt. Both Lorna and Eveline facilitated my professional development by granting me many valuable leadership experiences in the GGL.

In addition I would like to thank my previous supervisor Dr. Anna Petryk, for her ongoing mentorship and guidance as well my long-time friend and life mentor, Dr. Aaron McCabe.

I am especially thankful for the new graduate students in our lab, especially Alyona Moiseenko, Amit Shrestha, and Dr. Cho-Ming Chao. I thank them for giving me the opportunity to broaden their scientific understanding and professional development.

Furthermore, I am very grateful to my friends outside of the Excellenz Cluster who always gave my life a refreshing contrast. To my friend: artist, writer, and photographer, Anabel Plà who I met on my first day in Germany; at the wrong place and the wrong time at the Friederichshain Berlin Volkshochschule in 2009. By making her dreams a reality, not only has she always inspired me to push the boundaries in life and in art, she has also always been there to give me a hard slap in the face when I absolutely needed it.

I would also like to thank my first native-German friend, tango dancing conspirator, and Mainzer party co-hostess, sociologist and ethnographer, Dr.

Sarah Fitchner. With her openness to all things strange, and her love for tango, she has continued to support my professional and personal pursuits.

Meine Labor Leben war auch viel ergänzt wegen der Bildhauer und Lebens-Philosoph, Sebastian Schweikert. Mit seine beeinfluss, habe ich durch Tagebücher und Gedichte, meinem Deutsch versbessert und auch eine ganz neues perspektives für das Leben entwickelt. Mit seinem Instruktion, habe ich meine Zeichnung Fähigkeiten viel verbessert, Ausstellungen gemacht, Bilder verkauft, und ganz magische Erfahrungen gehabt in seinem Atelier in Mainz und auf dem Steinbruch in Untersberg, Osterreich. Außerdem, bin ich dankbar für den Freundschaft mit Schweizer Künstler Valentin Magaro, deren mit seinem Leben zusätzlich zu unsere Diskussionen waren auch inspirierende.

Bedanke ich auch, der bald Phd zu sein, Cyanobakterien Forscher und sehr attraktiver, Berliner nativ Nils Schürgers, deren Unterstützung und Einblick habe ich häufig wirklich gebraucht. Außerdem, mit ihm Tanzen in Gießen hat immer Spaß gemacht. Haben wir zusammen ganz wunderschöne, neue Erfahrung gesammelt, inklusive 1400km+ im Fahrrad gefahren vom Wien nach Kroatien Küste, zelten jeden Nacht und starke Gewittern überleben.

Schließlich, bedanke ich der Grafiker und Bassist für „Brain on Furs“, Lukas Kolar deren hat mit mir seinem Leidenschaft für Musik geteilt, und Gitarre Unterricht gegeben so hatte ich den Chance, eine wunderbare Gefühl zu fühlen,

das heißt, durch Musik mich endlich auszudrücken können. Ich bedanke ihm sehr für seine Offenheit und Geduld, und dass jemand wartet bei mir bis ich den nächste Schritt des Leben erreiche.

Lastly (and most largely) I would like to give my most enormous dankeschöns to the two individuals who were always here for me from the very beginning whether I needed extra money at the end of the month for food (beer) or a shoulder to cry on. Meine Lieblingskollegen, soon to be PhDs: Elie El Agha, and Athanasios Fysikopolous. Through my most challenging professional and personal moments, these two were always there for me like my caring, surrogate uncles with a whiskey in one hand and a cigarette in the other, and always a witty response to lift my spirits; because lets face it, this whole thing wasn't exactly a walk in the park for any of us. I will miss them profoundly for their friendship, understanding, hilariousness, sarcasm, and seemingly unconditional support, and will forever keep all of our memories close to my heart; memories which will only be retrieved in the future with their help. I wish them the best health, luck and happiness in life beyond Giessen.

Der Lebenslauf wurde aus der elektronischen Version der Arbeit entfernt.

The curriculum vitae was removed from the electronic version of the paper.